

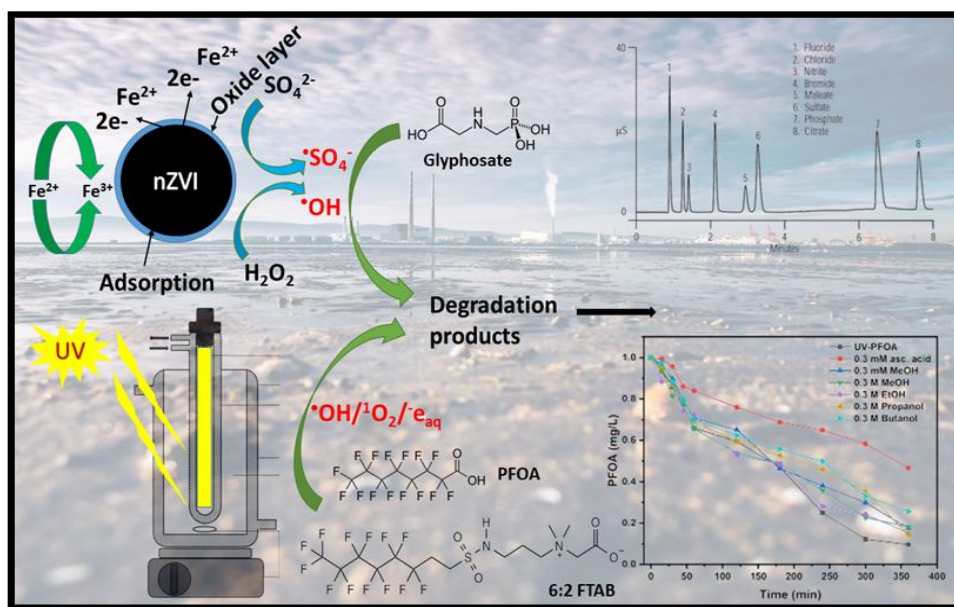


Università degli Studi di Torino

Doctoral School of the University of Torino

PhD Programme in Chemical and Materials Sciences XXXVI Cycle

Removal of Emerging and Persistent Pollutants by Fenton-like and
Photodegradation Processes



Naveed Ahmed

Supervisors:

Prof. Maria Concetta Bruzzoniti

Prof. Davide Vione



Università degli Studi di Torino

Doctoral School of the University of Torino

PhD Programme in Chemical and Materials Sciences XXXVI cycle

**Removal of Emerging and Persistent Pollutants by Fenton-like and
Photodegradation Processes**

Candidate: **Naveed Ahmed**

Supervisors: Prof. **Maria Concetta Bruzzone**
Prof. **Davide Vione**

Jury Members: Dr. **Luca Rivoira**
Department of Chemistry
University of Turin

Prof. **Gilles Mailhot**
Institut de Chimie de Clermont-Ferrand (ICCF).

Prof. **Marion Martienssen**
Chair of Biotechnology for Water Treatment
Brandenburg Technical University, Germany

Head of the Doctoral School: Prof. Eleonora Bonifacio

PhD Programme Coordinator: Prof. Bartolome Civalleri

Torino, 17/10/2024

Publications

1. Ahmed, Naveed, et al. "A review on the degradation of pollutants by Fenton-like systems based on zero-valent iron and persulfate: Effects of reduction potentials, pH, and anions occurring in wastewaters." *Molecules* 26.15 (2021): 4584.
2. Ahmed, Naveed, et al. "Feasibility of a Heterogeneous Nanoscale Zero-Valent Iron Fenton-like Process for the Removal of Glyphosate from Water." *Molecules* 28.5 (2023): 2214.
3. Ahmed, Naveed, et al. "Investigation on UV Degradation and Mechanism of 6: 2 Fluorotelomer Sulfonamide Alkyl Betaine, Based on Model Compound Perfluorooctanoic Acid." *ChemEngineering* 8.2 (2024): 32.

Contents

1	Introduction	6
2	Background	12
2.1	Introduction to Persistent Organic Pollutants	12
2.1.1	Introduction to GLY	14
2.1.2	Usage, Sorption, Functioning, and Fate in the Environment	16
2.1.3	Eco-toxicological effects of GLY	18
2.1.4	Recent Regulation and Policy related to GLY	20
2.1.5	Introduction to Aminomethylphosphonic acid (AMPA)	21
2.2	Introduction to PFAS	22
2.2.1	Physico-chemical Properties of PFAS	23
2.2.2	Sources and Their Dispersal into Environmental Sections	25
2.2.3	Toxicity of PFAS	31
2.3	Strategies for POP Treatment	34
2.3.1	Adsorption	34
2.3.2	Photolysis and Photocatalysis	36
2.3.3	Fenton and Fenton-like systems	42
2.3.4	Sulfate radical-based processes	46
2.3.5	Ozonation	53
2.3.6	Reductive degradation with hydrated electrons	55
2.4	PFOA and PFOS degradation pathways	69
2.4.1	Oxidative degradation pathways	69
2.4.2	Reductive degradation pathway	71
3	Materials and methods	73
3.1	Reagents and materials	73
3.2	Experimental setup and degradation of dyes (Malachite green, Rhodamine B, Acid Blue 74) by Fenton-like processes	73
3.3	Experimental setups and analysis for GLY removal	74
3.4	Experimental setup and photolysis of PFOA and 6:2 FTAB	76
3.4.1	Actinometry: Determination of Iron (II) and total Iron content:	76

3.4.2	Radical scavenging experiments	79
3.4.3	Quantification of PFOA, 6:2 FTAB, and their TPs by LC-MS.....	79
3.4.4	Fluoride and sulfate measurement by ion chromatography	80
3.4.5	Dissolved oxygen and hydrogen peroxide measurements	80
3.4.6	Data evaluation.....	80
4	Results and Discussions	82
4.1	Dyes removal	82
4.2	Glyphosate (GLY) removal.....	89
4.2.1	GLY removal at pH 3	90
4.2.2	GLY removal at pH 4	92
4.2.3	GLY removal at pH 5 and 6	94
4.2.4	GLY removal in tap water	94
4.2.5	Removal of Glyphosate by nZVI-metabisulfite.....	97
4.3	Removal of PFAS.....	99
4.3.1	Decomposition of PFOA at different pH values.....	99
4.3.2	Scavengers' Experiments for PFOA Decomposition	103
4.3.3	Decomposition of 6:2 FTAB at different pH values	110
4.3.4	Scavengers experiments for 6:2 FTAB decomposition	113
4.3.5	Proposed Mechanism of 6:2 FTAB decomposition.....	119
5	Conclusions and Future Work	121
6	References.....	125

1 Introduction

Water is essential for all life on Earth. However, out of all water resources on our planet, only 2.5% can be considered as freshwater, of which the majority occurs in the form of ice and permanent snow which is often not available for direct use. Currently, only 0.3% of freshwater is easily available to human beings [1]. Population growth, lifestyle improvements, and industrial production are among the reasons for which high amounts of sanitary sewage and industrial wastewater are discharged into natural water resources, resulting in severe environmental pollution. The discharged pollutants range from traditional persistent organic pollutants (POPs) e.g., polychlorinated biphenyls (PCBs), to emerging contaminants in the categories of dyes, pesticides, herbicides, pharmaceuticals, personal care products, and surfactants. Even though the production and application of several of these emerging contaminants are being restricted, the likelihood of human exposure due to accumulation in marine systems and contamination of groundwater used for drinking water production will continue for decades [2–5]. Among emerging pollutants, efficient strategies are required to detect and remove herbicides like phosphonates, and especially Glyphosate (GLY), as well as per- and polyfluorinated alkyl substances (PFAS) from wastewater effluents.

GLY and PFAS are reported to survive degradation in traditional wastewater treatment plants and to occur in treated water, thereby reaching aquatic environments where wastewater is discharged [2,6,7]. Treatment of GLY and PFAS is a huge challenge due to the following reasons:

- I) **Chemical stability:** PFAS are stable and not degraded for an extended period of time, they cannot be broken down through natural chemical processes or microbial degradation, thus they are able to resist degradation in wastewater treatment plants.
- II) **Low biological degradability:** Pollutant degradation potential in wastewater treatment plants mostly relies on microbial action, but it is quite challenging for bacteria to break down effectively either GLY or PFAS. Indeed, the latter have very

stable C-F bonds, while GLY is a phosphonate compound and the enzymes required to break it down are not very common in nature.

III) Adsorption: GLY and PFAS tend to adsorb onto particulate matter and suspended solids in wastewater. Thus, they might avoid entering into treatment processes and could settle down in the sludge, which may eventually be disposed off without further treatment.

IV) Dilution and transport: GLY and PFAS can be diluted below detectable concentration during mixing and transport within wastewater treatment plant systems, preventing detection and, sometimes as a consequence, removal (or removal assessment) from treated waters.

V) Incomplete treatment: Classical treatment plants are not typically optimized for the removal (e.g., breaking down or adsorption) of specific persistent organic pollutants like GLY and PFAS, although they are effective at removing many other pollutants.

VI) By-products formation: GLY persistent degradation by-products can be formed during treatment, some of which might be of high concern such as amino-methyl-phosphonic acid (AMPA) as they can have high levels of environmental persistence and toxicity [6,7]. PFAS degradation products (mainly PFOA or PFOS) are also persistent or very persistent.

Apart from the above reasons, the removal of PFAS is quite challenging due to the following, additional reasons:

I) PFAS are resistant to biological and traditional redox processes due to strong C-F bonds [8]. For example, they are inert to hydroxyl radicals as they have no C-H bonds available for H-abstraction, thus many $\cdot\text{OH}$ -based advanced oxidation processes (AOPs) fail to degrade PFAS [9].

II) The PFAS concentration in water bodies is quite low, i.e., in the range of ng L^{-1} to $\mu\text{g L}^{-1}$. Treatment of these PFAS traces in complex water bodies is quite difficult. Thus, there is an urgent requirement to develop innovative, low-cost, and useful techniques that can degrade PFAS efficiently [10].

In recent decades, AOPs have attracted much attention as promising methods to abate organic pollutants. They gather numerous techniques based on the in-situ formation of strong oxidants, among which the hydroxyl radical (HO^\bullet) plays a central role due to its high standard potentials (2.8 V vs. NHE) in acidic media. HO^\bullet is highly reactive and nonselective and can oxidize different organic compounds [11]. The main AOPs include ultraviolet (UV) irradiation, $\text{H}_2\text{O}_2/\text{UV}$, photocatalysis, ozonation, electrochemical oxidation, and Fenton-like processes. Many of these have removed GLY from wastewater [12–17].

In addition to other more conventional sources of iron (Fe^{2+} , FeO , FeS_2 , etc.), nano zero valent Iron (nZVI) has been used as an adsorbent as well as a reagent, coupled with hydrogen peroxide and metabisulfite, to degrade different pollutants [18]. The result is an efficient and cost-effective Fenton-like treatment technology that can operate at different pH values.

Preliminary experiments were performed to investigate the performance, suitability, and efficiency of nZVI-Fenton-like systems ($\text{nZVI}/\text{H}_2\text{O}_2$) using various dyes as model pollutants (Rhodamine B, Malachite green, and Acid Blue 74) at different pHs. The nZVI-Fenton-like system ($\text{nZVI}/\text{H}_2\text{O}_2$) was further replaced by nZVI/metabisulfite to study the role of sulfur-based radicals on one of the already investigated dyes (AB 74). All these nZVI-Fenton-like systems were proven to be efficient towards degradation of the studied dyes. Different loadings of chemicals (ZVI, H_2O_2 , and metabisulfite) were optimized to degrade the dyes at different pHs. Afterwards, optimized conditions were tested for degradation of persistent organic pollutants (glyphosate in our case).

In detail, we show that the heterogeneous nZVI-Fenton process ($\text{nZVI} + \text{H}_2\text{O}_2$) can achieve effective removal of GLY under different operational conditions. GLY removal

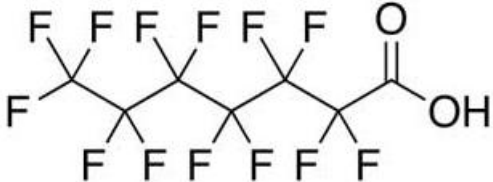
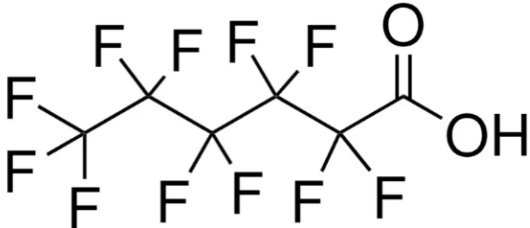
also takes place in the presence of excess nZVI, without H₂O₂, but the use of nZVI alone to remove GLY from water matrices would be very costly. GLY degradation by nZVI-Fenton was investigated in the pH range 3-6, with different H₂O₂ concentrations and nZVI loadings. We observed significant removal at pH 3 and 4, but as Fenton systems lose efficiency with increasing pH, the process was no longer effective at pH 5 or 6. GLY removal was also operational at pH 3 and 4 in tap water, despite the occurrence of several potentially interfering inorganic ions. Relatively low reagents costs, limited increase in water conductivity (mostly due to pH adjustments before and after treatment), and low iron leaching make nZVI-Fenton a promising tool to eliminate GLY from environmental aqueous matrices.

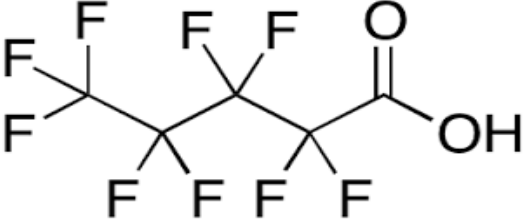
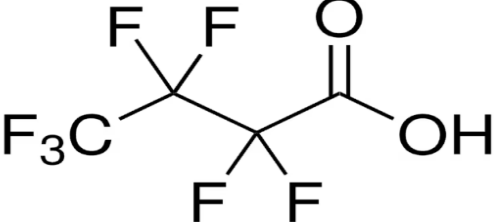
Aqueous photolysis is generally separated in direct and indirect photolysis. In the case of direct photolysis, an analyte of interest absorbs light radiation by itself and undergoes a chemical reaction. Indirect photolysis happens when light is absorbed by some other species to produce a reactive transient species that triggers degradation. Aqueous reactions with hydroxyl radicals ($\cdot\text{OH}$), peroxy radicals ($\cdot\text{OOR}$), carbonate radicals ($\text{CO}_3^{\cdot-}$), or singlet molecular oxygen ($^1\text{O}_2$) can be induced photochemically and, in such case, they are forms of indirect photolysis. If a compound does not absorb radiation, it can't undergo direct photolysis. In contrast, almost all compounds are labile to indirect photolysis, with the exception of the most persistent recalcitrant chemicals (e.g., perfluoroalkyl carboxylic and sulfonic acids) [19,20]. Previous studies have investigated the fate of some PFAS mainly by microbial degradation, as these generally remain in the wastewater treatment plant systems and interact with microbes. However, these water-soluble compounds are likely to be transported to surface waters where biodegradation classically plays a relatively minor role in comparison to photolysis for more or less biorecalcitrant compounds. In this thesis, the PFAS, perfluorooctanoic acid (PFOA) as well as aqueous film-forming foams such as 6:2 fluorotelomer sulphonamide alkylbetian (6:2 FTAB) have been degraded by direct photolysis using UV radiation (190-600 nm) at different pHs (4,7 and 10) as aqueous electrons were active species. The kinetics, half-life, and effect of scavengers

to study the reaction mechanism were here investigated and compared. The degradation pathway and formed byproducts were investigated and quantified; defluorination was also investigated by quantifying fluoride concentrations.

We used PFOA as a reference, finding 90% decomposition after 360 minutes at the original (unadjusted) pH of 5.6. At pH 4 and 7, degradation averaged 85% and 80%, respectively, while at pH 10 it went down to 57%. For 6:2 FTAB at its natural pH of 6.5, almost complete decomposition occurred. The primary UV transformation product was identified as 6:2 fluorotelomer sulfonic acid (6:2 FTSA), occasionally accompanied by shorter-chain perfluoroalkyl acids (PFAA) including PFHpA, PFHxA, and PFPeA etc. (Table:1.1).

Table 1.1: Short-chain Perfluoroalkyl acids with their structures

Compound	Structures
Perfluoroheptanoic acid (PFHpA)	
Perfluorohexanoic acid (PFHxA)	

Perfluoropentanoic acid (PFPeA)	
Perfluorobutanoic acid (PFBA)	

Interestingly, the overall decomposition percentages were unaffected by pH for 6:2 FTAB, although pH influenced rate constants and half-lives. In PFOA degradation, direct photolysis and reaction with hydrated electrons were presumed mechanisms, excluding the involvement of hydroxyl radicals. The role of superoxide radicals remains uncertain. For 6:2 FTAB, both direct and indirect photolysis were observed, with potential involvement of HO[•], superoxide radicals, and/or other reactive oxygen species (ROS). Clarification is needed regarding the role of e_{aq}^- in the degradation of 6:2 FTAB.

Overall, the given methodologies (ZVI Fenton-like systems as well as UV photodegradation) are promising and efficient treatment methods to degrade GLY in aqueous media in the presence of anions as water matrix and for the degradation of PFOA and 6:2 FTAB, respectively.

2 Background

2.1 Introduction to Persistent Organic Pollutants

Rampant industrialization and urbanization over the globe have caused an increased demand for new materials and substances, and a significant number of organic compounds are being used in our life. Indeed, innovation connected to these new materials has improved the quality of life but it also exerts pressure on our health due to environmental pollution [21]. Organic pollutants that persist in the environment and cause adverse effects on human health and the ecosystems, without being broken down into smaller compounds are known as persistent organic pollutants (POPs) [22]. Common pollutants belong to the families of dyes, pharmaceuticals, per- and poly-fluorinated alkyl substances (PFAS), pesticides, herbicides, phosphonates, personal care products, endocrine disruptors, and so on [23]. Overall, POPs are semi-volatile in nature and may enter the atmosphere, soil, and water bodies. Also, they are chemically stable and pose a continuous threat to the natural environment [23]. Furthermore, POPs can migrate in the environment through different routes facilitated by the atmosphere and water, and some of them are also absorbed by plants and animals thus making their way into the food chain, to ultimately affect human health. Due to persistency, long-term migration capability, and high toxicity of POPs, the regulation and abatement of pollution they cause have turned out to be challenging [24–26]. Thus, stability and toxicity of POPs are causing a serious threat to human health and the environment across the globe [26]. This calls for immediate attention by regulatory bodies, environmental scientists, as well as government organizations to tackle the problem in time and develop novel technologies to mitigate pollution across the globe. Some common POPs are here listed in Table. 2.1.

Table 2.1: Some common POP classes including their description and examples.

Class of POPs	Description	Examples	References
Organophosphates	Phosphorus-containing organic compounds that are frequently employed as insecticides ¹	Glyphosate ¹ , Malathion, Chlorpyrifos, and Parathion	Stockholm Convention on Persistent Organic Pollutants. (2001).
Organochlorines	Chlorinated organic substances are often bioaccumulative and resistant to breakdown	Chlordane, DDT, PCBs, and HCB	World Health Organization (WHO). (2005).
Polybrominated Diphenyl Ethers (PDBEs)	Used in many products as flame retardants	Decabromodiphenyl ether (BDE-209), Octabromodiphenyl ether (BDE-183)	European Chemicals Agency (ECHA). (2018).
Polycyclic Aromatic Hydrocarbons (PAHs)	Organic compounds with numerous fused aromatic rings, typical combustion by-products	Naphthalene, Benzo(a)pyrene, Anthracene	U.S. Environmental Protection Agency (EPA). (2018).

¹ As an exception to this, GLY is a herbicide.

Polychlorinated Biphenyls (PCBs)	Synthetic compounds used as coolants and in electrical equipment	PCB-180, PCB-101, PCB-153,	Agency for Toxic Substances and Disease Registry (ATSDR). (2000).
Dioxins and Furans	Combustion processes frequently produce chemicals that are extremely poisonous and persistent	2,3,7,8-Tetrachlorodibenzo-p-dioxin (TCDD)	U.S. Environmental Protection Agency (EPA). (2018).
Aldrin and Dieldrin	Insecticides used on crops regularly	Aldrin, Dieldrin	U.S. Environmental Protection Agency (EPA). (2017).
Perfluorinated Compounds (PFCs)	Organic substances with hydrophobic carbon chains that are completely fluorinated	Perfluorooctanesulfonic acid (PFOS), Perfluorooctanoic acid (PFOA)	U.S. Environmental Protection Agency (EPA). (2019).

2.1.1 Introduction to GLY

Glyphosate (N-(phosphonomethyl) glycine, $C_3H_8NO_5P$) is a polyprotic acid ($pK_{a1}=2.32$, $pK_{a2}= 5.86$, and $pK_{a3}=10.86$) and includes three polar functional groups: carboxylate, amine, and phosphonate [27]. It contains cations from the anionic commercial salt

part, which are of different compositions (e.g., trimethylsulfone, isopropyl amine, and diamine) [28]. GLY exhibits affinity for divalent and trivalent cations such as Cu^{2+} , Cd^{2+} , Al^{3+} , and Fe^{3+} , respectively, with which it can form metal complexes easily [29]. This herbicide is soluble in an aqueous solution (15.7 g L^{-1} at 25°C), but it is insoluble in organic solvents such as ethanol, benzene, acetone, and others. The commercial formulations of GLY use surfactants to increase its water solubility [6] but, once GLY reaches aqueous media, its half-life ($t_{1/2}$) can range from 63 days (shallow waters) up to 70 days (pond water), at concentrations $< 2 \text{ g mL}^{-1}$ and at neutral pH (7.2) [30]. This amphoteric, non-volatile compound has low Henry's law constant ($1.41 \times 10^{-5} \text{ mol/L atm}$ at 25°C), which favors its occurrence in the aqueous phase [31,32].

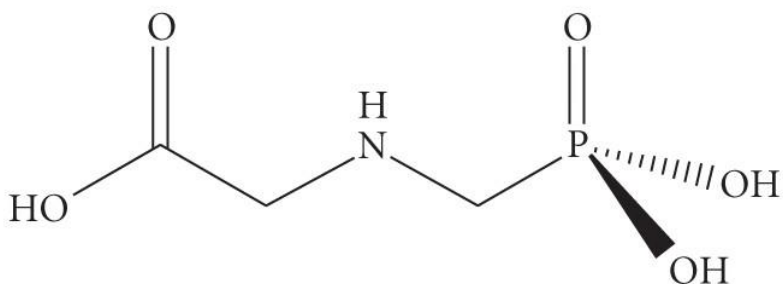


Figure:2.1 The molecular structure of Glyphosate

During spraying and dry-weather conditions ($6\text{--}20^\circ\text{C}$), GLY may not evaporate and may be suspended in dust particles up to 72 hours after its application. In soil, GLY stability occurs with a wide range of sorption coefficients ($K_{oc} = 9\text{--}60,000 \text{ L/kg}$). This condition varies depending on the pH ($3.5\text{--}7.5$) of soil and on di- and tri-valent cations concentrations (Cu^{2+} ; Al^{3+} ; Cd^{2+} ; Fe^{3+} , Mn^{2+} , Ni^{2+}), but it is not linked to soil type (sandy, silty, lime) or to its organic contents [6]. Nevertheless, GLY is sorbed more easily by clay loam soil than by sandy soil, suggesting that minerals in clay are responsible for sorption [33]. GLY adsorption varies directly with organic matter and inversely with pH, which is linked to the physicochemical properties of the soil. The half-life ($t_{1/2}$) of GLY can vary between 100 days for dry soil and 7 days for wet soil, with a biodegradation constant of 0.11 d^{-1} [30].

2.1.2 Usage, Sorption, Functioning, and Fate in the Environment

GLY is a post-emergence and non-selective broad-spectrum herbicide, used to control many perennial and annual weeds. It is one of the most used herbicides for forestry, agriculture, and urban planning in the world, owing to its low toxicity for non-target organisms. The total consumption of GLY used for agricultural and non-agricultural applications reached 126 million kilograms in 2014 [34]. Since its commercialization in 1970, the usage of GLY has increased steadily up to almost 600-700 tons annually and an expected 740-920 thousand tons to be used by 2025 [35]. The primary functional mechanism of GLY is through inhibition of the shikimate pathway that occurs in plants and some microorganisms. GLY inhibits the production of aromatic amino acids in plants during biosynthesis, by inhibiting the enzymes 3-deoxy-D-arabinoheptulosonate-7-phosphate synthase or 5-enolpyruvylshikimate-3-phosphate synthase, which is a precursor for aromatic amino acids and, ultimately, vitamins, hormones, and other essential metabolites for plants [36]. Owing to its enormous use in the environment, many harmful effects of GLY have been reported on plants, animals, and human health such as disrupting the metabolic system of terrestrial and aquatic animals, weakening plant systems, and causing endocrine disruption to humans [7]. In 2015, it was classified as probably carcinogenic to humans by the International Agency for Research on Cancer while authors disagree on this which required further research[37]. For this reason, many countries have banned the use of GLY due to its potential health risks. For instance, GLY concentration in the ground or surface water is in the range of 2-430 $\mu\text{g L}^{-1}$ in the US, higher than in Europe (0.59-165 $\mu\text{g L}^{-1}$). These values exceed the minimum contaminant level goal of 0.7 $\mu\text{g L}^{-1}$ for drinking water. Furthermore, after disposal, GLY-containing herbicides may contaminate the environment [7]. Usage of GLY/ha within Europe has been depicted in Figure 2.2 in comparison to other used herbicides.

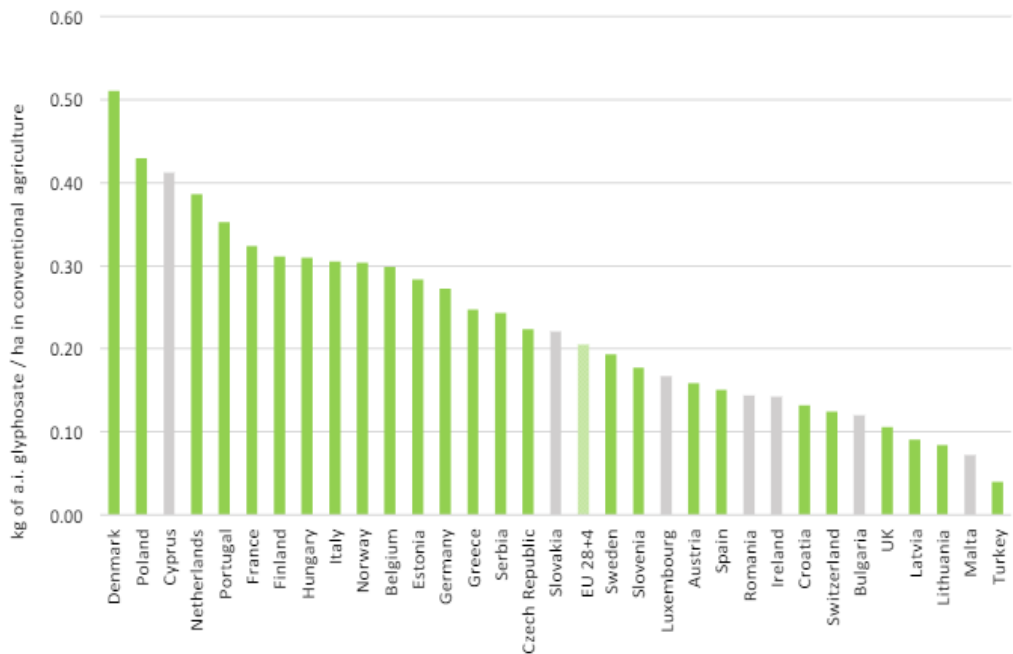


Figure:2.2 Average use of herbicides in the agricultural sector per hectare in the EU 28+3 countries in 2017, with a distinction of GLY vs. other herbicides (Source: ENDURE survey 2019).

Sorption and desorption strongly influence the mobility and bioavailability of GLY in soil due to complexation with soil components [6]. Sorption through soil minerals particularly involves Fe-oxides and Al-oxides. Sorption of GLY is strongly influenced by mineral characteristics (i.e., surface charge and specific surface area), pH, and competition with orthophosphate for sorption sites. GLY is also linked to soil minerals by ligand exchange with hydroxyl groups or coordinated with water molecules on mineral surfaces, or linked through specific sorption as monodentate or, less commonly, bidentate ligand. The sorption complexation of orthophosphate rather occurs through bidentate complexation, typically with higher affinity than GLY. Consequently, orthophosphate competes with GLY during sorption and desorption by occupying active sites on mineral surfaces [38]. Furthermore, more negative charge accumulation on the mineral surface due to orthophosphate sorption makes soil less susceptible to sorption of negatively charged GLY anions. Thus, soils with orthophosphate saturation are not expected to retain excess unbound GLY, which

ultimately leaches out to surface water and groundwater and poses further environmental concerns [39].

After spraying, GLY can directly enter the environment with, for instance, a rainwater concentration of up to 0.48 g L^{-1} [6]. Then, it reaches target organisms through foliar contact. The large roots of some weeds transport GLY into deep soil layers without degradation, and a fraction of GLY is absorbed into clay and organic matter, ultimately accumulating in soil over time. Meanwhile, GLY can be transported due to runoff. So, due to its extensive use, GLY has been detected frequently in the aquatic environment. Synthetic industries and some textile industries are also using GLY as raw material, thus they can also contaminate the aqueous environment via wastewater [40]. Major industrial synthesis methods for GLY production include diethanolamine, hydrocyanic acid, and glycine processes, which produce large amounts of wastewater. To get 1 ton of GLY, almost 5-6 tons of crystallized mother liquor is produced with $\sim 1\%$ GLY, 1-4% formaldehyde, and other byproducts [41]. Nanofiltration is used to recover most of the GLY from the mother liquor. Still, almost $200\text{-}3000 \text{ mg L}^{-1}$ GLY has been found to remain in the nanofiltration permeate in China. It is reported that, in industrial effluents, GLY concentration reached up to 2560 mg L^{-1} [41].

2.1.3 Eco-toxicological effects of GLY

2.1.3.1 Aquatic animals

The aquatic ecosystem is a critical part of our planet. GLY and its primary metabolite, Aminomethylphosphonic acid (AMPA) have been found in many plants and animals (especially fish) due to the accumulation in water bodies [42]. This is a consequence of large-scale use of herbicides containing GLY [43]. Both GLY and AMPA are water soluble and can persist in aquatic bodies for several weeks. It is reported that GLY can cause the death of several aquatic species including fish, birds, and herpetofauna [44]. Tsui and Chu were the first pioneers to conduct experiments to assess the occurrence of GLY in the aquatic environment. They investigated how GLY can affect crustaceans *Acartia tonsa* and *Ceriodaphnia dubia* as well as other organisms like

algae, bacteria, and protozoans. Their findings showed that *A. tonsa* among others showed the lowest lethal concentration (concentration of GLY in the air to kill 50% of test subjects in the air) i.e., LC50 of 1.77 mg L⁻¹ making it the most sensible to GLY [45]. Recently, Maraes et al. reported that zebrafish (*Danio rerio*) exposed to GLY and Roundup Transorb® had up to three times higher levels of adenosine triphosphate binding capacity. Furthermore, when the brain of zebrafish was exposed to Roundup Transorb®, it was found not to enhance the activity of some proteins (ABCC: Proteins that are transporters in living organisms) that were found to be activated after exposure to GLY [46].

2.1.3.2 Human health

Some significant properties of GLY involve biodegradation, quick soil sorption, and non-acute toxicity to organisms except for its intended recipients. However, it has been reported that GLY enhances the risk of cardiovascular issues, leaky gut syndrome, digestive disruption, autism, cancer, as well as hormonal and immunological dysfunctions [47]. Von Ehrenstein et al. reported that parents exposed to GLY have higher risk of autism disorder in their offspring compared to women who have not been exposed to GLY previously [48]. In another review article, it has been concluded that GLY has genotoxic and cytotoxic effects that rely on dosage. Moreover, it can increase oxidative stress, impair different cerebral processes, interrupt the estrogen system and, in some cases, it could lead to human cancer [49]. In recent times, Spinaci and coworkers investigated and compared the effect of GLY and its commercial formulation Roundup Transorb® on mammalian sperm. They measured the acrosome, motility, integrity, mitochondrial activity, and viability after half an hour of incubation at 37°C. Starting from 360 g/ml, Roundup Transorb® substantially reduced total and progressive motility, acrosome integrity, viability, mitochondrial activity, and the percentage of living spermatozoa with intact mitochondria [50].

2.1.3.3 Plants

Various studies have reported how GLY harms plants [44,51,52]. Typically, GLY binds and inactivates an enzyme that is required in shikimate pathways, blocking the production of essential amino acids [53]. A similar metabolic cycle provides various phenolic chemicals that are vital for plant immunity. Plants become more vulnerable to many soil-borne diseases due to the interference of GLY in the production of defensive chemicals [54]. Consequently, it may be stated that regular crops exposed to GLY are more susceptible to diseases. In most cases, diseases have been linked to excessive spraying, and it has for instance been found that GLY spraying was the primary cause of diseases like fusarium head blight in agronomic crops [55]. In addition, sublethal GLY concentrations sometimes produce an effect after a year or two on perennial crops, and the effect may last for two or more years [56]. GLY might also increase the risk of infections in plants by reducing their vigor and general growth, and by altering soil microbiota that influences the availability of nutrients required for disease resistance and, ultimately, physiological activity [57].

2.1.4 Recent Regulation and Policy related to GLY

The use of GLY dates to many years ago, but in the last 2 decades there have been political and health controversies regarding use indications and impacts on the environment. For instance, in 2015, GLY was classified as potentially carcinogenic for humans by the Agency for Research on Cancer (IARC) in group 2A. This claim is based on adequate evidence that it causes cancer in experimental animals, but on very little evidence that it causes cancer in humans. In the end, it should also be considered that pure GLY might not be equal to its mixed formulations. At the same time, the European Food Safety Agency (EFSA) claimed that the substance is not likely to cause cancer or to be genotoxic in humans. Some specialists from Member states, especially from Sweden, described neither any epidemiological data nor any evidence of cause and effect occurrence of cancer due to GLY exposure in humans. However, they proposed an idea to set a limit known as the acute reference dose of 0.5 mg/kg of body weight, an acceptable operator exposure level (LAEO) set at 0.1 mg/kg of body weight per day, and the acceptable daily intake (ADI) for consumers at 0.5 mg/kg of

body weight. In 2016, the Food and Agriculture Organization (FAO) and WHO concluded that it is questionable that GLY causes cancer and is a potential risk to humans. In the same year, in early August, the European Commission implemented regulations 2016/1313 that set the conditions for using the substance. After this, several plant-protecting products containing GLY, conditions, and its use in frequently populated areas such as green areas, gardens, parks, sports fields, recreational areas, within school facilities, and beside health facilities were modified by the Ministry of Health. Also, GLY was prohibited for use pre-harvest and measures were taken to protect groundwater and to avoid GLY use for non-agricultural purposes in soils containing 80% sand or more. In last regulations 2022/2364, the European Commission decreed to extend GLY use for one year, and the extension was renewed until December 15, 2023 [58].

2.1.5 Introduction to Aminomethylphosphonic acid (AMPA)

AMPA is a breakdown product resulting from phosphonates degradation (Figure 2.3). It can be a degradation product of amino-polyphosphonates in water or a metabolite in GLY biological degradation [59]. AMPA has been reported to occur extensively in air and in surface waters, agriculture areas, sediments, and shallow groundwater at a depth of 2m at the edge of the streams, as well as less commonly in deep groundwater. There are several AMPA sources like industrial, agricultural, and urban. Proof of the presence of AMPA has been found in wastewater-influenced streams depending on the hydroclimatic circumstances. Domestic and industrial phosphonates are other sources of AMPA [60].

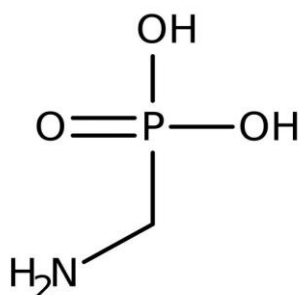


Figure:2.3 Structure of Aminomethylphosphonic acid (AMPA)

2.1.5.1.1 Toxicity

To date, no epidemiological reports on AMPA exposure have been found for water. Limited studies from *in-vitro* data are available, regarding its toxicity to animal cells and humans [61]. The metabolic nature of AMPA may lead to questions as to its probable formation in the body, as it is unusual that glyphosate degradation to AMPA happens in the human body [62,63]. There is a lack of deep knowledge about AMPA formation from phosphonates in the human body. Kwiatkowska et. al. showed that AMPA imparts slightly toxic effects on human erythrocytes: 0.05 mM AMPA induces hemolysis while, above 0.25 mM, AMPA can produce reactive oxygen species and enhances the level of methemoglobin in blood [64]. Regarding lymphocytes, it is reported that 1.8 mM AMPA has clastogenic effects (i.e., genetic mutations, chromosomal aberrations, cellular damage, cancer development, cancer etc.). Moreover, above 2.5 mM AMPA, Hep-2 DNA suffers substantial damage. Conclusively, Benachour and Seralini provide evidence that AMPA causes umbilical membrane cell damage and, sometimes, neonatal or embryonic cell death [60].

Although AMPA has been investigated to a lesser extent than GLY, Reddy et al. reported that chlorophyll biosynthesis was affected by AMPA leading to reduced plant growth, which means that AMPA can also be translocated to various plant tissues [65]. AMPA is also called phytotoxin, which can enhance the indirect effects of GLY on physiological processes. Moreover, due to its similarity with glycine, AMPA competes with it in biological pathways and sites, disturbing chlorophyll synthesis and, ultimately, impacting photosynthesis processes [66]. Plants exposed to AMPA exhibited decreased production of serine, glycine, and glutamate. According to reported data, AMPA seems to be highly toxic to aquatic organisms [67].

2.2 Introduction to PFAS

Among POPs, per- and polyfluoroalkyl substances (PFAS) are compounds that have been commonly used in industrial and commercial products since the 1940s. Described as “forever chemicals”, PFAS contain a polar head group and a fluorinated alkyl chain that give them surfactant-like properties. PFAS are resistant to water and

oil and can endure extreme temperatures. They can enter the environment in many ways, involving point source contamination from the production unit [68], effluent from wastewater treatment facilities, aqueous firefighting foams used at public or military sites, and landfill leachates [69]. In the past 30 years, many studies have reported the presence of PFAS in several environmental compartments such as rainwater, surface water, groundwater, drinking water, manufactured goods like cosmetics, food packaging, and agronomic foodstuffs [70]. Due to the physico-chemical properties of PFAS, they have minimal potential for excretion which ultimately produces biomagnification and bioaccumulation in wildlife and humans. Their persistence and ubiquity, in addition to adverse health effects posed by PFAS, justify the need to monitor and control these chemicals in food products, environmental compartments, and drinking water. PFAS can have prominently negative effects on wildlife and humans. Unintentional exposure to PFAS has been reported to cause cancer, decreased liver and immune functions, elevated cholesterol levels, and significant birth abnormalities. Under the Stockholm Convention, these findings related to health have led to the phase-out of long-chain PFAS [69]. Following this restriction, new PFAS substitutes were introduced that are easily degradable compared to previous ones. Substitutes contained smaller fluoroalkyl chains, and structures with chlorinated carbons or ethers linkages (C-O-C) instead of all fluorinated carbons.

2.2.1 Physio-chemical Properties of PFAS

Transport, environmental fate, and mechanisms are critical parameters connected with the physio-chemical properties of PFAS. The melting and boiling points of pure PFAS are dependent on their occurrence as liquid, solid, or gas at ambient temperature [71]. Most PFAS are solid (powder or crystalline) in atmospheric conditions, but shorter PFAS with chains in the range of C₄-C₆ occur in liquid form. For instance, the melting points of PFOA and Perfluorobutanesulfonic acid (PFBS) are 45–54 °C and -21°C, respectively [72]. How a PFAS behaves in the environment often depends on its density in the liquid form at ambient temperatures [73]. For now, a few of the PFAS compounds have been studied well, e.g., perfluorooctane sulfonate

(PFOS), perfluorinated carboxylic acids (PFCA), and fluorotelomer alcohols have been experimentally studied, which provided evidence for PFAS solubility in aqueous media [74].

Apart from truly solubilized molecules, PFAS also form micelles and hemi-micelles, which might be accounted in water solubility. According to laboratory results, the solubility of PFOS decreases in water with an increase in salt content [75]. These compounds form micelles because they have polar head groups (carboxylic) as well as tails (long fluorinated chain) that behave differently in water, and aggregate to form a micelle when present above a certain concentration known as critical micelles concentration (CMC). They can also form other aggregates such as semi-micelles or hemi-micelles [76,77]. Many studies have reported that, in groundwater, micelles occur at quite a lower concentration than the CMC because of interaction with soil co-contaminants and particles in soil matrices [78]. These assemblies can influence the transport and partition at the water-air interface. The carbon-fluorine (105.4 kcal mol⁻¹) bonds are the main cause of the persistence of PFAS in the subsurface. Fluorine due to its highest electronegativity ($\chi=3.98$) forms the strongest bonds with carbon in organic chemistry. Three lone pairs at the fluorine atom are held together closely due to strong electronegativity, and polarity stabilized the C-F bond. Consequently, PFAS compounds show low pKa values and low reactivity, with high chemical and thermal stability. These unique C-F bond properties can be understood using stereo-electronic or electrostatic-dipole interactions with neighboring lone pairs or bonds. Due to the low polarizability of fluorine, hydrophobic and lipophilic interactions produce surfactant-like properties in PFAS. However, these properties are not shared by all PFAS [69].

Currently, some of the properties of PFAS are not well known i.e., dissociation constant, stability, or rate constants. PFAS compounds possess several functional groups including carboxylates, amines, phosphates, sulfates, and sulfonates (figure 2.4) [79]. Many factors like transport and fate are affected by these functional groups involving dissociated and undissociated forms. The state (i.e., anionic or undissociated

acidic) of PFAS can affect the bio-accumulative potential and partitioning behavior. Apart from very acidic pH conditions, PFCA is negatively charged due to low acidic dissociation constants (pKa) [79,80]. Similarly, PFOA dissociates in water into a hydrogen ion and perfluorooctanoate. PFAS molecules can generally occur as positively charged cations, negatively charged anions, or zwitter ions [81]. Ultimately, PFAS can be divided into four groups based on functional groups: a) cationic (basic functional group); b) zwitterionic (contains two or more functional groups with at least an anionic and a cationic form); c) anionic (contains acidic functional groups), and d) non-ionic (does not dissociate) [82,83]. Cationic PFAS are supposed to have different transport behavior than anionic PFAS.

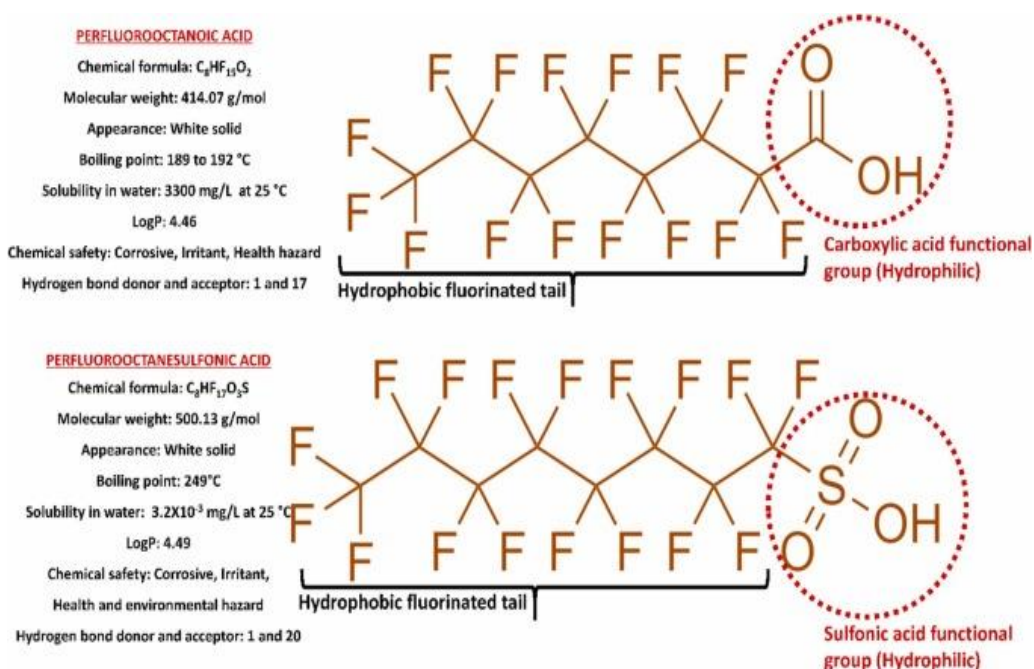


Figure:2.4 Molecular structures and physicochemical properties of PFOA and PFOS [83].

2.2.2 Sources of PFAS Their Environmental Occurrence

To date, more than 4,000 different PFAS have been produced by humans; hundreds of these PFAS have been found in environmental samples. Figure 2.5 presents the main

sources of PFAS contamination along with potential environmental effects. Point and non-point sources are the main routes of PFAS to environmental compartments. Diffuse sources of unknown location/origin mostly refer to non-point sources, such as degradation of precursor compounds, precipitation, surface runoff, atmospheric intrusion of volatile PFAS, etc. Point sources are stationary and discrete, such as landfills, firefighting training locations, wastewater treatment units, manufacturing, industrial plants, etc. Aqueous film-forming foams (AFFFs) used in firefighting operations have a long history of being implicated in PFAS pollution of water bodies in the United States [84]. The US military is the primary user of AFFFs; among the specific locations of these pollutants are airports and military bases. Chemically stable per- and polyfluoroalkyl substances (PFAS) can travel great distances after being released into environmental compartments and undergo processes of leaching, precipitation, partitioning, and deposition [85]. As a result, there are reports of their worldwide occurrence in a variety of environmental media. Following transport, the PFAS travel through many environmental compartments, including the air, soil, and water, where they may be bioaccumulated by local plants and animals. The most consistent sources of per- and polyfluoroalkyl substances (PFAS) are predicted to be air and landfill leachates, with typical values of 10^{1-2} pg/m³ and 10^{0-2} ng/L, respectively [86]. Worldwide, PFAS have been discovered in aquatic, plant, and animal habitats. For instance, freshwater fish from throughout the United States are commonly reported to contain PFAS. Between 2013 and 2015, the US EPA analyzed fish, and the median PFAS level was 11,800 ng/kg [87].

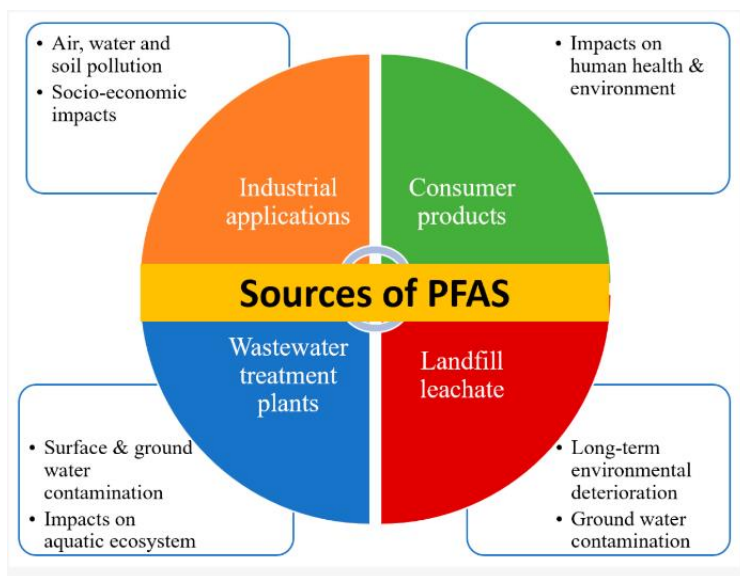


Figure:2.5 Principal PFAS sources and possible effects[88]

2.2.2.1 Exposure of Humans through Different Routes

PFAS often fall into the category of chemical compounds that are soluble in water and have a variety of uses. Actually, PFAS are composed of both hydrophobic (fluorinated carbon chain) and hydrophilic (functional group) moieties [89]. PFAS solubility is contingent upon functional moieties and chain length, both of which dictate their environmental prevalence. Longer-chain PFAS dissolve less readily in water and vice versa. While PFAS with long chains ($C > 8$) typically accumulate in sediments and fish tissues, those with short chains ($C < 8$) are typically found in surface water. Depending on the conditions of exposure (such as the amount, timing, and direction of exposure), they may have a wide range of detrimental effects on health. The industrial production of fluoropolymers, textiles, paints, food packaging, building construction, medical equipment, printing inks, and firefighting foams are the main sources of PFAS release into the ambient air. Nevertheless, consumer goods including makeup, food processing and storage supplies, and home and personal care items all play a part in the extra PFAS emissions into the atmosphere. In the end, air emissions are further increased by the recycling and incineration of items containing PFAS. By

dispersing dirty sludge, biosolids, and recycled effluent for agricultural use, municipal wastewater treatment plants indirectly encourage the dispersion of PFAS into soil, contaminating other environmental compartments (both water and soil) [88]. Even with tight landfill restrictions, the application of these contaminants during landfilling may result in leakage into soil and eventually into groundwater. Figure 2.5 shows the many ways humans are exposed to PFAS as well as their harmful impacts. In this section, the specificities of human exposure to PFAS are extensively illustrated. In light of these facts, it is unacceptable that PFAS have permeated the ecosystem and turned into such a widespread source of environmental pollution. Because of contamination through a variety of human exposure channels, including food supplies, milk, vegetables, fruits, cereals, indoor air, and drinking water sources, they are negatively impacting human health [88,90].

2.2.2.1.1 Exposure from Drinking Water

According to a thorough study done in Tarragona, Spain, drinking water is the primary source by which humans are exposed to PFAS [91]. Dietary intake comes in second. Groundwater, an important source of drinkable water in many regions, is severely impacted by PFAS contamination [92], which eventually has an impact on animals and people who drink this contaminated water. The most likely potential sources of PFAS contamination in Pennsylvania surface water, according to a research that sought to determine the possible sources, were electronic manufacturing sites and water pollution control facilities. Potential sources of both long- and short-chain perfluoroalkyl acids (PFAAs) in industrial wastewater treatment plants include both the influent and effluent [93]. There was also a report of an increase in PFAA concentration following treatment. Due to their high solubility in water, some PFAS accumulate in rivers and seas, endangering fish and aquatic life. In addition to polluting groundwater reservoirs, these PFAS have the potential to contaminate drinking water and endanger public health. An unexpected discovery was made about a municipal waterworks in Ronneby, Sweden, which had high levels of PFAS (>10,000 ng/L in outgoing potable water) [5]. A military airfield that has been utilizing AFFFs

since the mid-1980s was the source of contamination. Following the publication of these results, the contaminated waterworks were promptly shut down and replaced with a water supply from other municipal waterworks but unknowingly, for decades, about one-third of the local population had been exposed to PFAS poisoning. Even six months after the exposure, a significant level of PFAS has been found during the biomonitoring of Ronneby residents [88]. In conclusion, food and drinking water are two of the main ways that PFAS enter the human body [94].

2.2.2.1.2 Exposure from Soil and Vegetation

Industrial waste, polluted sludge, and foaming agents release PFAS contaminants into the soil matrix, surface water, and groundwater; PFAS are then absorbed by plants and consumed as food. The majority of PFAS found in landfill leachate and industrial effluent also contaminate the nearby rivers, posing a serious concern to the ecosystem [95]. The use of biosolids as fertilizers in agriculture and contaminated surface waters or groundwater for field irrigation are the primary sources of PFAS contamination in soils. Shorter-chain PFAS accumulate in the leaves and fruits of absorbing plants, while longer-chain PFAS compounds accumulate in the roots [96] and are subsequently assimilated into food webs. According to a recent study, field workers may be exposed to perfluorooctane sulfonic acid found in soil at manufacturing and storage locations[88].

2.2.2.1.3 Exposure during Occupational Activities

Because of the harmful consequences of PFAS on health, occupational exposure is a serious concern. High serum amounts of PFAS are associated with specific jobs, including professional ski waxers, firefighters, and workers in fluorochemical plants. Polyfluorinated alkyl compounds (PFAS) are unique chemicals that improve product quality and performance, which is why they have been used in electronic devices for a long time. But the presence of PFAS in electronics also increases the risk of PFAS exposure for people who handle and recycle e-waste through ingestion, inhalation, and skin absorption. These scavenging and recycling processes are also among the ways that PFAS are emitted. Furthermore, because samples taken from e-waste

collection, processing, and disposal sites were contaminated with per- and polyfluoroalkyl substances (PFAS), these areas have been recognized as possible sites of PFAS exposure [97–99]. Another study found that professional ski waxers and firefighters had higher serum PFAS levels when compared to serum PFAS levels of the general public exposed to PFAS-contaminated drinking water. The study also examined serum PFAS levels reported in various occupations. However, research on worker exposure to PFAS has only looked at employees at fluorochemical plants that produce PFAS [100]. In order to protect workers from the harmful health impacts of PFAS exposure, more studies on exposures across many industries and occupations is required for future recommendations.

2.2.2.1.4 Exposure to PFAS through Consumer Products, Dust and Indoor Air

When PFAS from household goods migrate into food, indoor air, and dust, the process can lead to human exposure [88]. It has been stated that PFAS are present in papers, carpets, upholstery, clothing, food, building supplies, paints, cleansers, polishes, impregnation agents, and ski waxes. Grease-resistant food packaging may allow PFAS to penetrate into food, increasing dietary exposure [101]. Moreover, numerous types of precursor compounds found in consumer goods, including powders, sunscreens, and other cosmetic products, have the ability to biotransform into PFAS that subsequently build up within the human body [102]. A volunteer's skin was treated with PFOA combined with sunscreen in an experimental study; this method showed that PFOA can be significantly absorbed by humans through transdermal absorption. A other investigation also demonstrated PFAS cutaneous penetration. The body may accumulate a greater amount of PFAS with intermediate hydrophobicity due to their advantageous skin penetration and unfavorable urine excretion [103]. When it comes to outdoor air pollution, the main sources of PFAS emissions into the air are manufacturing plants and work facilities. As a result, the surrounding ground and surface waters are heavily contaminated. Computational research suggests that emissions of GenX (2.5% of all emissions) and PFAS (5% of all pollutants) can readily settle within a 150 km radius around industrial locations [104]. Determining the relative importance of the many exposure pathways is therefore essential to

understand the causes of progressive blood alterations and project exposure risks into the future.

2.2.3 Toxicity of PFAS

Bioaccumulation and toxicity of PFAS have been much investigated, but the toxicity of PFAS in the environment as mixtures is still poorly known [69]. Most extensively investigated PFAS are perfluorooctanoic acid (PFOA) and perfluorooctane sulfonic acid (PFOS) [105–108], because of their wide use, stability, and persistence in the environment [109]. Moreover, they are the stable end products of several other PFAS precursors. Both PFOA and PFOS fall under the subclass of PFAS known as perfluoroalkyl acids (PFAA). Until May 2019, PFOA was not included among the persistent organic pollutants but since then it has been included in the list. PFOS and PFOA have long residence times of over 5 and 3.5 years, respectively, in human bodies. New research on the toxicity of PFOA and PFOS also referred to as “legacy PFAS”, plus replacement molecules are also termed as “alternative PFAS”, have shown that according to computational models, epidemiological studies in humans, cell, and animal studies, the alternative PFAS continue exhibiting similar toxicity and endocrine disruption properties as legacy PFAS.

2.2.3.1 Ecological Toxicity

Effects of PFAS contamination on animal and plant health have been deeply evaluated in areas where point source pollution is a recognized concern. It is reported that plant exposure to PFOA results in a reduction of shoot growth for *V. radiata* and *O. sativa* when grown in PFOA-contaminated soil (100, 300mg/Kg dry soil respectively) [110]. Lower seedling sizes were also noticed in the study. Algal soil biomass was also considerably reduced for *C. infusion* and *C. reinhardtii* in 50 and 700 mg/kg dry soil, respectively. Reproduction rates of nematodes were reduced as well after one-day exposure to soils contaminated with 300 mg/kg or more compared to control [110]. Plant phytotoxicity and uptake of PFOS and PFOA (5000 and 500 ng/L) were investigated in lettuce for exposure of over 28 days, which did not provide any data

on biomass or phenotype changes. The accumulation of PFOA was about 4.0-4.3 times higher than PFOS [111].

2.2.3.2 Animal Toxicity

Apart from environmental models, the impacts of PFAS on animals have been studied. Metabolomics was adopted in a study on *Ruditapes philippinarum* clams to compare the effect of PFOA and PFOA alternative, the difluoro [2,2,4,5-tetrafluoro-5-(trifluoromethoxy)-1,3-dioxolan-4-yl]oxyacetic acid (C₆O₄), on marine species [112]. Haemolytic size and cell count decreased due to the presence of both pollutants. PFAS alternative caused biomarker fluctuation for gills and haemocytes, and it affected DNA more than PFOA at lower concentrations. Two other PFAS, sodium p-perfluorooxobenzene sulfonate (OBS) and 6:2 chlorinated polyfluorinated ether sulfonate (6:2 Cl-PFESA) were also tested at a concentration of 1 µM in comparison to PFOS on zebrafish [113]. Prominent oxidative liver stress was observed in zebrafish by PFOS as compared to both OBS and 6:2 Cl-PFESA. However, all three PFAS exhibited gut disruptions, as well as anti-inflammatory in addition to immune-related gene expression. Early studies on mice and rats showed significant impacts on the kidney, liver, and spleen as well as other organs. It was observed that, by using perfluoro alkane sulfonyl fluorides (PFASF), a precursor class of PFAS inoculated into rat liver, reduction to form stable PFAS became operational upon oxidation of proteins containing cysteine and glutathione [69].

2.2.3.3 Human Toxicity

Humans can't be intentionally exposed to study the toxicological effect of environmental contaminants, thus the information related to toxicity is deduced from computational (in silico), in vivo, in vitro, and epidemiological evaluation. Computational modeling is usually a technique that is designed in a way to minimize the contaminant risk to understand the effect on human health without the involvement of invasive sampling of human subjects [69]. Different parameters were evaluated including adsorption, residence time, and transport of two PFOS and two novel PFAS alternatives, OBS and 6:2 Cl-PFESA, using molecular dynamics simulations

(MDS) on phospholipid bilayers. MDS can be chosen to predict the interaction of PFAS compounds with biomolecules at the atomic scale with very fine temporal resolution. Energy barriers were measured for these three compounds and were low, so they could enter effortlessly into the bilayer of the cell membrane. After entering, the interaction between cationic N-atoms in PFAS and the sulfonate head group led to the blockage of the bilayer head group and altered bilayer orientation [114].

The impact of PFAS exposure on early child development and childbirth has been evaluated in three epidemiological studies. In the first study, the weights of newborns and mothers were evaluated as well as parental exposure to PFAS. Higher concentrations were observed in old, first-time mothers, while all PFAS (PFOS, PFOA, and 6:2 Cl-PFESA) were found in all mothers. A very positive correlation was found between both 6:2 Cl-PFESA and PFOS and the body mass index, which is a common correlation for various lipophilic contaminants [115]. In addition, ponderal indices and birthweights of newborns were lower in mothers who were exposed to PFOS. Moreover, the PFAS substitute 6:2 Cl-PFESA has been detected in metal plating workers and Chinese surface waters [116].

Another evaluation comprising 1240 mother-child pairs about the developmental impacts of PFAS on children of up to 7 years of age was performed [117]. Both PFOS and PFOA were detected in all samples of maternal plasma, while perfluorohexanoic acid (PFHxA) and Perfluorononanoic acid (PFNA) were found in the majority of samples, almost 96 and 99% respectively. Differently from most of the other studies on human subjects, the mentioned study revealed that there is no significant effect of PFAS on child development from 14 months to 7 years of age. A few studies exhibited some links between exposure and verbal skills as well as memory at the age of 4-5 years, but results were statistically not significant. Controversial studies are found in the literature when a small sample size is adopted. Thus, in epidemiological studies, unfavorable interferences can lead to skewed results. In addition to recent discoveries on the toxicity of PFAS, there is an urgency and need to isolate, control, and degrade these persistent environmental pollutants [69,117].

2.3 Strategies for POP Treatment

Typical wastewater treatment plants are not designed to process POPs. Ultimately, any POPs that encounter wastewater plants usually end up in treated waters after the plant. As discussed earlier, most the POPs are resistant to conventional oxidation and reduction processes due to their persistence, stability, and conversion into harmful by-products. Recently, some POPs removal technologies have been described, including adsorption, photolysis, photocatalysis, Fenton and Fenton-like systems, ozonation, sulfate radical-based processes, hydrated electron-based degradation, electrochemical oxidation, etc.

2.3.1 Adsorption

Adsorption is a surface phenomenon where substances become attached to the outer layer of a material. In general, it involves atoms, molecules, and even ions from a liquid, solid, or gas which are linked to the surface. This method of removal is adopted in many treatment facilities because of its lack of toxicity, great efficiency, and low cost [7]. For instance, several studies for GLY as well as PFAS removal through adsorption from environmental matrices have been conducted. Many materials like biochar, zero-valent iron (ZVI), clay compounds, adsorption membranes, resins, activated carbon, etc., have been used as potential adsorbent mediums. To extract GLY from the medium, different processes involve different interactions between the adsorbent and the pollutants including molecular interactions among entities in the system or diffusion through pores having different volumes (micro, meso, and macro) or sizes [118]. Furthermore, GLY removal can also occur through electrostatic interaction between the adsorbent system and GLY molecules in the form of metal-based complexes from an aqueous solution. A typical example involves a zirconium-based metal-organic framework (Zr-MOFs), which can be used for the adsorption of GLY from an aqueous solution. In this study, Tao et al. removed GLY in the presence of other pollutants like acephate, sulfamethoxazole, methyl parathion, sulfanilamide, sulfamethazine, etc. Electrostatic interaction, hydrogen bonding, and Zr-phosphate bonding were responsible for GLY removal due to adsorption from the aqueous solution[119].

Biochar and activated carbon, typically two adsorbents having porous structures and high efficiencies have been useful for many environmental applications, especially for GLY removal [120]. For instance, waste newspaper-activated carbon (WNAC) has been employed to achieve GLY removal from water. Three different adsorption models including Langmuir, Freundlich, and Redlich-Peterson isotherms were used to check for GLY removal efficacy. The best-suited model was Langmuir adsorption isotherms and WNAC was reported to have an optimal performance of 48.8 mg L^{-1} at 2.5 pH for GLY removal. In an additional study, Herath and Wickramasinghe investigated the steam-activated biochar generated from rice husk at 700°C , for GLY removal from an aqueous system. Batch adsorption using Elovich, Langmuir, and Freundlich isotherms was used to check adsorption kinetics. Parameters including pseudo-first-order (PFO), pseudo-second-order (PSO), pH, reaction time, and GLY dosage were also investigated. Maximum GLY removal was observed at pH 4 and removal did not increase with increasing pH.

Resin's surface chemistry and porous structure favor GLY adsorption in aqueous systems. Jia et al., [121] examined the potential of resin for GLY removal by producing a composite resin by crosslinking nanoiron oxide with polystyrene. Lower pH favors GLY removal through adsorption and PSO was shown to be the best fit for removal kinetics. Chen et al., [122] reported about the thermodynamics and kinetics of GLY removal using resin D301. The optimal removal was as high as 833 mg/g at 318.15K . The Langmuir adsorption model suggested formation of a monolayer using resin D301. Also, the sorption mechanism was exothermic as examined by experimental parameters that are governed by intricate mechanisms, which are neither purely physical nor chemical. Adsorption of GLY on resin D301 followed a PSO kinetic model with an ordinary activation energy of 83.11 kJmol^{-1} .

Considering PFAS removal through adsorption, activated carbon and ion-exchange resin have been reported. Ochoa-Herrera and coworkers [123] studied various adsorbents for PFOS removal, i.e., high silica zeolite NaY, activated carbon, and anaerobic sludge. Among these adsorbents, activated carbon exhibited maximum

adsorbent affinity towards PFOS. Besides, they also investigated the adsorption of PFOA, PFOS, and perfluorobutanesulfonate (PFBS) on activated carbon. They discovered that PFOS has a stronger affinity towards activated carbon than PFOA and PFBS. Apparently, the replacement of the sulfonic by a carboxylic group and reduced fluorocarbon chain length led to weaker interaction with activated carbon for adsorption. In addition, Saeidi et al., [124] studied the performance of activated carbon felts (ACF) for PFOA and PFOS removal. They observed a higher affinity of defunctionalized ACF towards PFAA due to the combined effect of electrostatic attraction and hydrophobic interactions, between PFAA anions and positively charged adsorbent sites. They discovered the adsorption behavior on different ACFs was considerably affected by the surface chemistry due to the cation/anion exchange capacity, oxygen content, and point of zero net proton charge.

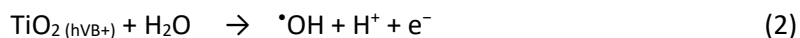
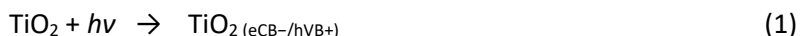
The adsorption strategy is extensively used for wastewater treatment. It is adopted because of simplicity, cost-effectiveness, and ease of operation. Regarding POPs removal efficiency and relevance through adsorption, there are still numerous limitations and challenges that should be considered. First, acidic conditions for adsorbents may be required for maximum removal of POPs from the aqueous environment. These acidic conditions might affect the water treatment, and acidic-waste release to the environment might be risky to human and animal health. Also, the disposal of residues from the adsorption process is still a major challenge and it needs further investigation. Thus, additional efforts are needed after adsorption, and attention must be paid to secondary pollution during these treatments.

2.3.2 Photolysis and Photocatalysis

Photolysis and heterogenous catalysis (photocatalysis) are two processes to degrade different persistent pollutants. Photolysis is a technique in which UV or Visible light is utilized to degrade various pollutants directly, by breaking bonds between atoms or molecules. In alternative, the photolysis of pure water can yield strong oxidant species like $\cdot\text{OH}$ that interact with pollutant molecules in water. It is well known that the most abundant source of energy is solar energy, which is eco-friendly, produces

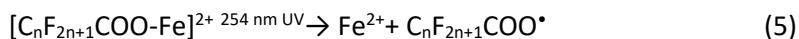
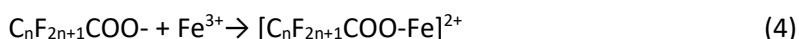
no emissions, requires no fossil fuels during utilization, and yields no greenhouse gases. However, according to the nature of pollutants, the nature of light is also important, i.e., only a limited UV range can be used for PFAA degradation.

Heterogenous photocatalysis is a process where the most extensively used semiconductor catalyst is titanium dioxide (TiO₂). It absorbs light radiations or photons with energy equal to or greater than the band-gap energy ($h\nu \geq E_g$), which in the case of TiO₂ is 3.2 eV for anatase and 3.05 eV for the rutile phase. Absorption of photons causes electrons to exit from the valence band (VB) and migrate to the conduction band (CB) leaving a VB hole or vacancy bearing a positive charge. These electron/hole (e_{CB^-}/h_{VB^+}) pairs, by which redox reactions are carried out, are thus generated (eq. 1) and holes (h_{VB^+}) are strong oxidizing agents, which carry out water oxidation to form $\cdot OH$ radicals or interact directly with pollutants molecules on the catalyst surface (eq. 2). In contrast, e_{CB^-} reacts with electron receptor species such as O₂ to form superoxide radicals, which is also a mild oxidant species (eq. 3) or a precursor of oxidants.

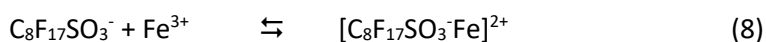


Chen et al., [125] discovered PFOA degrades quite slowly by direct irradiation under 254 nm UV light, and degradation can be considerably enhanced by photolysis under 185 nm because PFOA has strong absorption at 190-220 nm. This issue makes decarboxylation easier under 185 nm UV light (Figure. 2.6). Jin et al.,[126] investigated the fast degradation of PFOS under 185 nm radiation in anaerobic alkaline conditions. They discovered the degradation of PFOS is enhanced by anaerobic alkaline compared to aerobic neutral conditions. Also, the branched PFOS isomers exhibited faster degradation rates than linear PFOS, indicating the possibility of involvement of hydrated electrons as active species for PFOS degradation. In addition, a few fluorinated intermediates were detected and quantified. Direct

photolysis can be a possible degradation pathway under 185 nm UV, but this is not applicable while using solar energy. To mitigate the issue, researchers introduced some reactive reagents to attain higher efficiency and a broader absorption spectrum. Hori and coworkers [127] introduced trace amounts of ferric ions and improved the degradation of PFAAs under 254 nm UV light. The results were interesting considering rate constants which were 3.6-5.3 times higher compared to direct photolysis alone. This can be explained by photo-redox reactions between oxygen, PFAAs, and ferric/ferrous ions through complex formation between ferric ions and PFAAs (Eqs. 4-7).



Wang et al., [128] also investigated PFOA degradation in the same way and found initial ferric ions concentration affects the process. Apart from ferric ions they also introduced cupric, magnesium, zinc, and manganese ions, etc. They discovered that Cu and Zn ions improved the degradation rate of PFOA. Jin et al. found the addition of ferrioxalate ions enhanced the photodecomposition rate of PFOS by 50 times compared to direct photolysis. From scavenger experiments, they deduced that molecular oxygen could be involved in the defluorination process without hydroxyl radicals ($\bullet OH$). Moreover, PFOS decomposition can't be governed by $\bullet OH$ due to the inertness of these radicals on PFOS, they can just accelerate defluorination. The authors suggested that the key step during PFOS degradation was ligand-to-metal charge transfer (Eqs. 8-9).



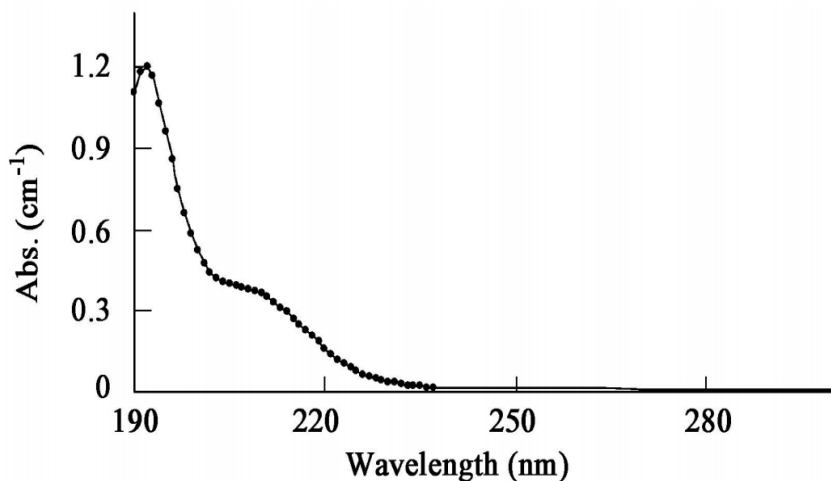
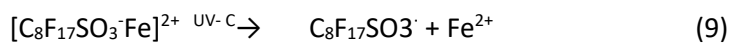


Figure:2.6 UV Absorption of a 50 mgL⁻¹ PFOA solution [125].

Photodecomposition is an eco-friendly technique for PFAA removal. Still, the high demand for energy and low PFAA degradation rate will limit its applicability.

Photocatalysis of various PFAS has been tested using TiO₂ under irradiation by 254 nm UV light. Panchangam et al., [129] reported and claimed that oxidative holes are the active sites for PFAS degradation in excited TiO₂ during UV irradiation. After exposure to UV light, electron-hole pairs were generated as discussed earlier and electrons are accepted from PFAA anions to produce PFAA radicals. Li et al., [130] studied and compared In₂O₃ and TiO₂ as photocatalysts for PFOA degradation under 254 nm UV light, finding that In₂O₃ has higher photocatalytic activity for PFOA removal. It is explained that the terminal carboxylate group can strongly coordinate to the In₂O₃ surface with bidentate or bridging configuration that, in turn, is helpful for direct PFOA removal by holes generated in In₂O₃. In contrast, the TiO₂ surface is coordinated to PFOA through monodentate configuration, preferentially resulting in the formation of hydroxyl radicals from photogenerated holes which are inert toward PFOA degradation (Figure 2.7).

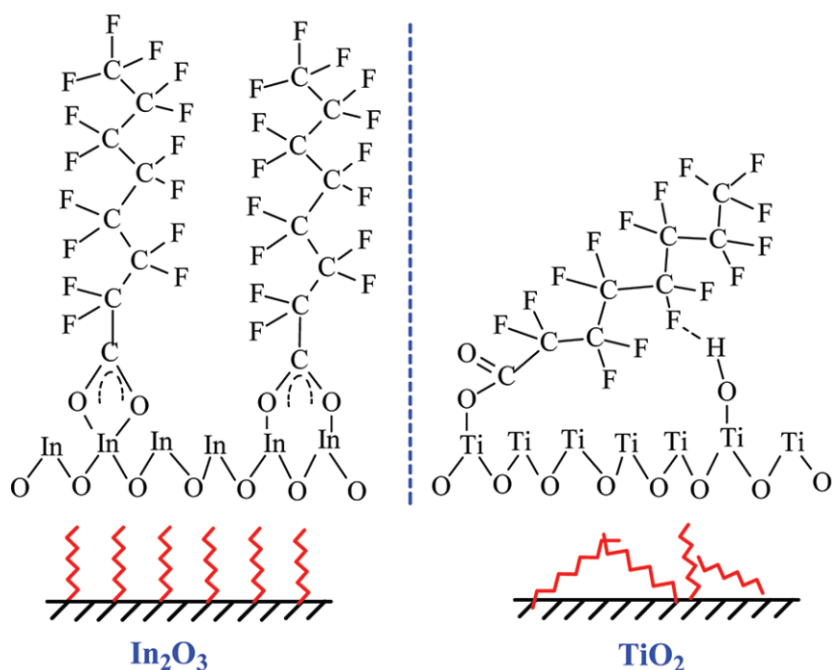


Figure:2.7 Schematic diagram for PFOA configuration adsorbed on TiO₂ and In₂O₃

Zhao et al. [131] conducted photocatalytic degradation of PFOA using a wide band gap photocatalyst (β -Ga₂O₃) under 254 nm UV light. The reaction followed a pseudo-first-order kinetics. They discovered that upon excitation of the catalyst surface, photogenerated electrons interact with water to produce hydrated electrons, which are responsible for PFOA degradation. Also, by irradiation, the direct photogenerated electrons from β -Ga₂O₃ can degrade PFOA molecules.

Photodecomposition of PFAS through photocatalysis is a promising technology that is also applicable to a wide range of organic pollutants in water. An extensive amount of research has been concerned with TiO₂-related photocatalysts at the laboratory scale, which has considerable limitations including limited reactivity, low quantum yield, and narrow band gap absorption. These issues should be considered for industrial-scale applications[132].

In photolysis of pure water using vacuum-ultraviolet (V-UV, $\lambda = 172\text{nm}$), generation of oxidant species ($\cdot\text{OH}$) occurs to ultimately degrade pollutants in water according to reaction 10. Azrague et al. reported the production of hydroxyl radicals without the

addition of any catalyst or supplementary oxidant (i.e., ozone or H₂O₂). Moreover, a combination of UV light with hydrogen peroxide (UV/H₂O₂) or ozone (UV/O₃) enhances the quantity of produced •OH radicals. Wang and Xu reported that upon photolysis of ozone ($\lambda < 300\text{nm}$), O₃ decomposes to O₂ and an oxygen atom O(D¹). This oxygen atom is very reactive and potentially reacts with all substrates including water, to form H₂O₂ via reaction 11. To end the reaction, H₂O₂ could form oxidant species based on reaction 12. The hydroxyl radical is particularly important in AOPs because of its relatively high standard potential in an acidic medium [133]. This radical can oxidize and break down organic pollutants until they are converted to water, carbon dioxide, and related inorganic salts. For example, GLY is attacked by hydroxyl radicals, resulting in the formation of intermediates like sarcosine, AMPA, or final breakdown products that include NO₃⁻, NH₄⁺, CO₂, and PO₄³⁻.



Manassero et al., reported GLY removal using UVC/H₂O₂ at GLY concentration of 50-75 mgL⁻¹ [134]. These average concentrations were present in wastewater due to rinsing of herbicide containers. Effects of different parameters were evaluated including pH, incident irradiation, and H₂O₂ concentration. According to the hypothesized mechanism, the initial stage in the formation of glycine involves the oxidation of the C-P bond by oxidant species, which prevents the formation of sarcosine and AMPA. As a result of glyphosate's breakdown, nitrate, formic acid, formaldehyde, ammonium, and phosphate ions were detected. Lopez et al., and Vidal et al., [7] also investigated the degradation of a commercial GLY-based herbicide using UVC/H₂O₂ system. Both compared the results of mathematical models and experimental data. Vidal et al. reported that after 12 hours of treatment time, 80% glyphosate degraded alongside 70% TOC, and the percentage results were consistent with Lopez et al. Also, Assalin et al., investigated GLY removal through heterogeneous

photocatalysis using TiO_2 and monitored the degradation intermediates. After 30 min of reaction at pH 10, TOC removal was 92%. Also, Chen and Liu obtained similar removal percentages i.e., 92% using 6 g/L of TiO_2 as the optimum amount for the used GLY concentration (0.25 mL^{-1}) after 3.5 hours of reaction time. It was reported that GLY removal was accelerated at pH 3-7 [12].

2.3.3 Fenton and Fenton-like systems

The primary mechanism underlying these systems is the production of extremely reactive radical species, the main one being the hydroxyl radical, $\cdot\text{OH}$. Radical species are produced in homogeneous systems in a variety of methods, including electron transfer during the activation of oxidants by transition metals, photolysis, thermolysis, and sonolysis [135]. The Fenton process, in which H_2O_2 is activated by ferrous ions to generate $\cdot\text{OH}$, is the most traditional homogeneous AOP. The breakdown of organic and inorganic contaminants in wastewater is commonly achieved by the Fenton process, which is reliable, practical, and simple and can be used to reduce wastewater toxicity or to cleanse it, thereby allowing for discharge. In the conventional homogeneous Fenton process, soluble iron ions (Fe^{2+}), which work as catalysts in acidic environments, combine with H_2O_2 to produce powerful oxidants ($\cdot\text{OH}$ and/or reactive high-valence Fe species, such as ferryl, FeO^{2+}) [18]. If we disregard the mass transfer restrictions between active reagents, the use of soluble Fe salts (Fe^{2+}) in conventional Fenton affords the maximum efficiency. The primary flaw in the traditional Fenton method is Fe(III) precipitation in the form of ferric hydroxide brought on by pH adjustment and catalyst (Fe^{2+}) oxidation, which results in sludge waste. In actuality, Fe^{2+} remains dissolved even at a pH of 4, but Fe^{3+} precipitates at pH 4 and forms ferric hydroxide sludge. Due to the high expense in reagents required to acidify the effluents before treatment and then neutralize them before drainage, the least extreme acidic conditions (pH 4 instead of the optimum pH 3) are often used to maintain and carry out the procedure for practical applications [18].

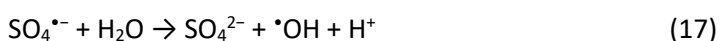
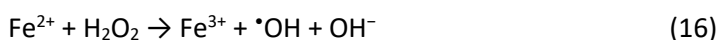
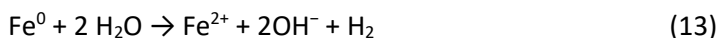
In the past few decades, numerous ways have been developed to move forward more effectively and use heterogeneous Fenton and Fenton-like systems to mitigate these

limitations. Different insoluble iron compounds (Fe_2O_3 , Fe_3O_4 , FeO , FeS_2 , etc.) are introduced as catalysts in the heterogeneous Fenton reaction, along with H_2O_2 , to decontaminate or decompose contaminants in aqueous solution[18]. The use of iron oxide supports or the incorporation of Fe oxides into composite porous materials (clay, zeolites, activated carbon, polymers, and multiwalled carbon nanotubes, Nafion films, pumice particles, ashes, and aluminates) are additional options to increase the efficiency of the Fenton reaction. Because the support adsorbs the pollutant molecule and, in some cases, can also facilitate the reaction, the overall performance of the Fenton reaction may even be enhanced in such heterogeneous processes [18].

The production of free radicals and/or other oxidizing species also occurs in heterogeneous Fenton-like systems when the heterogeneous catalyst is combined with ultrasonic energy, magnetic field, ultraviolet radiation, microwave radiation, or a combination of them [18,136].

2.3.3.1 ZVI-Fenton-like system

Researchers have focused a lot on zero-valent iron (ZVI), one of the catalysts utilized in Fenton-like or heterogeneous Fenton reactions. ZVI is a promising material to be used for water and wastewater treatments, due to its eco-friendliness, cost-effectiveness, non-toxicity, and ability to transform different pollutants such as halogenated compounds, nitrate, heavy metals, phosphate, arsenic, phenol, polycyclic aromatic hydrocarbons, and dyes. ZVI can be employed alone by taking advantage of its reductive (electron-donor) characteristics or combined with H₂O₂ in a heterogeneous Fenton reaction that results in the generation of oxidizing species, mainly •OH [18,136]. Last but not least, current research has attracted attention to using ZVI in combination with persulfate (S₂O₈²⁻) or peroxymonosulfate (SO₅²⁻) to create a heterogeneous Fenton-like reaction with the primary goal of producing the sulfate radical (SO₄^{•-}) as a substitute for •OH as an oxidizing agent. While SO₄^{•-} is more selective than •OH, it is slightly less reactive. This indicates that when compared to •OH-based approaches, the SO₄^{•-}-based processes can achieve pollutant degradation with less interference from water components (vide infra). In particular, the mixture of ZVI with persulfate can trigger a series of reactions (13–17) with the generation of reactive radicals (•OH, SO₄^{•-}), which can be extensively exploited for the decontamination of wastewater [18].



It should be noted that reactions (14) and (16) describe the formation of oxidizing species via Fenton and Fenton-like reactions, and their interconversion is shown by

reaction (17). Fenton reagents can also be produced through the interactions of iron species with dissolved molecular oxygen (not shown here). Reactions (13-16) illustrate how Fe species with different redox state cycle [18].

Numerous water characteristics could influence how well the ZVI-Fenton and Fenton-like systems degrade pollutants. They comprise, among other things, solution chemistry, pH, reagent concentration, and the presence of various anions. One of the most important operating parameters is pH, which regulates the chemistry, radical generation potential, catalyst behavior, and overall effectiveness of almost every Fenton process [18].

Because ZVI nanoparticles have a favorable surface-to-volume ratio that increases their reactivity, nanoscale ZVI (nZVI) is frequently employed as Fe^0 form in these procedures. On the other hand, the quick surface oxidation that nZVI experiences may prevent it from being reused. However, it has been discovered that passivated nZVI (i.e., nZVI covered with a layer of Fe oxides) retains considerable Fenton reactivity, which would be advantageous in the case of potential reuse, at least in the case of ZVI/ H_2O_2 [18]. In addition, it has been demonstrated that the nZVI dosages required to break down pollutants are low and do not significantly impair the process economics, even in the situation of challenging reuse. Additionally, a group of potential composite materials based on amorphous Fe (metallic glasses) have recently been created, and they exhibit fascinating reusability and the capacity to activate H_2O_2 , ZVI/persulfate (PS), and SO_5^{2-} [18].

Deng et al. used acetaminophen (APAP) as a representative pollutant for wastewater from the pharmaceutical industry and applied the iron/persulfate (Fe^0/PS) Fenton-like process to APAP degradation, to provide some instances of the application of ZVI/PS to decontamination operations. They investigated how pH, iron dose, and chelating agent addition affected the Fe^0/PS system. With a 1:1 molar ratio of iron to PS, the highest efficiency (around 93%) was attained. In a wide pH range (3-8.5), efficient degradation (>90%) was seen, and the presence of Fe^0 was thought to be crucial for

the regeneration of Fe^{2+} , by reaction 16 with Fe^{3+} . It was discovered that the degradation of APAP involves both $\text{SO}_4^{\bullet-}$ and $\cdot\text{OH}$. Radical production and interconversion have been noticed here [137]. Zhang et al. have created nanosized ZVI (nZVI) to obtain a nZVI/PS system for Norfloxacin (NOR) degradation. With 100 mgL^{-1} nZVI, 12 mM PS, and pH 7.0, the maximum degradation efficiency (93.8%) of 100 mgL^{-1} NOR was accomplished. The reaction followed a pseudo-first-order kinetic model, and it was concluded from quenching tests and EPR analysis that $\text{SO}_4^{\bullet-}$ and (especially) $\cdot\text{OH}$ were both engaged in NOR degradation. An optimum nZVI dose for degradation was discovered: above this dosage, it can be predicted that nZVI would significantly scavenge $\cdot\text{OH}$. Furthermore, the degradation process was aided by high PS concentration and temperature [138]. According to Jiang et al., Fe^0 is a reliable supply of Fe^{2+} that can be used to activate persulfate ($\text{S}_2\text{O}_8^{2-}$) to $\text{SO}_4^{\bullet-}$ for the breakdown of bisphenol A (BPA). High initial persulfate or Fe^0 concentrations reduced BPA concentration, while subsequent additions enhanced the breakdown efficiency from 49 to 97%. Contrary to a large, single initial addition, the use of repeated additions of reagents, which are then consumed in the Fenton reaction, is advantageous to prevent the reagents from reaching excessive concentration values at any time point. The fact that extra reagents scavenge reactive species ($\cdot\text{OH}$ and/or $\text{SO}_4^{\bullet-}$) can be detrimental to the degradation process. The pH at which the system operates most effectively is 3, however, maintaining this pH level is difficult because the necessary reagents are expensive [18,139].

2.3.4 Sulfate radical-based processes

Despite the high energy requirements, sulfate radicals ($\text{SO}_4^{\bullet-}$) have been shown in several studies to be successful at degrading PFAS with different chain lengths [127,140,141]. There have been numerous reports of the complete mineralization of PFOA using light-activated persulfate, with PFOA degrading to F^- and carbon dioxide (CO_2) ions. Small levels of shorter-chain PFAAs were found in the solution, and the oxidation process further mineralized them. Under a 23 W low-pressure mercury lamp emitting at 254 nm and 185 nm, potassium persulfate ($\text{K}_2\text{S}_2\text{O}_8$) photolysis was

compared to photolytic breakdown, and the results showed that persulfate-activated photolysis considerably increased PFOS degradation. Additionally, PFOA degraded and mineralized more quickly in an oxygen compared to a nitrogen atmosphere. Hori et al., [140] examined the effects of heat-activated persulfate on the effectiveness of PFOA and other C5-C9 chains PFAAs degradation. While the thermal breakdown of PFAS was ineffectual by itself, adding 50 nM $S_2O_8^{2-}$ and heating the aqueous solution with 374 μ M of PFOA for 6 hours at 80°C under pressurized air was able to completely mineralize PFOA [83]. Similar outcomes were seen when various PFAA compounds were subjected to the heat-activated persulfate oxidation method. For PFOA, the F^- ions production was around 78%, while for other PFAAs, it ranged between 80% and 90%. Intriguingly, when the reaction temperature was raised to 150 °C, the yields of F^- and CO_2 ions decreased and they were replaced with large amounts of C4-C7 chain PFAAs, proving that temperatures higher than subcritical water were ineffective in achieving PFAA decomposition when combined with persulfates [83].

It has been asserted that PFAAs would be attacked by generated sulfate radicals via one electron transfer (eq. 18). After decarboxylation, many radical reactions will follow, as well as hydrolysis procedures, till PFCA fully mineralize [140].



Research using heat- and microwave-induced breakdown has supported this conclusion. Transitional metals, such as Ag, have been used to activate persulfate for PFAS degradation at room temperature. It was suggested that the decarboxylation of PFAS could be accomplished via the production of sulfate radicals and the oxidation of Ag^+ to Ag^{2+} . The mentioned study emphasized that there is an ideal PS/Ag ratio that results in the best PFAS breakdown, which in this case was 0.6 M PS/0.6 mM Ag. However, while this approach works well for PFAAs, it is useless for PFOS. It has been shown that activated persulfate oxidation is effective in PFOA degradation, especially in groundwater, and could degrade PFOA and PFOS in situ. Persulfate has a low breakdown efficiency in alkaline environments. The inability of sulfate radicals to

decompose perfluorinated sulfonic acid, such as PFOS, is a drawback of using sulfate radical-based techniques to treat PFAAs [83].

The second-order rate constants for sulfate radicals with various PFAAs (C4 to C8) are in the range of $1.7\text{-}4.4 \times 10^4 \text{ M}^{-1}\text{s}^{-1}$, according to Lutze et al., [141] The chain length of various species does not affect the relative reaction rate constants. PFAAs, however, should rather be viewed as experimental mistakes. Additionally, Kutsuma and Hori, [142] showed that PFAAs and sulfate radicals have comparable second-order rate constants ($1.3 \times 10^4 \text{ M}^{-1}\text{s}^{-1}$ for PFBA, PFPrA: $1.4 \times 10^4 \text{ M}^{-1}\text{s}^{-1}$). On the other hand, Qian et al., [143] recorded various rate constants between PFCAs and sulfate radicals. These constants were calculated by fitting experimental data to the model. Information on the breakdown of PFOA and the emergence of shorter-chain PFCAs (PFHpA, PFHxA, PFPeA, PFBA, and PFPrA) via a stepwise degradation of PFAAs is here provided (Table 2.3).

Table: 2.3 Rate constants for reaction of sulfate radicals with PFAAs from model simulations [143].

PFCAs	k ($\text{M}^{-1} \text{s}^{-1}$)
PFOA ($\text{C}_8\text{HF}_{15}\text{O}_2$)	2.59×10^5
PFHpA ($\text{C}_7\text{HF}_{13}\text{O}_2$)	2.68×10^5
PFHeA ($\text{C}_6\text{HF}_{11}\text{O}_2$)	7.02×10^5
PFPeA ($\text{C}_5\text{HF}_9\text{O}_2$)	1.26×10^6
PFBA ($\text{C}_4\text{HF}_7\text{O}_2$)	1.05×10^7
PFPrA ($\text{C}_3\text{HF}_5\text{O}_2$)	9.31×10^7

It has been shown that the carbon chain lengths and the rate constants between sulfate radicals and PFCAs are correlated (rate constants rise with decreasing carbon chain lengths). The competition between PFOA and shorter-chain PFAA products for sulfate radicals, however, can only be disregarded in situations when all compounds

have extremely high rates of degradation and shorter-chain PFAA products have extremely low yields. Consequently, the rate constants obtained by model simulations are not very compelling. Sulfate radicals are scavenged by different anions and the oxygenated species thus generated will be discussed in later sections.

Sulfate radicals ($\text{SO}_4^{\bullet-}$), produced by sulfate-based substances like persulfate (PS) are used in these procedures. The sulfate-based radical reactions can break down GLY, and they typically begin by adding a sulfate-based substance (such as persulfate or peroxymonosulfate) to the contaminated area or treatment system. There are several ways to activate these chemicals, including heat, UV light, or transition metal catalysts. Sulfate radicals ($\text{SO}_4^{\bullet-}$) are highly reactive species with a substantial oxidative potential, and are formed by activation of sulfate-based molecule. They attack GLY by removing hydrogen atoms from different functional groups. The glyphosate's carbon-phosphorus (C-P) bond is broken during one of the crucial processes [144].

As GLY is degraded by sulfate radicals, intermediate breakdown products are produced. For instance, aminomethylphosphonic acid (AMPA) and sarcosine can be produced when the C-P link is broken [11]. In general, these products are less harmful than GLY. Sulfate radicals could further oxidize these intermediates, converting them into less dangerous and simpler molecules, and these reactions can occasionally result in the formation of inorganic phosphates as well. The mineralization of GLY and its breakdown byproducts into harmless compounds including carbon dioxide, water, and inorganic ions can occur over time because of sulfate-based radical reactions [144].

Because sulfate radicals are potent oxidizing agents capable of degrading the molecular structure of GLY into smaller, less hazardous components, sulfate-based radical reactions are efficient at degrading GLY. These procedures are frequently employed in water treatment and environmental remediation to lessen the impact of GLY and other organic contaminants. To guarantee efficient GLY breakdown, the

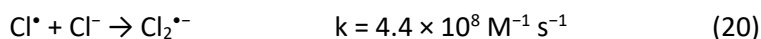
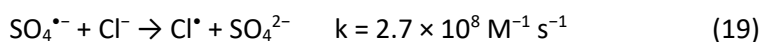
treatment system must be properly designed and optimized, including the selection of sulfate-based chemical and reaction conditions [11,18].

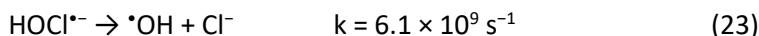
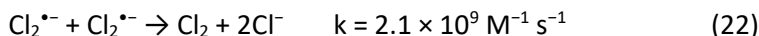
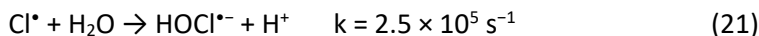
2.3.4.1 Reactive Oxygen species

One of the key characteristics of the hydroxyl radical is its high reactivity toward most compounds found in water and wastewater. On the one hand, this allows for the possibility of degrading a variety of contaminants in the framework of water treatment. On the other hand, $\cdot\text{OH}$ can be scavenged by many constituents of natural water and wastewater, such as organic matter and some inorganic anions (e.g., Cl^- , NO_2^- , HCO_3^- , and CO_3^{2-}), which leads to a decrease in method efficiency [18]. The ability of natural water constituents to scavenge $\cdot\text{OH}$ will primarily prevent the breakdown of contaminants, because natural water constituents do not always need oxidation for water to be fully decontaminated. Increased costs and/or decreased process efficiency are the results of $\cdot\text{OH}$ scavenging by organic matter and inorganic anions, which operate as interfering agents [11].

2.3.4.1.1 Chloride

Because chloride can trigger some opposing reactions in Fenton-like systems, the impact of chloride ions on the ZVI/PS process has generated some debate. Cl^- can accelerate the corrosion of Fe^0 and can also scavenge $\text{SO}_4^{\cdot-}$ and/or $\cdot\text{OH}$ by producing reactive chlorine species (RCS) like $\text{Cl}_2^{\cdot-}$, Cl^\bullet , and Cl_2 [145]. It is important to consider that while net scavenging of $\cdot\text{OH}$ by Cl^- happens only at acidic pH values, scavenging of $\text{SO}_4^{\cdot-}$ by Cl^- can occur at any pH. The overall action of chloride can either increase or hinder pollutant breakdown, depending on the circumstances. The scavenging by chloride of strong oxidizing species ($\text{SO}_4^{\cdot-}$, $\cdot\text{OH}$) that are replaced by less reactive species such as $\text{Cl}_2^{\cdot-}$ has been cited as the explanation for the chloride inhibition effect [146].





It is interesting to note that Fenton-like systems based on ZVI/PS should operate better in the presence of chloride when the latter's concentration is low (about 1 mM), however, degradation becomes noticeably worse at high chloride (10 mM). Cl⁻'s ability to promote ZVI corrosion and stimulate PS activation by Fe²⁺ at low concentrations is a plausible explanation for this effect. On the other hand, increased Cl⁻ concentration would instead result in SO₄^{•-} (and/or •OH) scavenging, with less reactive RCS (Cl₂^{•-}, Cl[•], Cl₂) replacing them [18,147].

Distinct chloride concentrations have distinct effects on ZVI/PS. For instance, Kim et al. concluded that there is a maximum concentration of [Cl⁻] at which degradation is most effective (170 mM Cl⁻, or about 1% dissolved salts, which is in the range of brackish waters). Indeed, based on those data it was deduced that brackish waters, which contain 600 mM Cl⁻ or about 3.5% of the dissolved salts found in seawater, may be more conducive to pollutant breakdown by ZVI/PS than freshwater or more saline waters. However, RCS may produce chlorinated by-products that have the potential to be hazardous, although this topic has not yet received considerable attention. In the presence of RCS and electron-rich substrates, the production of chlorinated by-products is extremely likely. The chlorinating agents Cl[•], Cl₂ that is generated following radical condensation, and Cl₂^{•-} formed upon interaction between Cl[•] and Cl⁻ can all be produced by the oxidation of Cl⁻ by SO₄^{•-} [18].

2.3.4.1.2 Nitrate/nitrite

There hasn't been much research done on how nitrate and nitrite ions behave in Fenton systems based on hydroxyl and sulfate radicals. However, one can anticipate

the scavenging of sulfate radicals as demonstrated in equations (24) and (25), as well as of $\cdot\text{OH}$, in the presence of nitrate and particularly nitrite.

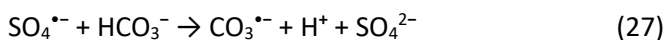
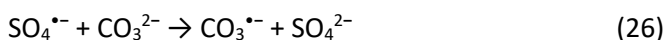


Although it is anticipated that the scavenging process will result in the substitution of $\text{SO}_4^{\cdot-}$ (and $\cdot\text{OH}$) with less reactive radicals (NO_3^\cdot and especially NO_2^\cdot), the actual result will depend on the environment and the target substrate. Nitrate concentration is not expected to change in these processes because the nitrate radical will eventually give back NO_3^- . On the other hand, nitrite is oxidized into nitrate [18].

For instance, Guo et al. just published a paper on the impact of nitrate on the ZVI/PS-mediated decontamination of sulfadiazine. A low concentration of nitrate (10 mM) was discovered to improve the removal efficiency for unidentified reasons. Higher nitrate concentrations (10–50 mM), on the other hand, prevented the elimination of sulfadiazine. Due to the reduced reactivity of NO_3^\cdot compared to $\text{SO}_4^{\cdot-}$ and a scavenging mechanism (reaction (24)), the latter effect was tentatively explained [148,149]. Also seen in the presence of nitrite at relatively high concentration values (>100 μM) was the inhibition of pollutant breakdown by PS/ $\text{SO}_4^{\cdot-}$. The oxidation of NO_2^- to NO_2^\cdot by $\text{SO}_4^{\cdot-}$ (reaction 25) is expected to induce a double effect: (i) inhibition of pollutant degradation, because NO_2^\cdot is considerably less reactive than $\text{SO}_4^{\cdot-}$ (and than NO_3^\cdot as well: indeed, nitrite has the potential to inhibit degradation at a higher extent than nitrate if concentrations are comparable), and (ii) formation of nitrated by-products, because of the activity of NO_2^\cdot as nitrating agent. According to reports, several chloronitrophenols, including 2C4NP and 2C6NP, are produced when 2-chlorophenol degrades in the presence of $\text{SO}_4^{\cdot-}$ and nitrite. These nitro-derivatives that are created throughout the process should be considered and their formation prevented wherever feasible because they could be hazardous [18].

2.3.4.1.3 Carbonate/Bicarbonate

Both HCO_3^- and CO_3^{2-} could scavenge $\text{SO}_4^{\bullet-}$ (as well as $\bullet\text{OH}$) and ultimately lead to the formation of carbonate radicals, $\text{CO}_3^{\bullet-}$ (reactions (26) and (27)). Although $\text{CO}_3^{\bullet-}$ and $\text{SO}_4^{\bullet-}$ both primarily react through the transfer of electrons and hydrogen, $\text{CO}_3^{\bullet-}$ is significantly less reactive than $\text{SO}_4^{\bullet-}$ due to its lower one-electron reduction potential [148,149]. One may anticipate that in the presence of ZVI/PS, carbonate and bicarbonate would limit the breakdown of pollutants due to reactions (26) and (27). This is frequently seen but, under other conditions, the situation is more complicated because the concentration, pH, and type of the target pollutant all affect how carbonate and bicarbonate affect degradation.



Using p-nitrosodimethylaniline as an example, Bennedsen et al. studied the effect of carbonate on PS activation for the degradation of the pollutant [150]. Notably, carbonate's function in such a situation could not be reduced to that of a simple scavenger. Hayat et al. have reported a comparable, advantageous effect of $\text{HCO}_3^-/\text{CO}_3^{2-}$ on pollutant elimination by PS activation [151].

Zhao et al. [152] investigated the influence of water matrices containing NOM and bicarbonates on the degradation of 2-chlorophenol via PS activation. They discovered that bicarbonate prevents $\text{SO}_4^{\bullet-}$ scavenging-related deterioration. Bicarbonate, however, also needs to be considered because it buffers the reaction solutions. Similar adverse $\text{CO}_3^{2-}/\text{HCO}_3^-$ effects on degradation have been noted for propranolol and sulfamethoxazole [18].

2.3.5 Ozonation

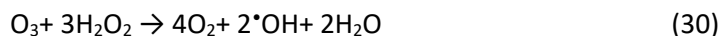
An efficient AOP for treating wastewater containing GLY quickly and at the lowest concentration is ozone oxidation. To encourage the breakdown of ozone and promote the generation of $\bullet\text{OH}$, H_2O_2 can be added to the reaction system [153]. Additionally,

by raising the pH of the system, which encourages $\cdot\text{OH}$ formation, the efficiency of ozonation can be improved. To remove GLY, ozonation can in fact either take place directly by ozone or indirectly by hydroxyl radicals, which subsequently attack and break down GLY. Studies have shown that GLY can be completely broken down as a result of the oxidation process caused by ozonation. GLY elimination was accomplished with a high efficiency (99%) and a high percentage (85%) using O_3 and H_2O_2 combined in a relatively short period of time [154]. Despite this method's high efficacy, it still has certain drawbacks, such as high costs, difficulties with ozone's solubility in water, a problem with waste management, and the unstable nature of ozone.

Finally, several studies have reported the use of hybrid systems, which combine two or more approaches, to boost the effectiveness of GLY degradation. According to Xing et al., who combined AOPs with adsorption, a catalytic wet oxidation process using modified activated carbon as the catalyst could completely degrade GLY in an effluent. Because they break down GLY and numerous of its intermediate products, these hybrid methods are advantageous. Even though the aforementioned techniques have shown promise in treating wastewater containing GLY at the laboratory scale, further study is still required before they are applied on an industrial scale. The price of these technologies continues to be a barrier, thus it is advised that this procedure be utilized after a first step or route that lowers GLY concentration to minimize the financial commitment required [7].

According to Dombrowski et al., PFOA and PFOS are two organic pollutants that can be degraded using ozone (O_3) gas [155]. According to Lin et al., ozonation may remove 80–100% of perfluorooctanoic acid and perfluorooctane sulfonate under basic conditions (pH 11). However, when exposed to O_3 at a lower pH (between 4 and 5), the breakdown of PFOA and PFOS was not seen [156,157]. The production of superoxide radicals that contribute to the mineralization of PFAS was thought to be more likely under basic conditions (Eqs.28-30) [156].





Regarding PFAS removal, innovative ozonation techniques for their elimination from drinking water were evaluated. Laboratory tests revealed that the mixture of persulfate, ozone, and a catalyst was the most effective treatment. All of the 18 tested PFAS decreased significantly within three hours of treatment in pilot-scale testing; moreover, while CF12–CF17 PFAS underwent 64% removal and CF4–CF6 PFAS reached an average of 55%, longer-chain PFAS (CF7–CF11) showed outstanding removal effectiveness, exceeding 98%. These results demonstrate the potential of this ozonation technique for the elimination of PFAS on a wide scale, but additional studies are required to determine any potentially harmful consequences [158].

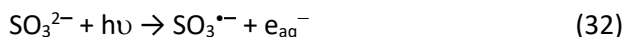
2.3.6 Reductive degradation with hydrated electrons

In recent years, reductive degradation has been studied as a wastewater treatment method. Reductive processes produce hydrated electrons and hydrogen atoms, which are active reducing species. These characteristics can be combined with activation techniques like UV light, ultrasound, and electron beam irradiation, as well as reducing reagents like iodide, sulfite, and indole acetic acid. The reductive degradation processes are especially promising for some hardly degradable contaminants in water, such as chlorinated and fluorinated organic compounds and inorganic pollutants (bromate and perchlorate), because the produced active reducing species, such as hydrated electrons, can donate an unpaired electron to the target compound and reduce it chemically.

Park et al.'s [159] study looked at the iodide photolysis-based degradation of PFOA and PFOS under UV-C light. Iodine radical and hydrated electrons are produced when iodide is photolyzed in the presence of UV-C rays, Eq. 31.



It was discovered that the iodide concentration, headgroups, length of the perfluorocarbon chain, and starting concentrations of PFOA and PFOS all affected the breakdown of these compounds, while pH had no effect. One drawback of photolysis-induced hydrated electron production via iodide is that the intermediate tri-iodide will scavenge the hydrated electrons that are created. In addition to iodide, sulfite was employed as a reductant in photolysis to produce hydrated electrons Eq. 32.



Bentel et al., [160] investigated the connections between structure and reactivity using 34 common PFAS and hydrated electrons produced by exposure of sodium sulfite to UV light. They discovered that fluorinated carboxylic acids (PFCAs) varying in length from 2 to 10 carbon perfluorocarbon chains had a comparable rate of defluorination and degradation. The perfluorinated sulfonic acids (PFSA), on the other hand, showed evidence of a correlation between chain length and reactivity. The mentioned authors suggested numerous chemical pathways of PFAS degradation driven by hydrated electrons by combining their findings with theoretical estimates on carbon-fluorine bond dissociation energy. These include the following: HF removal, H/F exchange, terminal function group dissociation, and decarboxylation-induced hydrolysis. Huang et al., [161] reported on the laser flash photolysis reactivity of hydrated electrons towards a series of perfluorinated carboxylates.

The second-order rate constants for the reactions of hydrated electrons with PFOA, PFBA, and TFA at an ionic strength of 0.01 M NaClO₄ were estimated to be $(1.7 \pm 0.5) \times 10^7 \text{ M}^{-1} \text{ s}^{-1}$, $(8.8 \pm 0.2) \times 10^6 \text{ M}^{-1} \text{ s}^{-1}$, and $(2.3 \pm 0.2) \times 10^6 \text{ M}^{-1} \text{ s}^{-1}$, respectively. The lengthening of the fluorocarbon chains seemed to increase the rate constant. Furthermore, it was observed that the hydrated electrons had second-order rate constants with PFOS (in the form of tetraethylammonium salt) of $7.3 \times 10^7 \text{ M}^{-1} \text{ s}^{-1}$ [162].

Table 2.4 illustrates how certain coexisting scavengers in wastewater can readily quench hydrated electrons. Therefore, before implementing hydrated electron-based

treatment for PFAA degradation, careful consideration must be given to these coexisting scavengers. It has been shown that hydrated electrons can be used in reduction-based degradation procedures to effectively break down and defluorinate PFAA. However, the majority of researchers used artificially simulated water for their investigations. Certain conditions are typically needed for these operations, such as deionized or Milli-Q water, an anaerobic atmosphere, an alkaline pH, and large reagent dosages. The efficacy and efficiency of hydrated electron-based procedures for PFAA treatment in natural water matrices still need to be assessed, given the high reactivity of hydrated electrons towards some coexisting scavengers in wastewater.

Table:2.4 Rate constants for reaction of hydrated electrons with other species

Solute	K (M⁻¹ s⁻¹)
H ⁺	$(2.4 \pm 0.2) \times 10^{10}$
[•] OH	$\sim 3 \times 10^{10}$
CO ₂	$(7.7 \pm 1.1) \times 10^9$
O ₂	$(1.9 \pm 0.2) \times 10^{10}$
NO ₃ ⁻	$(1.1 \pm 0.1) \times 10^{10}$
Cl ⁻	$<10^6$
SO ₄ ²⁻	$<10^6$
CO ₃ ²⁻	$<10^6$

Here we see the critical comparison of the various treatment techniques for GLY removal (Table 2.5) [118].

Table: 2.5 Critical comparison of various Treatment Techniques for GLY removal

Treatment Techniques	Description	Advantages	Disadvantages
Adsorption	<ul style="list-style-type: none"> • Removal of GLY from aqueous environment using adsorbents or membranes including biochar, resins, clay compounds, activated carbon, polymers, etc. 	<ul style="list-style-type: none"> • User-friendly and simple. • High productivity with a low concentration. • Low cost and low risk of secondary pollution 	<ul style="list-style-type: none"> • Presence of competition for adsorption sites. • Adsorbents are hard to clean, recycle, and use again. • Challenge with disposal of residues after adsorption.
Biological treatment	<ul style="list-style-type: none"> • Degradation of GLY using microorganisms including bacteria, fungi, and algae. 	<ul style="list-style-type: none"> • Cost-effective and eco- friendly. • Outstanding performance with high amounts of wastewater. 	<ul style="list-style-type: none"> • Pretreatment is required to decrease effluent toxicity. • Time-consuming method. • Low efficiency in the mineralization process.
Electrochemical oxidation	<ul style="list-style-type: none"> • Use of high anodic energy to break down GLY molecules to complete mineralization. 	<ul style="list-style-type: none"> • Outstanding performance with high amounts of wastewater. • Very clean 	<ul style="list-style-type: none"> • Mass transfer limitation. • Electrode lifespan is limited. • High energy

		method	requirement.
Photolysis-assisted oxidation	<ul style="list-style-type: none"> • Use of UV light to produce hydroxyl radicals for the removal of GLY in water. 	<ul style="list-style-type: none"> • Outstanding performance with high amounts of wastewater 	<ul style="list-style-type: none"> • Complicated due to low UV penetration in important media. • Difficult to scale-up.
Ozonation oxidation	<ul style="list-style-type: none"> • Using ozone or hydroxyl radicals to remove and degrade GLY. 	<ul style="list-style-type: none"> • Outstanding performance at low concentration levels 	<ul style="list-style-type: none"> • Mass transfer limitation of ozone. • Maintenance- heavy. • Ozone is unstable. • Solubility challenges prompting a complex mixing method.
Fenton-assisted oxidation	<ul style="list-style-type: none"> • Iron (Fe^{2+}) ion is employed as a catalyst, to break down H_2O_2 into reactive hydroxyl ($\cdot\text{OH}$) radicals for degrading GLY. 	<ul style="list-style-type: none"> • Outstanding performance at low concentration levels. • User-friendly. • Unlimited mass transfer. 	<ul style="list-style-type: none"> • Acidic pH requirement. • Ferrous ion recycling is difficult. • Generation of sludge. • Additional treatment is required.
ZVI-Fenton like process	<ul style="list-style-type: none"> • Fe^0 is used as catalyst to produce Fe^{2+} and activate H_2O_2, recycle Fe^{3+}, 	<ul style="list-style-type: none"> • Outstanding performance at low concentration levels. 	<ul style="list-style-type: none"> • Acidic pH requirement. • Additional treatment

	and generate $\cdot\text{OH}$ to degrade GLY.	<ul style="list-style-type: none"> • No sludge production. • Fe^{2+} recycling is easier. • User-friendly. • Unlimited mass transfer. 	is required.
Hybrid process	<ul style="list-style-type: none"> • Combination of two or more treatment methods to achieve a high degradation efficiency. 	<ul style="list-style-type: none"> • Outstanding performance. • Addresses the inherent limitations of specific treatment methods 	<ul style="list-style-type: none"> • Complexity of systems and operations. • Difficult to investigate and compare to other methods

Figure 2.8 summarizes many GLY oxidation processes with various AOPs. It has been shown that GLY oxidation normally proceeds according to two biological mechanisms that are connected to the hydroxyl radical-caused cleavage of C-P and C-N bonds. Hydroxyl radicals attack GLY to produce sarcosine, PO_4^{3-} or AMPA, and glycolic acid. Throughout the GLY oxidation process, the two pathways may operate independently or together.

Table: 2.6 Removal of GLY from polluted water by advanced oxidation processes (AOPs) [11].

AOPs	Operating Conditions	GLY Concentration (mg a.i. L ⁻¹)	Removal (%)	Ref.
UV/Ferrioxalate	V = 80 mL (eight quartz tubes/10 mL); pH = 3.5–6.0; UV-vis Lamp 250 W ($\lambda \geq 365$ nm); t = 180 min	1.0–5.0	-	[163]
UV/TiO ₂	V = 400 mL, pH from 2.0 to 12.0; UV Lamp at 365 nm; illumination time = 1 h	42.25	9.8–50.2	[12]
Photocatalytic degradation(UV-TiO ₂)	V = 200 mL; high-pressure mercury lamp (125 W, $\lambda > 290$ nm); amount of catalyst = 0.1 g·L ⁻¹ of TiO ₂ ; t = 30 min.	42.3	99.9	[13]
H ₂ O ₂ /UV	V _{reactor} = 110 cm ³ ; [H ₂ O ₂] = 75–200 mg·L ⁻¹ ; t = 5 h; 2 UV lamps, each at 40 W	50.0	70.0	[167]
Photocatalysis Ce-TiO ₂	0.15% Ce-TiO ₂ nanotubes annealed at 400 °C; V = 500 mL; t = 1 h; pH 7; 125 high-pressure mercury lamps.	22.8	76.0	[168]
UV/H ₂ O ₂ experimental and mathematical model	V = 2000 mL (quartz cylindrical reactor, 110 mL, flow rate = 5×10^{-2} cm ³ ·s ⁻¹ ; UV Lamp at 253.7 nm; pH 5.2; [H ₂ O ₂] = 0 - 403 mg·L ⁻¹ ; t = 12 h	140.0	80.0 GLY 70.0 TOC	[169]

UV/H ₂ O ₂	V = 1000 cm ³ ; two low-pressure mercury vapor lamps with emission wavelength at $\lambda = 253.7$ nm; Q = 2 L·s ⁻¹ ; t = 8 h	30.0	-	[170]
UV/Goethite	incident light intensity 500–2000 W/m ² ; T = 20 °C, pH 3–9	10.0	92.0 99.3	[16]
Aeroxide TiO ₂ -P25	Volume 250 mL, stirring 600 rpm, UV-A light, 60 W/m ² , $\lambda = 365$ nm, Time = 240 min	25.0	100	[171]
Photochemical degradation over CuS/Bi ₂ WO ₆	Hierarchical CuS/Bi ₂ WO ₆ Illumination time: 180 min; 44 W light-emitting diode (LED) light irradiation ($\lambda > 400$ nm)	16.9	85.9	[172]
Photo-Fenton	V = 50 L; closed recirculating system at a flow rate of 2.37 L·min ⁻¹ ; [Fe ²⁺] or [Fe ²⁺ /Fe ³⁺] = 0.27 mmol·L ⁻¹ ; [H ₂ O ₂] = 10.3 mmol·L ⁻¹ ; pH 2.8 ± 0.2	100.0 100.0	- -	[173]
Electro-Fenton Mn ²⁺	V = 200 mL; 100 mA constant current; catalyst = 0.1 mM Mn ²⁺	22.8	92.0– 100.0	[165]
Electro–Fenton	t = 360 min; pH 3; current intensity = 0.36 A; 1 mM Fe ²⁺ ; pure O ₂ flow rate = 100 mL·min ⁻¹	22.8	-	[174]
Electrochemical oxidation with	i = 50 mA·cm ⁻² ; t = 4 h; electrode composition =	1000.0	24.0	[175]

RuO ₂ /IrO ₂ electrodes	Ti/Ir _{0.30} Sn _{0.70} O ₂ ;			
Adsorption and POA's (H ₂ O ₂)	V = 150 mL GLY residue solution; pH = 2–4; adsorbent = nano-tungsten/D201 resin + H ₂ O ₂	258.0	60.5	[176]
Electrochemical degradation with MnO ₂	V = 400 mL; acidic pH; i = 10 mA·cm ⁻² ; t = 120 min	22.8	80.0	[177]
Electrochemical degradation	Anode: Ti/PbO ₂ ; pH: 3–10; current intensity: 4.77 A; reaction time: 173 min; electrolyte: Na ₂ SO ₄	4–16	95.16	[15]
Electrochemical oxidation BDD	Electric charge = 6.0 Ah·dm ⁻³ ; pure GLY; t = about 150 min; Chloride media	100.0	- -	[178]
Photochemical Oxidation with BDD	UV lamp (λ = 254 nm); i = 100 mA·cm ⁻² ; t = about 200 min; supporting electrolyte = NaCl	100.0	-	[179]

Considering the PFAS removal by different treatment methods, many methods have been described and each has its advantages and disadvantages. Here we see a comparison of different adopted methods in the literature, mentioning their advantages and disadvantages in Table: 2.7.

Table: 2.7 Summary of some existing methods/technologies for the removal of PFAS

Method/Technology	Advantages	Disadvantages	Ref.
<p>Advanced photochemical oxidation using chemicals or Ozone, O₃/UV, Fenton's reagents, activated persulfate, UV/H₂O₂</p>	<p>Ozone, O₃/UV:</p> <ul style="list-style-type: none"> • These reagents are effective in oxidizing physiologically resistant organic materials. • Activated persulfate and Fenton's reagents: Under mild circumstances, activated persulfate is useful for the oxidative breakdown of PFOA in groundwater, making it a feasible solution for use in large-scale applications. • It is not necessary to use further treatment to eliminate PFOS and PFOA. 	<p>Activated persulfate:</p> <ul style="list-style-type: none"> • While standard alkaline-activated persulfate degrades PFOA with very poor effectiveness, activated persulfate is good at oxidatively breaking down the chemical in acidic conditions in aqueous solution. <p>Fenton's reagent, O₃/UV, O₃/H₂O₂, and Ozone:</p> <ul style="list-style-type: none"> • Certain advanced oxidation technologies have not been able to effectively degrade PFOS and PFOA at the mg/L level. At low temperatures (40 °C, for example) the pace of reaction is quite sluggish. • High amount of energy needed to speed up the process. • Regarding PFOS breakdown, the Fenton 	<p>[83,180]</p>

	<ul style="list-style-type: none"> • Possibility of in situ degradation of PFOS and PFOA. • UV/H₂O₂: • Quick response time and reduced environmental impact 	<p>system is only useful in alkaline and neutral conditions. Additional research should be conducted for broad use.</p> <p>UV/H₂O₂:</p> <ul style="list-style-type: none"> • secondary pollution production 	
Sonochemical decomposition	<ul style="list-style-type: none"> • This procedure achieves elimination of both PFOS and PFOA. 	<ul style="list-style-type: none"> • The process is still in its early phases. Before being used in the field, more studies are required. 	[181,182]
Electrochemical oxidation	<ul style="list-style-type: none"> • Practical technique for full mineralization of PFOA and PFOS at room temperature and atmospheric pressure, with fast mineralization and minimal energy usage. Also relevant under in situ circumstances like co-contaminants and PFAS mixtures. 	<ul style="list-style-type: none"> • The production of perchlorate, HF, bromate, adsorbable organic halides, and poisonous chlorine gas. • Since the oxygen evolution potential (OEP) is essential to the breakdown of PFOA, electrode manufacturing is a crucial component. Furthermore, the hydroxyl radical generated through water electrolysis is ineffective when applied to perfluorinated surfactants. 	[183,184]

	<ul style="list-style-type: none"> • Because of its high oxidation efficiency, quick reaction rate, ease of operation and automation, environmental compatibility, and affordability, electrochemical oxidation can break down hazardous or persistent organic contaminants. 		
<p>Adsorption</p> <p>Activated carbon</p> <p>Biochar</p>	<ul style="list-style-type: none"> • Established technology. • Broad pH range of operation. • Low cost in comparison with ease of use. • Effective against long-chain PFAS. 	<ul style="list-style-type: none"> • Poor selectivity • Adsorbents need to be regenerated • Poor capacity for reuse of absorbent • Ineffective for short-chain PFAS 	[83]
Photocatalysis	<ul style="list-style-type: none"> • Regeneration of the catalyst to enable reuse. • Functioning in the 	<ul style="list-style-type: none"> • Large volumes of chemicals and harsh operating conditions are occasionally required. 	[185]

	<p>presence of visible light.</p> <ul style="list-style-type: none"> • Many catalytic materials are available. • TiO₂-based photocatalysts can remove PFAS up to 100%. • Operation at ambient temperature. • Minimal use of energy. 	<ul style="list-style-type: none"> • Degradation can result in the production of secondary pollutants. • Poor effectiveness. 	
Treatment train (combined technologies for treatment)	<ul style="list-style-type: none"> • Enhanced overall effectiveness of PFAS degradation, in situ treatment possible. • Reduced possibility of secondary pollution as a result of byproducts of PFAS breakdown. • Decreased use of 	<ul style="list-style-type: none"> • The costs associated with the combination of technologies have not been reported yet. 	[185]

	chemicals and energy, which, in contrast to technologies employed separately, eliminates the need for harsh conditions (high acidity, alkalinity, temperature, etc.).		
--	---	--	--

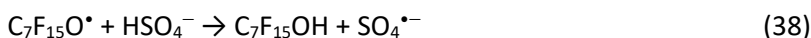
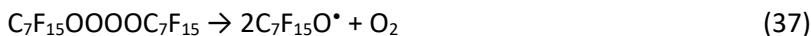
2.4 PFOA and PFOS degradation pathways

2.4.1 Oxidative degradation pathways

The breakdown of PFOA was reported to begin with an attack of the reactive species at its carboxylic headgroup in the majority of its oxidative degradation processes covered in Chapter 2.3 (e.g., photocatalysis, Fenton process, etc). $C_7F_{15}COO^{\bullet}$ will be produced following the loss of one electron from the PFOA headgroup (eq. 33) [128,129,140]. After undergoing a Kolbe decarboxylation reaction, the radical $C_7F_{15}COO^{\bullet}$ becomes $^{\bullet}C_7F_{15}$ (eq. 34), which is then expected to react further with (i) molecular oxygen, (ii) hydroxyl radicals, (iii) water, and (iv) it can recombine with other (perfluorinated) radicals.

When $^{\bullet}C_7F_{15}$ and oxygen combine in the (i) case, perfluoroalkyl peroxy radicals are created. These radicals then undergo a bimolecular radical-radical interaction to form two perfluoro-alkoxy radicals, $^{\bullet}OC_7F_{15}$ (eqs. 35-37)[141,142]. $^{\bullet}OC_7F_{15}$ will abstract H from water to create perfluoroalkyl alcohol ($C_7F_{15}OH$), or from HSO_4^- (in sulfate radical-based processes) (eqs. 38 and 39). Fast elimination of one HF results in $C_6F_{13}COF$, which is subsequently hydrolyzed to $C_6F_{13}COOH$. The breakdown mechanism of $C_6F_{13}COOH$ will be comparable to that of PFOA (eqs. 40 and 41). PFOA

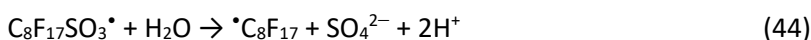
can finally be completely degraded or defluorinated. When (ii) occurs, $\cdot\text{C}_7\text{F}_{15}$ and $\cdot\text{OH}$ may react to form $\text{C}_7\text{F}_{15}\text{OH}$ (eq. 42)[186], which is subsequently further degraded according to (i). Furthermore, according to several researchers, $\bullet\text{C}_7\text{F}_{15}$ may react directly with water (the (iii) case) to produce $\text{C}_7\text{F}_{15}\text{OH}$ and $\cdot\text{H}$ [178,179]. However, because $\cdot\text{H}$ is far more reactive than $\cdot\text{C}_7\text{F}_{15}$, this process is suspicious.



Fluorinated radicals recombine to produce volatile perfluoroalkanes that have the potential to escape from the aqueous solution ($\cdot\text{C}_n\text{F}_{2n+1} + \cdot\text{C}_m\text{F}_{2m+1} \rightarrow \text{C}_{n+m}\text{F}_{2(n+m+1)}$). This may be the cause of their lack of consideration in many response methods. Recombination when applied to peroxy radicals can produce peroxides ($\text{RF}\text{-OO}\cdot + \cdot\text{RF}' \rightarrow \text{RF}\text{-O-O-RF}'$), which have been hypothesized by Lutze et al. [141] but have not yet been identified.

In oxidative degradation methods, oxidizing species attack at PFOS's sulfonate head group will also start the decomposition process [189,190]. $\text{C}_8\text{F}_{17}\text{SO}_3\cdot$ will be generated following the loss of one electron from the PFOS head group (eq. 43). When reacting with water, the loss of one electron causes the C-S bond to stretch, which facilitates

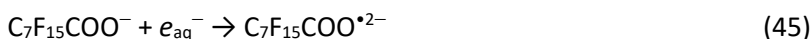
desulfurization and produces sulfate anions and perfluorinated alkyl radicals ($\cdot\text{C}_8\text{F}_{17}$) (eq. 44). C_8F_{17} will undergo the same conversion as PFOA, following the same chemical route as C_7F_{15} .

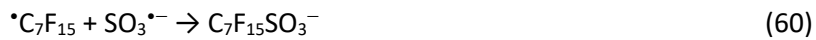
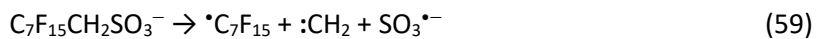
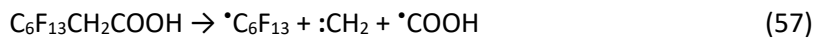
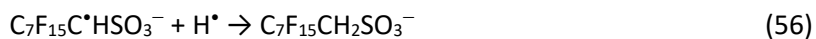
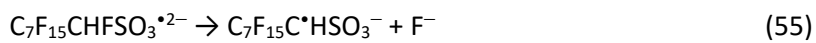
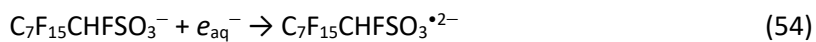
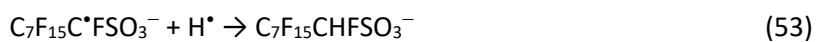
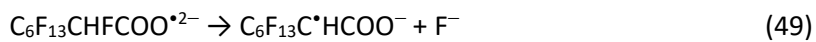
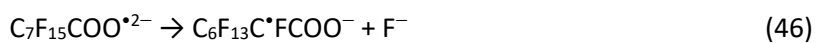


2.4.2 Reductive degradation pathway

The documented methods of reductive PFOA and PFOS breakdown are mostly hydrated electron-based. Degradation of PFOA or PFOS occurs via two main pathways: H/F exchange and decarboxylation/desulfurization[160]. In the first scenario, the hydrated electron preferentially targets the carbon on the PFOA or PFOS α -position. Following two successive H/F exchanges on the α -position, the relatively stable $\text{C}_6\text{F}_{13}\text{CH}_2\text{COO}^-$ (eqs. 45-50) or $\text{C}_7\text{F}_{15}\text{CH}_2\text{SO}_3^-$ (eqs. 51-56) are produced [191]. There's also a chance that further H/F exchange occurs in the middle CF_2 groups. PFOA and PFOS cannot, however, be completely defluorinated using this breakdown process. Moreover, some researchers claimed reactions 57–60 would further change the intermediates $\text{C}_6\text{F}_{13}\text{CH}_2\text{COO}^-$ and $\text{C}_7\text{F}_{15}\text{CH}_2\text{SO}_3^-$ to $\text{C}_6\text{F}_{13}\text{COO}^-$ and $\text{C}_7\text{F}_{15}\text{SO}_3^-/\text{C}_7\text{F}_{15}\text{COO}^-$, respectively [192,193].

PFOA and PFOS can also undergo desulfurization and decarboxylation when hydrated electrons attack their headgroups [194–196]. Following further radical reactions and hydrolysis, shorter-chain polyfluoroalkyl compounds (PFCAs) with one CF_2 unit less are generated. There were other suggested reaction paths, but they all seemed suspicious. It is for instance unclear what is the electronic state of the hypothetical intermediate dianion $\text{C}_7\text{F}_{15}\text{COO}^{*2-}$. Furthermore, there are still doubts regarding the availability of free $\text{H}\cdot$ radicals for the reductive saturation of fluorinated radicals in aqueous solution.





3 Materials and methods

3.1 Reagents and materials

All chemical reagents used here were of analytical grade and were used without further purification. Nanoscale zero-valent iron (nZVI, $\geq 99.5\%$ purity), Acid Blue 74 ($C_{16}H_8N_2Na_2O_8S_2$), Malachite Green ($C_{23}H_{25}ClN_2$), Rhodamine B ($C_{28}H_{31}ClN_2O_3$), sodium metabisulfite ($Na_2S_2O_3$), hydrogen peroxide (H_2O_2 , 30% w/w), H_2SO_4 (98%), glyphosate (GLY, $(OH)_2P(O)CH_2NHCH_2CO_2H$), NaOH ($\geq 97\%$), HCl (37%), sodium phosphate dibasic heptahydrate ($Na_2HPO_4 \cdot 7H_2O$), and sodium phosphate monobasic monohydrate ($NaH_2PO_4 \cdot H_2O$) were obtained from Sigma-Aldrich (Darmstadt, Germany). All solutions were prepared by using Milli-Q water (Elix-Milli-Q Academic system, Millipore-Merck, Vimodrone, Italy).

PFOA was purchased from Acros Organics (USA). 6:2 Fluorotelomer sulfonamide alkyl betaine (6:2 FTAB) was purchased as Capstone 1157 from Chemours (Meyrin, Switzerland). Methanol (CH_3OH) and ethanol (C_2H_5OH) were purchased from Merck (Darmstadt, Germany), and 2-propanol (C_3H_7OH) from VWR (Darmstadt, Germany). Butanol (C_4H_9OH), iron trichloride ($FeCl_3 \cdot 6H_2O$), and formic acid ($HCOOH$) were purchased from Merck (Darmstadt, Germany). L-Threoascorbic acid was purchased from VWR (Leuven, Belgium). H_2SO_4 was purchased from Roth (Karlsruhe, Germany) and LC-MS grade acetonitrile from VWR (Dresden, Germany). Ultrapure water (LC-MS grade) was generated in-house (Adrona Sia Crystal EX, Lithuania).

3.2 Experimental setup and degradation of dyes (Malachite green, Rhodamine B, Acid Blue 74) by Fenton-like processes

Some preliminary experiments were carried out to investigate the performance of Fenton-like processes with different dye solutions (Acid Blue 74, Rhodamine B, Malachite Green). The solution's pH (3-4) was adjusted using HCl/NaOH, while pH 5-6 was adjusted by means of a phosphate buffer. A suitable dye solution (Acid Blue 74, Rhodamine B, or Malachite Green) (100 mL) was taken in a 250 mL beaker with a magnetic stirrer. The beaker was placed on a stirring plate, the required amount of H_2O_2 was added and, subsequently, a suitable amount of nZVI was added from a

homogenous solution. After regular intervals, a sample was withdrawn from the reaction beaker and put into a 5 mL vial containing the same amount of methanol as the quenching agent. The residual dye concentration was measured with a UV-Vis spectrophotometer (Cary 100 Scan) at the wavelength of maximum absorption. In each experimental series the reaction pH was increased from acidic to near neutral conditions and pH > 4 was maintained using phosphate buffers. Moreover, in some experiments H₂O₂ was replaced by sodium metabisulfite (Na₂S₂O₃) to investigate the degradation of Acid Blue 74 by nZVI-metabisulfite (Fenton-like system). The remaining procedures were followed as described earlier.

3.3 Experimental setups and analysis for GLY removal

All experiments were performed at room temperature (20–22 °C), and the initial pH values were adjusted using dilute solutions of sulfuric acid (see below for the choice of H₂SO₄). In a typical experiment, 1 L of ultra-pure water containing 2 mg/L GLY was placed in a 1.2 L beaker. The value of the pH was monitored with a Checker pH meter (Hanna Instruments, Woonsocket, RI, US), and it was adjusted whenever required using diluted H₂SO₄. The required amounts of directly weighed (or pipetted) nZVI and H₂O₂ were added to an already-prepared 2 mg/L GLY solution, and the whole system was then magnetically stirred for 1 h of reaction time (longer times would be uninteresting within the framework of water treatment). After 1 h, a few mL of the sample were withdrawn, filtered (nylon 0.45 µm, VWR, Radnor, PE, USA), and injected into an ion chromatograph (Thermofisher-Dionex DX-100, Sunnyvale, CA, USA) equipped with a 200 µL loop, using 17 mM NaOH as the eluent. GLY was separated and detected with an IonPac AS16 column (250 × 4 mm, Thermofisher-Dionex, Sunnyvale, CA, USA), a Dionex ASRS 4 mm membrane suppressor, and a conductivity detector using isocratic elution. The same experimental procedure was adopted to check for the adsorption efficiency of GLY using nZVI, with the exception that H₂O₂ was not added in this case. All experiments were conducted in triplicate.

The concentration of dissolved iron leached during the nZVI–Fenton treatment was determined via inductively coupled plasma–optical emission spectroscopy (ICP–OES,

Agilent 5100, Santa Clara, CA, USA). The emission of atomic Fe was quantified at 238.204 nm, and the Fe-detection limit with this technique was at the level of $\mu\text{g/L}$. By comparison, the limit for Fe in wastewater is 4 mg/L according to the Italian law [Law decree 152/06].

In tap-water experiments, tap water (from Turin, Italy) was spiked with GLY to achieve the desired 2 mg/L concentration. Then, the same procedure described earlier was followed, but conductivity was also monitored throughout the reaction. Common inorganic anions in tap water were determined via suppressed anion chromatography.

Before deciding how to adjust pH, preliminary experiments were performed to minimize chromatographic interferences of acids (HClO_4 , HCl , H_2SO_4) and buffers (phosphate, acetate) with the detection of GLY. Chromatographic interference was observed between GLY and HClO_4 , which was thus excluded. Although chloride did not interfere with GLY detection, HCl was not chosen because of the ability of chloride ions to scavenge HO^\bullet in acidic solution [197,198]. Phosphate buffer was not selected owing to the very close elution of phosphate and GLY, caused by the similar selectivity usually exhibited by chromatographic columns for these anions. Acetate buffer was tested, but excluded due to ineffectiveness (the orange-red Fe^{2+} -acetate complex is possibly unreactive in the framework of $\text{nZVI} + \text{H}_2\text{O}_2$). Therefore, H_2SO_4 was finally selected to adjust pH, also in consideration of the high chromatographic resolution between sulfate and GLY ions.

Ion chromatography (IC) was chosen because GLY is easily ionized and detected by conductimetry, while its functional groups are poor chromophores. Moreover, phosphate is a degradation product of GLY and it is also easily detected by IC. Also, the effects of other anions (Cl^- , SO_4^{2-} , NO_3^- , NO_2^-) were studied and these ions can easily be detected by IC with different retention time. Moreover, the selection of different acids (HClO_4 , HCl , H_2SO_4) and buffers (acetate, phosphate) were done to minimize their chromatographic interferences. Last but not least, IC is robust,

reproducible, can handle complex matrices and requires minimum sample preparation.

3.4 Experimental setup and photolysis of PFOA and 6:2 FTAB

In our UV irradiation experiments, a 150 W medium pressure mercury lamp (TQ 150, Heraeus Noblelight, Germany) was used, which has wavelength range from 190 to 600 nm and emission maximum at 366 nm. The system configuration has been described earlier as open system configuration 1 (open quartz-glass vessel) with an outer cooling jacket [199], and is here shown in Figure 3.1. Light intensity was determined by chemical actinometry.

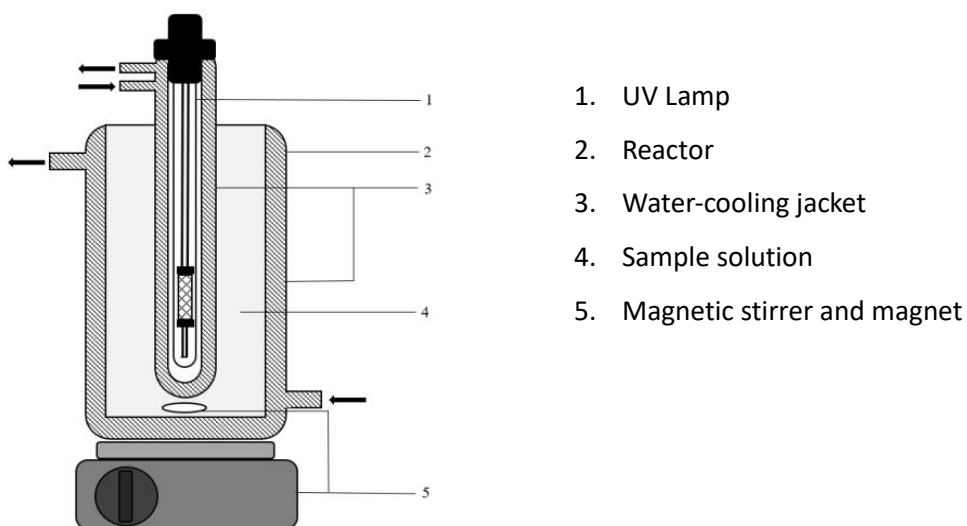


Figure:3.1 System Configuration 1 with outer cooling jacket.

3.4.1 Actinometry: Determination of Iron (II) and total Iron content

The determination of iron (II) and the total iron concentration was based on the House method according to Balcke (cf. Jensch, 2015 according to UFZ Leipzig). In detail, a potassium tris oxalate-ferrate complex ($K_3[Fe(C_2O_4)_3] \cdot 3H_2O$) that is light-sensitive was synthesized. The entire synthesis process was done in the dark. First, 50

mL of ultrapure water was used to dissolve 60 mM KHC_2O_4 . Then, 50 mL of ultrapure water was used to dissolve 20 mM $\text{FeCl}_3 \cdot 6\text{H}_2\text{O}$. The two solutions were combined for 30 min at room temperature and 500 rpm of steady stirring in the dark. The solution was kept at 4 °C for crystallization overnight. The resulting ferrioxalate complex crystals were dried for an entire night at 35 °C before being placed on a cellulose acetate filter with a pore size of 0.45 μm (Sartorius, VWR, Dresden, Germany) to eliminate water traces by vacuum filtration. Before usage, the dried ferrioxalate complex was kept in a vial with light protection. Actinometry was carried out using 7.5 mM ferrioxalate complex dissolved in ultrapure water that had been acidified (0.05 mol L^{-1} H_2SO_4). After every 20 seconds, samples were taken from under the lamp (vide infra) obtained. It was discovered how much ferrous iron (Fe^{2+}) was released [200].

The basic principle of iron (II) determination is based on the selective reaction of dissolved iron (II) ions with complexing agents such as ferrozine to form a violet complex. The addition of ascorbic acid reduces the iron(III) contained in the sample so that total iron determination is made possible. The difference in the amount of absorption with and without the addition of ascorbic acid is proportional to the content of iron(III) ions, which can be calculated according to eq.61:

$$C_{(\text{Fe}^{3+})} = C_{(\text{Fe total})} - C_{(\text{Fe}^{2+})} \quad (61)$$

To determine the iron (II) concentration, 2 mL of a sample solution is mixed with 2 mL of the required detection reagent. This is achieved by adding 50 mg of 3-(2-pyridyl)-5,6-diphenyl-1,2,4-triazine-4',4''-disulfonic acid monosodium salt to a buffer solution containing 200 mM citric acid and 200 mM trisodium citrate (pH 4.6). As mentioned above, the total iron content of the sample is determined upon addition of 100 μL of a 10% ascorbic acid solution. The photometric measurement is made after 90 minutes at the wavelength of 562 nm. The measuring range is in the interval of 0.1-5 mg/L. Because of higher iron contents, the sample was diluted. Figure 3.2 shows the time trend of Fe(II), Fe(III), and total Fe during the actinometry measurements.

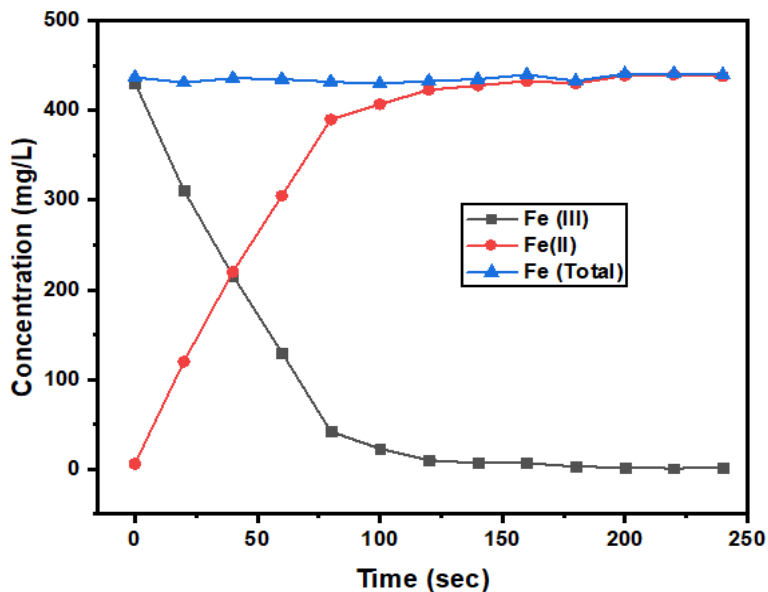


Figure:3.2 Concentration of Fe (II), Fe (III), and Fe (total).

This lamp we used produced an incident photon flux of $(3.81 \pm 0.19) \times 10^{-5} \text{ E sec}^{-1}$, according to actinometry results using $P_e = a N_A h c / \lambda$, where P_e is radiation flux, a is incident photon flux, N_A is Avogadro's Number ($6.022 \times 10^{23} \text{ mol}^{-1}$), h is Planck's constant ($6.63 \times 10^{-34} \text{ Js}$), c is speed of light ($3 \times 10^8 \text{ m/s}$) and λ is 366 nm, which corresponds to a light intensity of $1.24 \pm 0.1 \text{ mW cm}^{-2}$ (calculated by $I(\lambda=366 \text{ nm}) = P_e \times 100 / A = P_e v / 100 / \pi \cdot D \cdot H$, where $D=6 \text{ cm}$ and $H=19.5 \text{ cm}$).

In irradiation experiments, a magnetic stirrer was used for continuous mixing of the solution. The pH of the treatment solutions was adjusted by adding either ammonia or formic acid before the UV treatment. The temperature in the reactor was kept between 20-25°C throughout the experiment. All UV treatments were carried out using either PFOA or 6:2 FTAB (1 mg L^{-1}) in a total reactor volume of 320 mL. The UV lamp was turned on 10 to 15 min before each experiment. Samples (5 mL) were collected at $t = 0$ and subsequently at 15-minute intervals for 180 min, then at 30-minute intervals for a further 180 min (i.e., total treatment time 360 min).

3.4.2 Radical scavenging experiments

Scavenger experiments were carried out with either PFOA (pH 5.6) or 6:2 FTAB (pH 6.5). A concentration of 0.3 M alcohols or 0.3 mM ascorbic acid was used to scavenge reactive species and, whenever required, the scavenger was added before the UV treatment. Samples were collected at the starting point and, afterward, at 15-minute intervals for 180 min followed by 60-minute intervals up to 180 min, for a total of 360 min (180 min + 180 min). All tests were performed in triplicates. Liquid samples were analyzed by LC-MS for either PFOA or 6:2 FTAB and their transformation products (TPs). The release of fluoride and sulfate ions was analyzed by ion chromatography (IC).

3.4.3 Quantification of PFOA, 6:2 FTAB, and their TPs by LC-MS

PFOA and potential TPs were identified and quantified by analyzing the samples with liquid chromatography-electron spray ionization-mass spectrometry (LC-ESI-MS), using an LC-MS-IT-TOF system from Shimadzu (Tokyo, Japan). The instrument was equipped with (Shimadzu) LC Spectral System P4000, LCQ MS Detector, and Autosampler AS 3000. A 10 μ L aliquot of each sample was injected into the LC system. The sample was separated using an Ultra AQ C18 column (150 x 2.1 mm, 3 μ m/200 \AA , Restek, USA). The column temperature was 35°C and the flow rate was constant at 0.2 mL min⁻¹. Linear gradient elution was performed with solvent A (0.1% formic acid in ultra-pure water) and solvent B (0.1% formic acid in acetonitrile). The analysis was run for 35 min with the following gradient: 20% B for 3 min, then up to 60% B in 1 min and held for 15 min, then up to 80% B in 1 min and held for a further 5 min, and finally back to 20% B in 3 min and held for another 7 min. The MS detector settings were as follows: negative ionization at 1.7 kV, capillary spray temperature of 220 °C, and 10 msec ion accumulation time. In scan mode, the mass-to-charge ratio (m/z) was measured in the 150 – 750 range. In SIM mode the following m/z ratios were measured: 569.0785, 426.9742, 412.9682, 362.9699, 312.9731, 262.9762, and 212.9887, corresponding to 6:2 FTAB, 6:2 FTSA, PFOA, PFHpA, PFHxA, PFPeA, and PFBA, respectively. For quantification, sample volumes of 1 mL were mixed with 10 μ L internal standard (¹³C8 PFOA/¹³C8 PFOS, Cambridge Isotopes, US). Calibration was

done with the multi-component standard ITA-70 (5 to 200 $\mu\text{g L}^{-1}$, Agilent Technologies, USA).

3.4.4 Fluoride and sulfate measurement by ion chromatography

UV-treated samples were analyzed for fluoride release using a DX-120 ion chromatograph (IC) (Dionex, CA, USA) equipped with an IonPac AS22 column (250 \times 4 mm, Dionex, CA, USA) and a Dionex ASRS 4 mm membrane suppressor for suppressed ion conductivity detection. A total volume of 20 μL was injected into the IC system by using autosampler Gynkoteck GINA 50 (Germering, Germany) equipped with a 20 μL loop, using 4.5 mM NaCO_3 and 1.4 mM NaHCO_3 as the eluent. Fluoride and sulfate were eluted at retention times of 2.8 min and 11.9 min, respectively.

3.4.5 Dissolved oxygen and hydrogen peroxide measurements

Preliminary experiments were performed to monitor the consumption of dissolved oxygen (DO) and release of H_2O_2 during UV treatment of PFOA. DO was measured by an optical dissolved oxygen sensor (Fibox 3 minisensor oxygen meter from PreSens, Regensburg, Germany). The potential release of H_2O_2 was measured by the DPD (N, N-diethyl-p-phenylenediamine) method.

3.4.6 Data evaluation

We assumed the PFAS degradation was a pseudo-first-order reaction of the parent compound according to equation (62), where k is the rate constant (s^{-1} or min^{-1} , depending on the time units used), t is the time (in seconds or minutes, depending on the time units used), \ln represents the natural logarithm, A_0 is the initial concentration of the PFOA or 6:2FTAB in mg/L , and A_t is the concentration of the PFOA or 6:2 FTAB at time interval t .

$$k = 1/t \ln(A_0/A_t) \quad (62)$$

The half-life of the reaction has been calculated by the following equation (63).

$$t_{1/2} = \ln 2/k \quad (63)$$

where $t_{1/2}$ is the half-life time of the reaction and k is the rate constant of the reaction according to the time units used.

The percentage degradation efficiency has been calculated by the following equation (64).

$$\text{Degradation efficiency} = C_t/C_o \times 100 \quad (64)$$

For Fluoride release measurements, the percentage was calculated by using the formula given below in equation (65).

$$\% \text{age fluoride release} = C_t/C_{\text{max}} \times 100 \quad (65)$$

4 Results and Discussions

4.1 Dyes removal

To investigate the performance, efficiency, and degradation of dyes, a heterogeneous Fenton-like system was evaluated using different loadings of nZVI and H₂O₂ (or metabisulfite) at different pHs. These are preliminary experiments, and dyes were used as a fast and easily detectable tool to check for conditions that led to better or scarcer degradation performance. Preliminary results were later used to adjust the conditions for GLY removal.

Different dyes were tested using different loadings of nZVI-H₂O₂ at different pH values, with the goal of achieving extensive dye degradation. Here in Figure 4.1, we observed the reaction is fast and AB74 (C₀=10μM) was degraded within 5-10 minutes at pH 3 and 4, in the presence of 10 mg/L nZVI and 50 μM H₂O₂. However, AB 74 did not show fast removal at pH 5 with the same nZVI/H₂O₂ loadings.

At lower pH, the Fenton process works efficiently but, as far as we go beyond acidic pH the efficiency of Fenton is minimized and we need to add more chemicals to optimize the removal efficiency. At pH 3, it is clearly seen that there is complete removal of AB74. At pH 4 the Fenton process worked more or less similarly to pH 3. At pH 5 the removal efficiency was reduced significantly.

An alternative strategy, proposed by Minella et al. (2019) and consisting in stepwise addition of H₂O₂ was followed. This procedure allows for the use of a relatively high overall amount of H₂O₂ (thus, with sufficiently high total amount of generated HO^{*}), at the same time minimizing HO^{*} scavenging by H₂O₂ itself. The rationale is that H₂O₂ gets progressively degraded as the reaction goes on and, if H₂O₂ is added stepwise, it never reaches excessive concentration values at any time point [201]. In Figure 4.2 we can observe a significant removal of AB74 at pH 5-6 by stepwise addition of H₂O₂. The optimized amounts were 20 mg/L of nZVI with 50 μM initial H₂O₂ + 5 μM H₂O₂ added after every 10 minutes. The reactions were monitored for one hour.

In figure 4.2 the degradation of AB74 was initially faster at pH 6 than at pH 5 but then slowed down. It is possible that, compared to pH 5, reaction between ZVI and H₂O₂ is

faster at pH 6, but the recycling of Fe species for the Fenton reaction is slower. This issue could explain the different time trends of AB74 degradation at the two pH values.

ZVI-Fenton degradation was also studied with additional dyes, to see if and to what extent the results obtained with AB74 could be generalized and to find which dye was most reactive under Fenton conditions.

The removal of Malachite Green (MG, $C_0=3 \mu\text{M}$) at pH 3-4 by nZVI (10-20 mg/L) with 50-100 μM of H_2O_2 is shown in Figures 4.3 and 4.4. The removal of MG at pH 3 was faster as compared to pH 4. As we proceeded from acidic to near-neutral pH, the loadings of reagents (nZVI, H_2O_2) had to be increased because a Fenton-like system works efficiently at acidic pH. Removal of MG was also optimized with different loadings of nZVI and H_2O_2 at pH ≈ 5 (Figure 4.4). We observed maximum removal of MG with nZVI (60 mg/L) and H_2O_2 (100 μM). At pH 6, the optimized amounts were 60 mg/L nZVI and 50 μM H_2O_2 (Figure 4.5).

In the case of Rhodamine B (150 μM), higher initial concentration was used and we observed significant removal with nZVI (10 mg/L) and H_2O_2 (50-100 μM) at pH 3-4 (Figure 4.6). However, the direct addition method did not work in case of pH 5-6, in which case we used the stepwise addition method to remove Rhodamine B. The optimized loadings were 20-50mg/L nZVI and, as per H_2O_2 , 50 μM initially +5 μM added after every 10 minutes (Figure 4.7).

Degradation of these dyes using the Fenton process was successful, and we decided to study the performance of the system while replacing H_2O_2 with metabisulfite as alternative reagent.

Of all dyes (Rhodamine B, Malachite Green, Acid Blue 74), AB74 proved to be a very suitable model compound to allow for the study and optimization of Fenton-like degradation conditions. For this reason, it has been used to optimize the nZVI-metabisulfite system towards degradation. In Figures 4.8-4.10 we show the removal of AB74 ($C_0=10 \mu\text{M}$) by different loadings of nZVI-metabisulfite, which were: at pH 3,

0.01 g/L nZVI and 150 μM $\text{Na}_2\text{S}_2\text{O}_5$; at pH 4, 0.01 g/L nZVI and 150 μM $\text{Na}_2\text{S}_2\text{O}_5$; at pH 5, 0.02 g/L nZVI and 100 μM $\text{Na}_2\text{S}_2\text{O}_5$ (unstable system); at pH 6, 0.02 g/L nZVI and, initially, 300 μM $\text{Na}_2\text{S}_2\text{O}_5$. Then, stepwise addition of 15 μM $\text{Na}_2\text{S}_2\text{O}_5$ was carried out after every ten minutes.

The studied dyes were efficiently degraded by Fenton-like systems (either nZVI- H_2O_2 or nZVI-metabisulfite). It was deduced from these results, that these Fenton-like systems could be explored and implemented for the removal of persistent organic pollutants like GLY at different pH values.

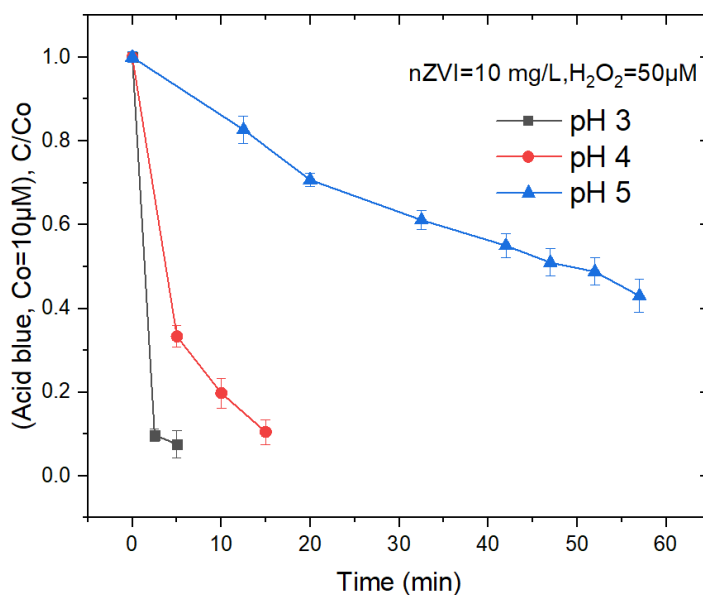


Figure:4.1 Removal of Acid blue 74 by nZVI- H_2O_2 at pH 3-5

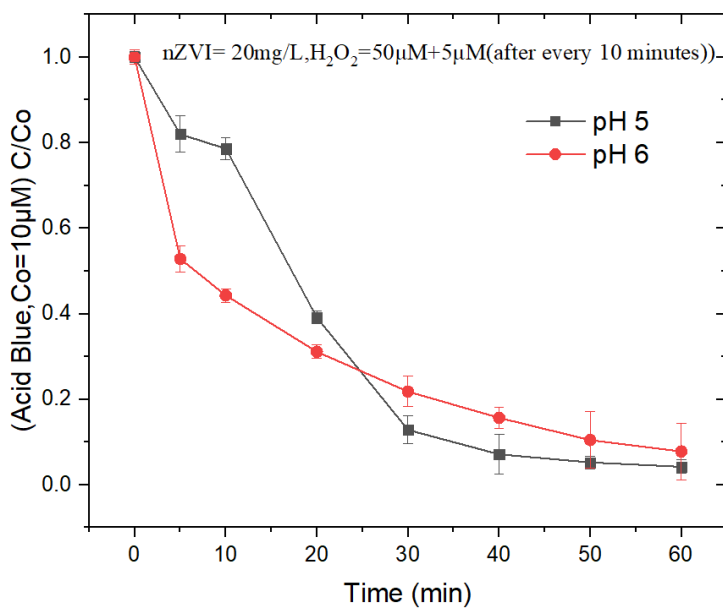


Figure:4.2 Removal of Acid blue 74 by nZVI-H₂O₂ at pH 5-6 by stepwise addition method

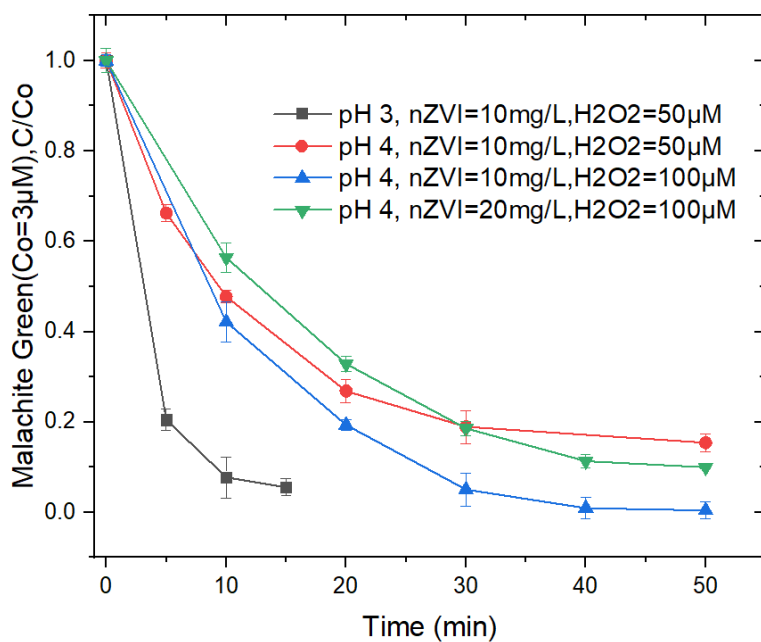


Figure:4.3 Removal of Malachite Green at pH 3-4 by nZVI (10-20 mg/L) and H₂O₂ (50-100 µM)

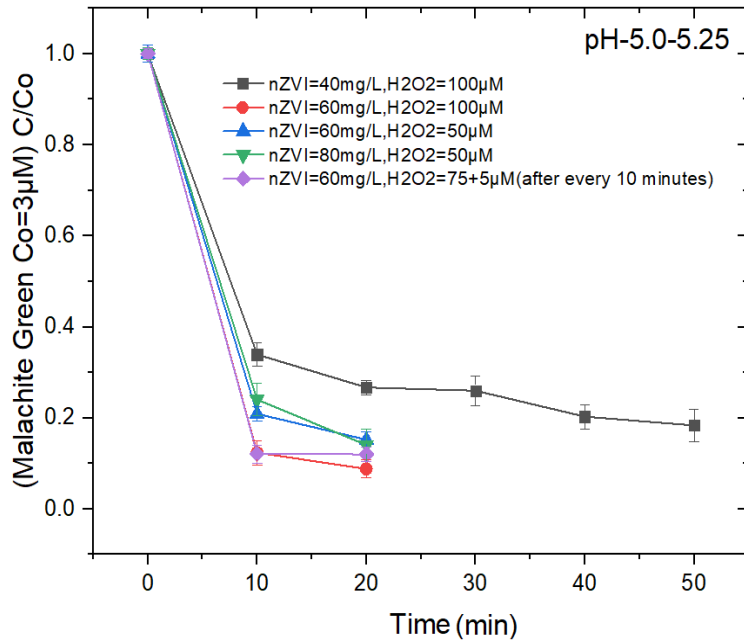


Figure: 4.4 Removal of Malachite Green at \approx pH 5 by nZVI (40-60 mg/L) and H₂O₂ (50-100 μ M)

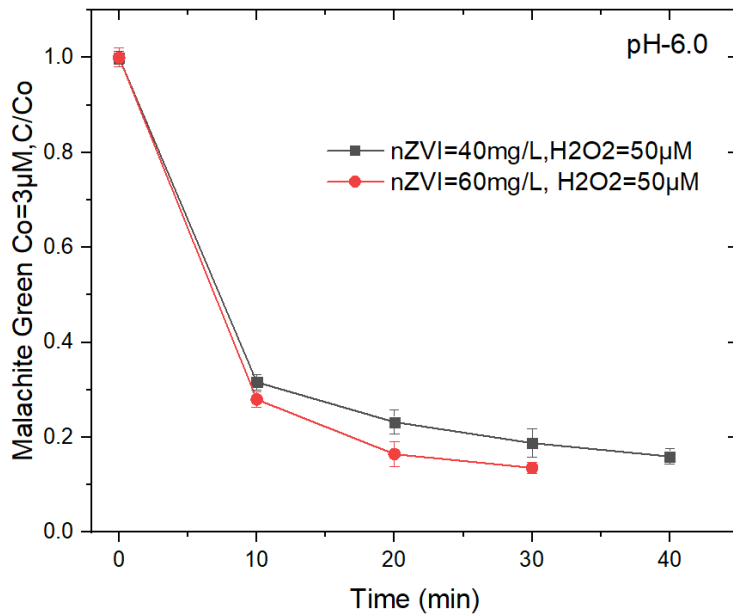


Figure: 4.5 Removal of Malachite Green at pH 6 by nZVI (40-60 mg/L) and H₂O₂ (50 μ M)

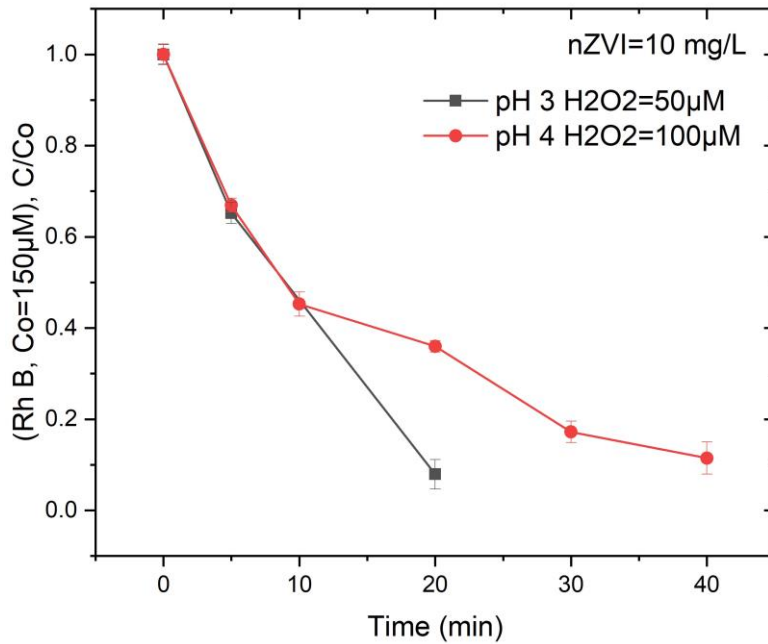


Figure: 4.6 Removal of Rhodamine B at pH 3-4 by nZVI (10 mg/L) and H₂O₂ (50-100µM)

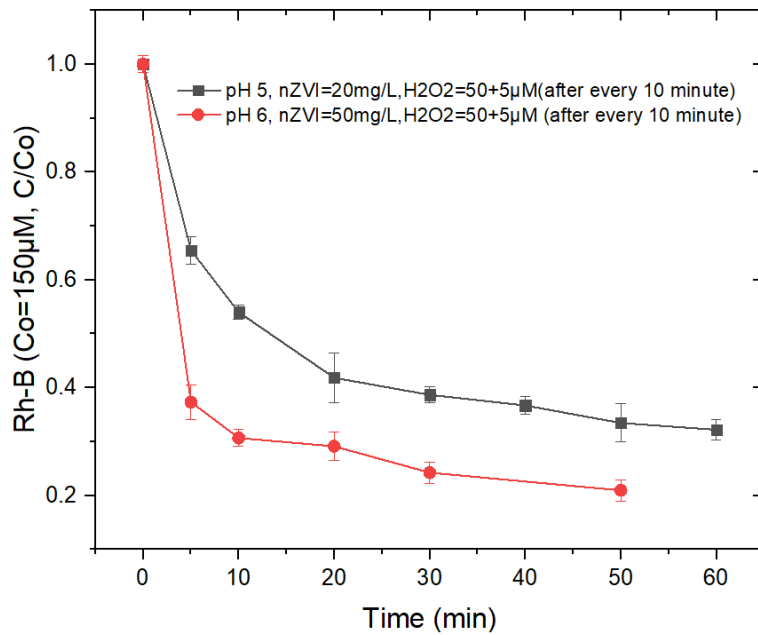


Figure:4.7 Removal of Rhodamine B at pH 5-6 by nZVI (20-50mg/L) and H₂O₂ (50µM initially +5 µM after every 10 minutes).

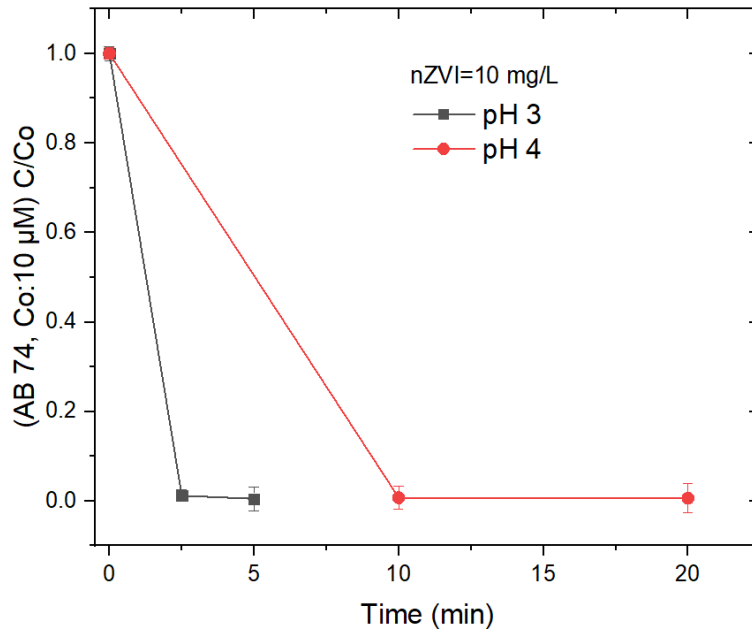


Figure :4.8 Removal of Acid Blue 74 at pH 3-4 by nZVI (10 mg/L) and metabisulfite/MBS (50μM)

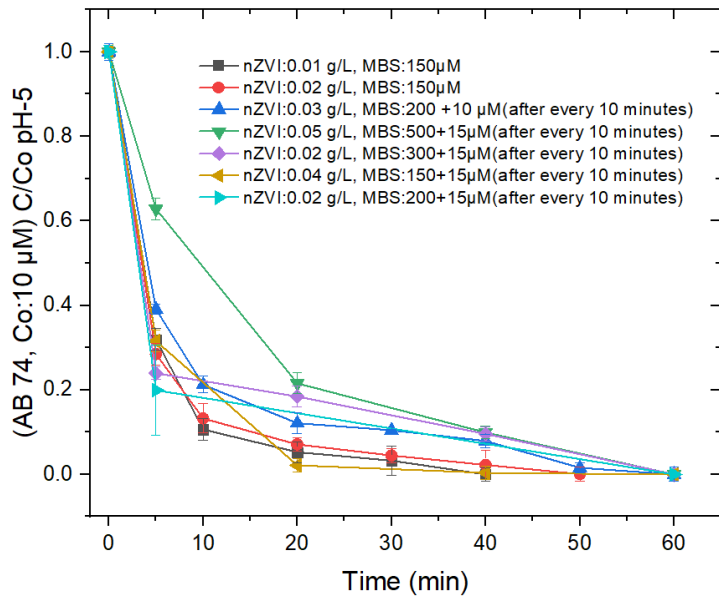


Figure:4.9 Removal of Acid Blue 74 at pH 5 by nZVI (0.01-0.05g/L) and Na₂S₂O₅ (150-500 μM) (unstable system).

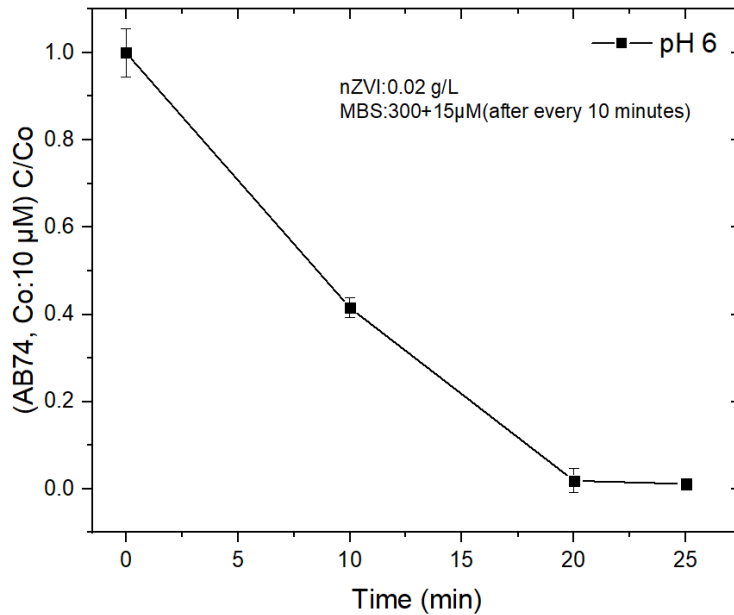
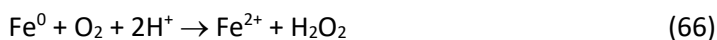


Figure:4.10 Removal of Acid Blue 74 at pH 6 by nZVI (0.02g/L) and Na₂S₂O₅ (300 μM initially +15 μM added after every 10 min).

4.2 Glyphosate (GLY) removal

All experiments were performed for 60 minutes reaction time. To optimize the concentrations/loadings of nZVI and H₂O₂, several experiments were performed at different pH values to investigate GLY degradation efficiency. Preliminary experiments with nZVI + H₂O₂ at pH 3 were carried out to highlight Fenton degradation (Fig. 4.11). The loading of nZVI (varied in the range of 0.001-300 mg/L) was optimized while minimizing GLY removal by nZVI alone (which could involve adsorption at least in part, Fig. 11b). Indeed, although complete GLY removal could be achieved by using 300 mg/L nZVI without H₂O₂ (Fig. 11b), such a high nZVI loading would be impractical in water-treatment applications, due to elevated costs of chemical reagents (300 mg/L nZVI would cost around 0.24 \$/m³; [202]).

Note that adsorption is not the only phenomenon that could account for the removal of GLY shown in Fig. 11b. Indeed, the nZVI-Fenton process could be activated by O₂ alone, without H₂O₂, with the generation of both Fenton reactants [203] (eq.66):



The minimum tested amount of nZVI (0.001 mg/L) was effective at minimizing adsorption, but it did not induce effective GLY degradation in the presence of H₂O₂. Moreover, such low loading could not be obtained by direct weighting but rather by dilution of a stock nZVI suspension. Presumably due to the difficulty in making the stock suspension fully homogeneous, the system lacked reproducibility in results. Therefore, compromise loadings (10 mg/L, i.e., the lowest loading that could be achieved by direct weighting, or 20 mg/L) were chosen for nZVI.

4.2.1 GLY removal at pH 3

As shown in Fig. 4.11a, complete GLY removal could be achieved at pH 3 by using 10 mg/L nZVI and 300 μM H₂O₂. However, by using a lower amount of H₂O₂ (50-200 μM), complete GLY removal was not observed as the removal efficiencies were 55-96%. Here, a constant amount of nZVI (10mg/L) along with variable concentrations of H₂O₂ (50-200 μM) produce different amounts of HO[•] which in turn degrades GLY. Lower H₂O₂ concentrations were less effective, most likely because of lower hydroxyl radical (HO[•]) generation when H₂O₂ is low. Higher H₂O₂ concentrations (>300 μM) were not tested because their use would increase treatment costs (300 μM H₂O₂ would cost around 0.009 \$/m³; [202]) and because effectiveness would decrease, at a certain point, due to HO[•] scavenging by H₂O₂ itself (eq. 67) [197]:



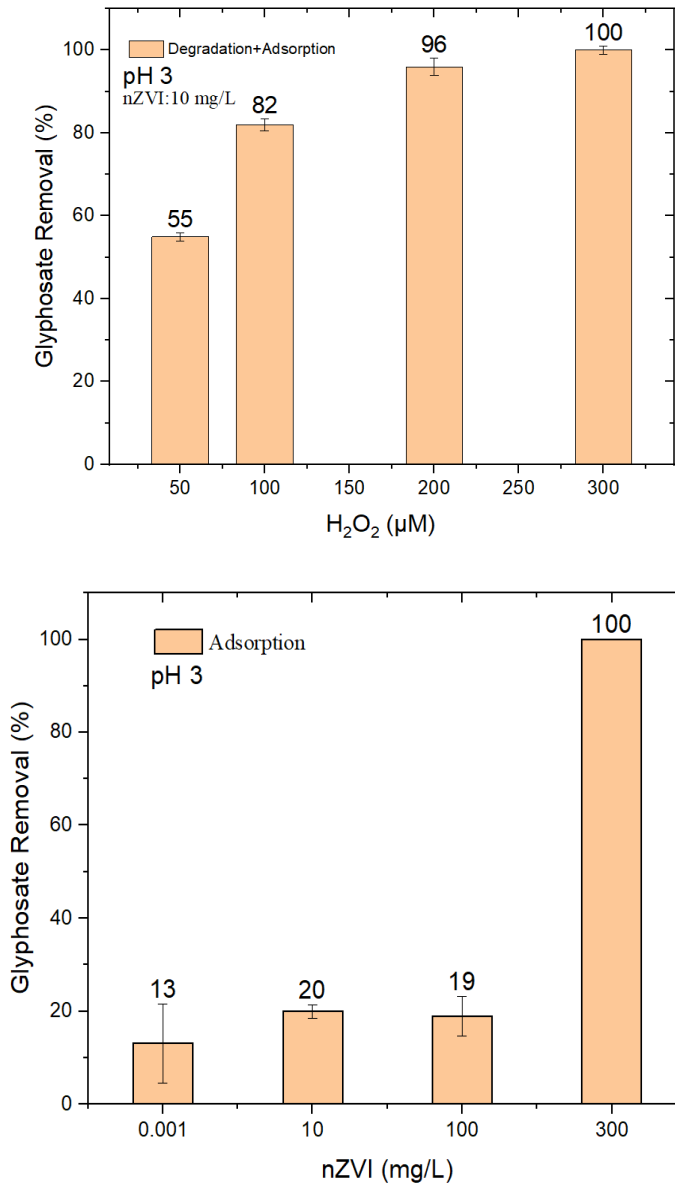
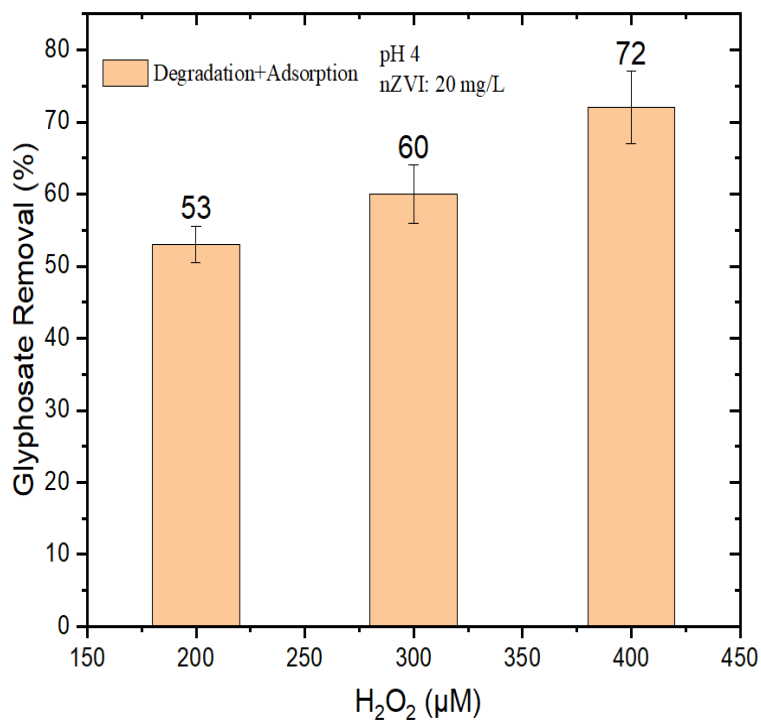


Figure 4.11. (a) Effect of H₂O₂ concentration (50-300 μM) on GLY removal by nZVI-Fenton at pH 3, at optimized nZVI loading (10 mg/L, to minimize adsorption). Reaction time (60 minutes). **(b)** GLY removal by different amounts of nZVI alone, without H₂O₂, at pH 3. The error bars represent the standard deviation of triplicate experiments. Reaction time: 60 minutes.

4.2.2 GLY removal at pH 4

It was not possible to achieve satisfactory GLY removal at pH 4, in the presence of 10 mg/L nZVI + H₂O₂. For this reason, higher loadings of nZVI (20 -40 mg/L) were tested, but adsorption of GLY on nZVI alone (i.e., without H₂O₂) was also checked. Limited adsorption was observed with 20 mg/L nZVI, which was then used to perform further degradation experiments at different concentrations of H₂O₂ (200-400 μM). However, as shown in Fig. 4.12a, the maximum GLY removal by nZVI + H₂O₂ was at most only 72% when using 400 μM H₂O₂ at pH 4.

As described earlier, stepwise addition has been shown proven to be better than direct addition by Minella et al. By adding 150 μM of H₂O₂ at the beginning, plus an additional 50 μM at 30 minutes after the start of the reaction, we obtained 87% GLY removal with 20 mg/L nZVI at pH 4 (Fig. 4.13).



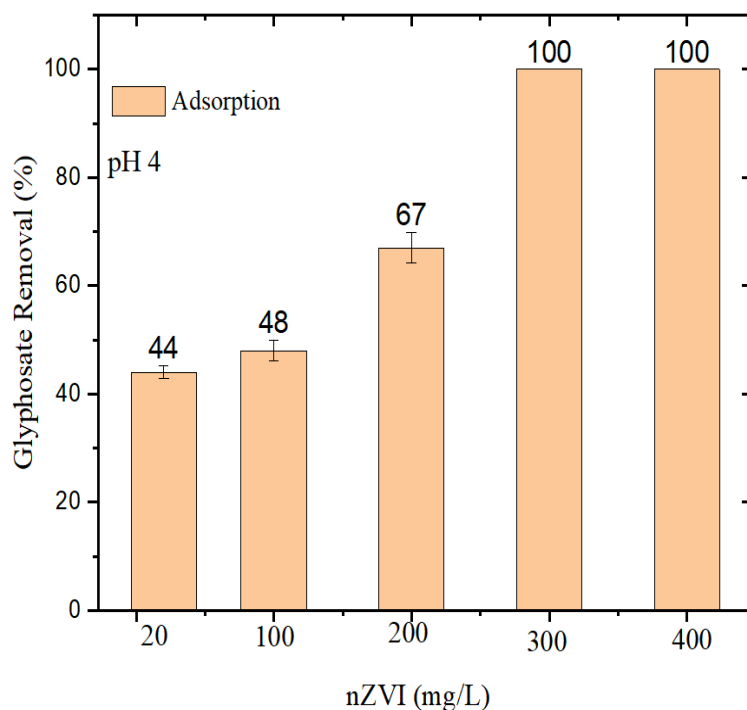


Figure 4.12. (a) GLY removal (%) by nZVI (20 mg/L) and H₂O₂ (200-400μM) at pH 4. **(b)** GLY removal at pH 4 by nZVI alone (different loadings). Reaction time: 60 minutes.

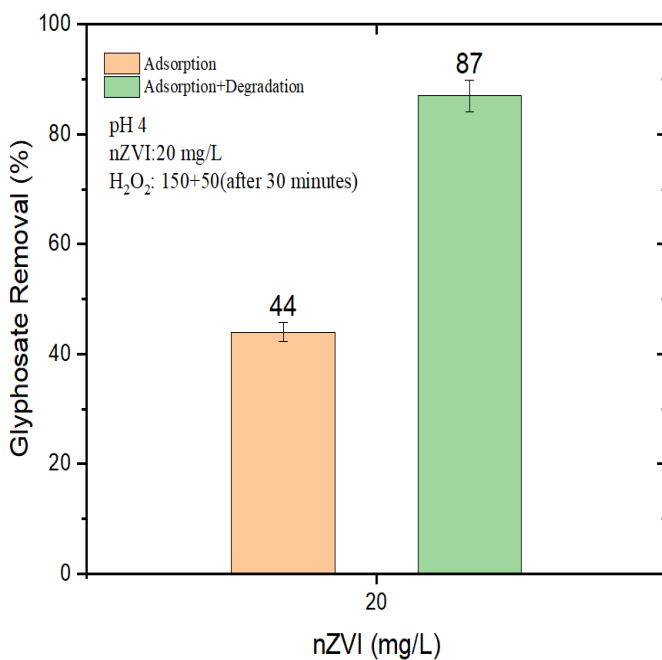


Figure 4.13. GLY removal (%) by nZVI (20 mg/L) and H₂O₂ (150 μM at t = 0 + 50 μM at t = 30 min) at pH 4. Reaction time: 60 minutes.

4.2.3 GLY removal at pH 5 and 6

Several combinations of nZVI loading (10-30 mg/L) and H₂O₂ concentration, including multiple additions of different amounts of the latter, were tried to remove GLY at pH 5 and 6 by nZVI-Fenton. However, no GLY degradation at all was observed under any conditions. The most likely explanation is the decrease in efficiency of the Fenton reaction with increasing pH (and of the nZVI-Fenton one as well [201,202]).

4.2.4 GLY removal in tap water

GLY removal was then studied in GLY-spiked tap water at pH 3 and 4 (pH was adjusted by H₂SO₄; the original tap-water pH was 7.6-7.7), starting with the loadings/concentrations of nZVI and H₂O₂ already optimized in ultra-pure water. At pH 3, with 10 mg/L nZVI and 300 μM H₂O₂, the GLY removal efficiency achieved 80%. Unfortunately, it was not possible to improve these removal percentages, even by employing the stepwise addition method or different initial concentrations/loadings of the Fenton reagents (GLY removal ranged between 54-76%). The lower GLY removal in tap water, compared to ultra-pure water, might be tentatively ascribed to the presence of common inorganic anions in tap water (Cl⁻, SO₄²⁻, NO₃⁻, NO₂⁻) (see Table 4.1). Some anions, and especially chloride, can scavenge HO• to produce different reactive transient species that are, however, significantly less reactive than HO• itself [197], thereby lowering the nZVI-Fenton efficiency [18]. Furthermore, scavenging of HO• by H₂O₂ would become comparatively less important in tap water that already contains HO• scavengers, thereby decreasing the effectiveness of the stepwise H₂O₂ addition method.

Very interestingly, it was possible to achieve 100% GLY removal in tap water at pH 4 by using 20 mg/L nZVI, 150 μM of H₂O₂ at the beginning of the reaction, plus an additional 50 μM at 30 minutes' reaction time. Complete removal of GLY was achieved in 40 minutes, and degradation at 30 minutes was around 66% (Fig. 4.14). Possible reason for the better performance of nZVI-Fenton at pH 4 compared to pH 3 is that the reaction rate between chloride and HO• decreases with increasing pH, because the HO• + Cl⁻ reaction step becomes partially reversible [197].

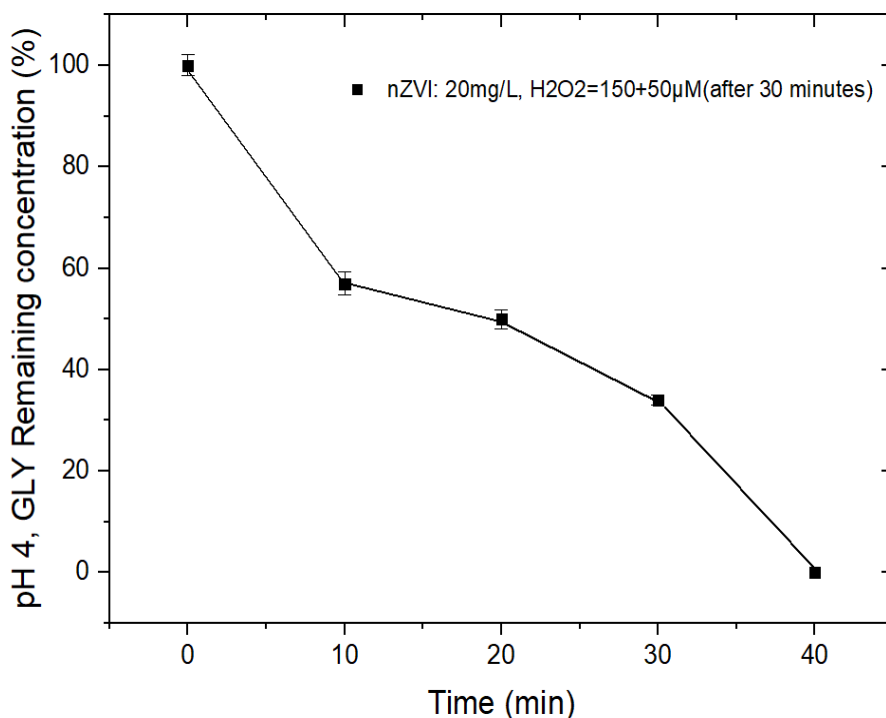


Figure 4.14. Kinetics of GLY removal at pH 4

The pH and conductivity values of GLY-spiked tap water were monitored during nZVI-Fenton treatment. Interestingly, initial tap-water conductivity was around 0.5-0.55 mS/cm, and it increased to around 0.6 mS/cm upon acidification to pH 4. A further increase by ~0.1 mS/cm units is expected to take place in the final neutralization step, intended to bring pH to at least 6 to allow for discharge in the environment. Despite the conductivity increase, it would still be possible to reuse treated water in several fields, including some of the most demanding in terms of water conductivity (e.g., agriculture [204]). The pH value was reasonably stable during the reaction (4.0-4.3). Leached iron was quantified as well: the concentration of dissolved Fe was undetectable before treatment and amounted to 2.5 mg/L at the end of the treatment. This means that around 12% of the initially added nZVI (20 mg/L) underwent dissolution at pH 4. When compared with Fe wastewater limits (4 mg/L according to the Italian law), a dissolved Fe concentration of 2.5 mg/L suggests that treated water could be safely discharged, without the need for additional steps of iron removal (except easy magnetic separation of nZVI).

Under optimal conditions in tap water (pH 4, 20 mg/L nZVI, 150 + 50 μ M H₂O₂), the GLY removal capacity of nZVI-Fenton can be calculated as at least 100 mg_{GLY}/g_{nZVI}. This value exceeds the capacity of adsorption systems based on metals having high complexation capabilities towards P-containing ligands [205] and, to an even higher extent, the adsorption capacity of activated carbon [206], which is a widespread adsorbent used in the tertiary treatment of any potabilization facility. Therefore, the studied Fenton-like process appears to make better use of the solid reagent compared to adsorptive techniques.

On these premises, a preliminary and partial estimate of the costs of the nZVI-Fenton process could be carried out, in the framework of expenditure in chemical reagents per m³ of treated water. This estimate is significant, in that reagents are a major expenditure in Fenton treatments [207]. Cost estimates are 0.016 \$/m³ for 20 mg/L nZVI, and 0.006 \$/m³ for 200 μ M H₂O₂ (i.e., 150 μ M + 50 μ M; [202]). The cost of H₂SO₄ can be estimated by carrying out tap-water titration, and by measuring the amount of H₂SO₄ that is required to adjust water pH to any given value (pH 4 in the present case, see Fig. 15). On this basis, one can conclude that the adjustment of pH to 4 would require 1.8 mol H₂SO₄ m⁻³, which translates into a cost of 0.041 \$ m⁻³ for H₂SO₄ [202]. Moreover, again based on water titration data, one would also need 1 mol CaO m⁻³ to finally adjust pH to at least 6 for eventual discharge or reuse, which entails an added cost of 0.0067 \$ m⁻³ [202]. Overall, the elimination of GLY from water with the ZVI-Fenton technique at pH 4 would cost 0.070 \$ m⁻³ in chemical reagents. By comparison, the cost of traditional wastewater treatment (including sedimentation and activated sludge, unable to remove glyphosate) is in the range of 0.3-0.4 \$ m⁻³ [201,202]. Treatment at pH 3 would cost 0.008 \$ m⁻³ in nZVI, 0.009 \$ m⁻³ in H₂O₂, 0.052 \$ m⁻³ in H₂SO₄, and 0.010 \$ m⁻³ in CaO, for a total of 0.079 \$ m⁻³ (i.e., a slightly higher cost compared to pH 4, to achieve lower GLY removal). Moreover, a higher conductivity increase (up to 1-1.5 mS/cm) was observed upon water treatment at pH 3 compared to pH 4, and 8 mg/L iron was leached from 10 mg/L nZVI at pH 3. This means that a further step of dissolved iron removal before discharge would be required for treatment at pH 3.

Table 4.1. Concentration values of different anions in tap water.

Anion	Measured Value (mg/L)
Chloride (Cl ⁻)	26
Sulfate (SO ₄ ²⁻)	44
Nitrate (NO ₃ ⁻)	16
Nitrite (NO ₂ ⁻)	< 0.05

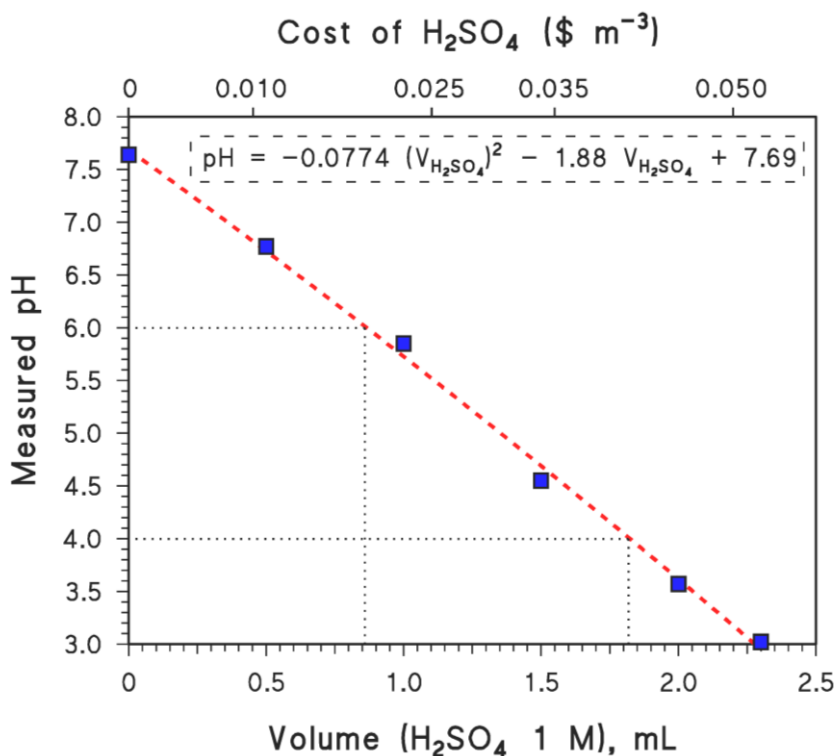


Figure 4.15. Results of tap water titration with H₂SO₄ (measured pH, as a function of added volume of H₂SO₄ 1 M). The upper X-axis reports the cost of H₂SO₄ addition, based on an estimate of 240 \$ (ton H₂SO₄)⁻¹ [202]. The reported phenomenological equation is a 2nd-order polynomial fit. The volumes of H₂SO₄ needed to bring pH to 4 and 6 are highlighted (the latter allows for the calculation of the amount of CaO needed to fix pH to 6 at the end of the treatment).

4.2.5 Removal of Glyphosate by nZVI-metabisulfite

In order to obtain glyphosate removal with a heterogeneous Fenton-like system, nZVI-metabisulfite was also used to carry out degradation by sulfate radicals. Many

approaches were tried to optimize GLY removal at pH 3, but it did not work significantly, and the removal was different at different concentrations of nZVI and metabisulfite. The addition of nZVI (0.01-0.02 g/L) was also investigated along with direct or stepwise addition of bisulfite, and maximum removal (46%) was observed with nZVI (0.01 g/L) - metabisulfite (150 μ M) at pH 3. To enhance the removal percentages, stepwise addition was also performed but the nZVI-metabisulfite Fenton-like system did not exhibit significant removal. This presumably happens because the reactive species in metabisulfite-based Fenton-like systems is considerably less reactive than HO \cdot . The results are shown in Figures 4.16 and 4.17.

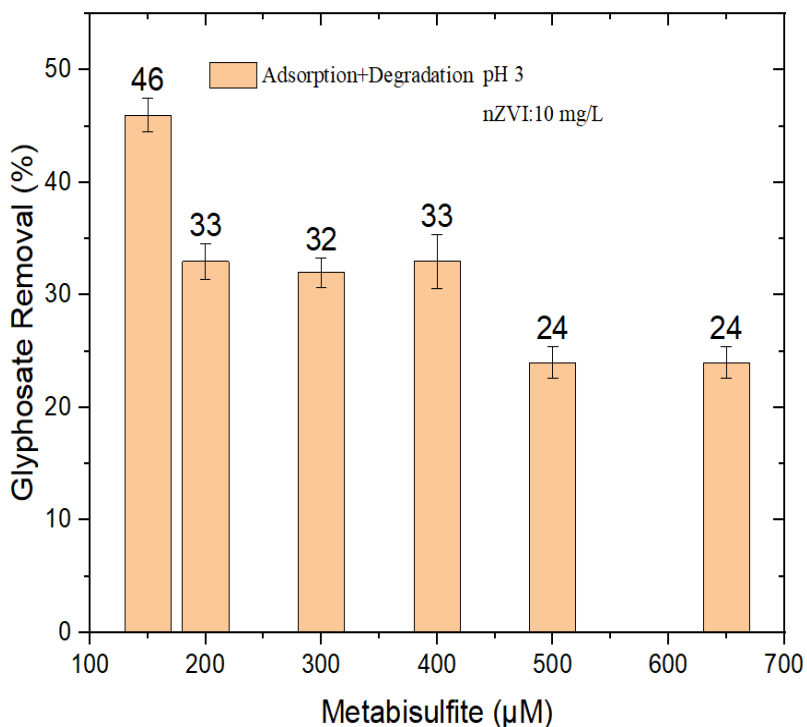


Figure:4.16 Removal of GLY through nZVI (0.01g/L) and different metabisulfite (100-650 μ M) concentrations at pH 3. Reaction time: 60 minutes.

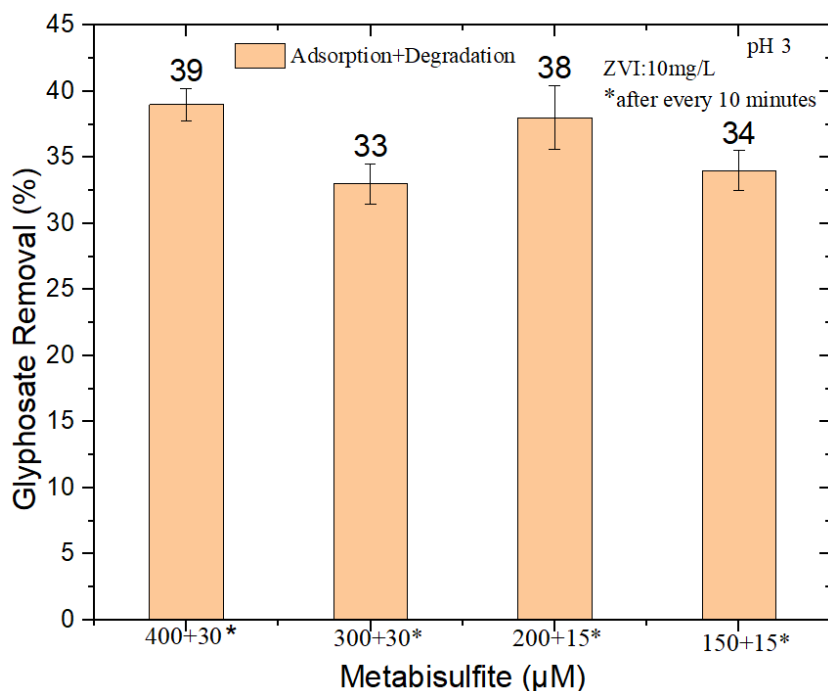


Figure:4.17 Removal of GLY through nZVI (0.01g/L) and different metabisulfite (stepwise) concentrations at pH 3. Reaction time: 60 minutes.

4.3 UV Treatment for the Removal of PFAS

4.3.1 Decomposition of PFOA at different pH values

We investigated the influence of three different pH values on the decomposition kinetics and mechanism of UV-treated PFOA, as well as TP formation. Among many reported factors such as temperature, dosage of oxidant, or dissolved oxygen, pH plays a crucial role because it affects both the generation rate of radicals and the speciation of many contaminants. Both radical formation and contaminant speciation highly affect the decomposition performance [18,208].

In our experiments, PFOA (1 mgL^{-1}) in aqueous solution had a pH of 5.6 and degraded rapidly during UV irradiation (Fig. 4.18). After 360 min treatment, $90.3 \pm 2.5 \%$ of PFOA was degraded. Assuming pseudo-first-order kinetics (Fig. 4.18 b) produced by the involvement of one or more steady-state reactive species in PFOA decomposition, we determined a half-life $t_{1/2}^{\text{PFOA}} = 106.8 \pm 2.0 \text{ min}$ (Tab. 4.2). Interestingly, PFOA

decomposition percentages at pH 4.0 and pH 7.0 were only slightly lower as compared with pH 5.6 ($85.2 \pm 1.6 \%$ and $80.5 \pm 4.0 \%$, respectively; Fig. 4.18 a and c). However, the calculated half-lives were significantly different (Tab. 4.2), with $t_{1/2}^{\text{PFOA}} = 130.4 \pm 2.4$ min at pH 4.0 and 152.4 ± 2.9 min at pH 7.0. Besides, we determined a significant decrease in PFOA decomposition at pH 10.0 that averaged $57.9 \pm 1.8 \%$, with $t_{1/2}^{\text{PFOA}} = 288.4 \pm 2.6$ min (Fig. 4.18 d). Thus, the highest decomposition and shortest half-life were determined at the natural pH of aqueous PFOA. Compared to pH 5.6 (k_{dec}), the decomposition rate constants at pH 4.0, 7.0, and 10.0 were $0.82 k_{\text{dec}}$, $0.70 k_{\text{dec}}$, and $0.37 k_{\text{dec}}$, respectively.

The initial pH during UV irradiation of PFOA affected both decomposition kinetics and TP formation. The most TPs were found for the UV treatment at pH 5.6 and the fewest for the treatment at pH 4.0, which only yielded PFHpA in significant amounts. By comparison, we determined and quantified PFHpA, PFHxA, PFPeA, and PFBA at pH 5.6. The choice of PFOA as a model compound can be justified because shorter-chain PFAA is released as TP during the decomposition of both PFOA and 6:2 FTAB (*vide infra*).

The release and amount of fluoride (F^-) as a major mineralization product of PFOA seemed to be affected by pH also. The defluorination was almost comparable at acidic and neutral pH, averaging 30 % after 360 min treatment. However, at pH 5.6 F^- release was first detectable after 30 min while, for pH 4.0 and pH 7.0, the F^- release was detectable only after 50 min (Fig. 4.18). At alkaline pH, the defluorination started even later, i.e., after 60 min from the beginning of the UV treatment and it averaged 20 % after 360 min (Tab. 4.2). Our results indicate a two-stage decomposition reaction of PFOA, except at pH 4.0. At this pH value, produced protons are not quenched by OH^- , thus reaction between protons and $e_{\alpha q}^-$ reduces the availability of electrons that may be responsible for PFOA decomposition [209].

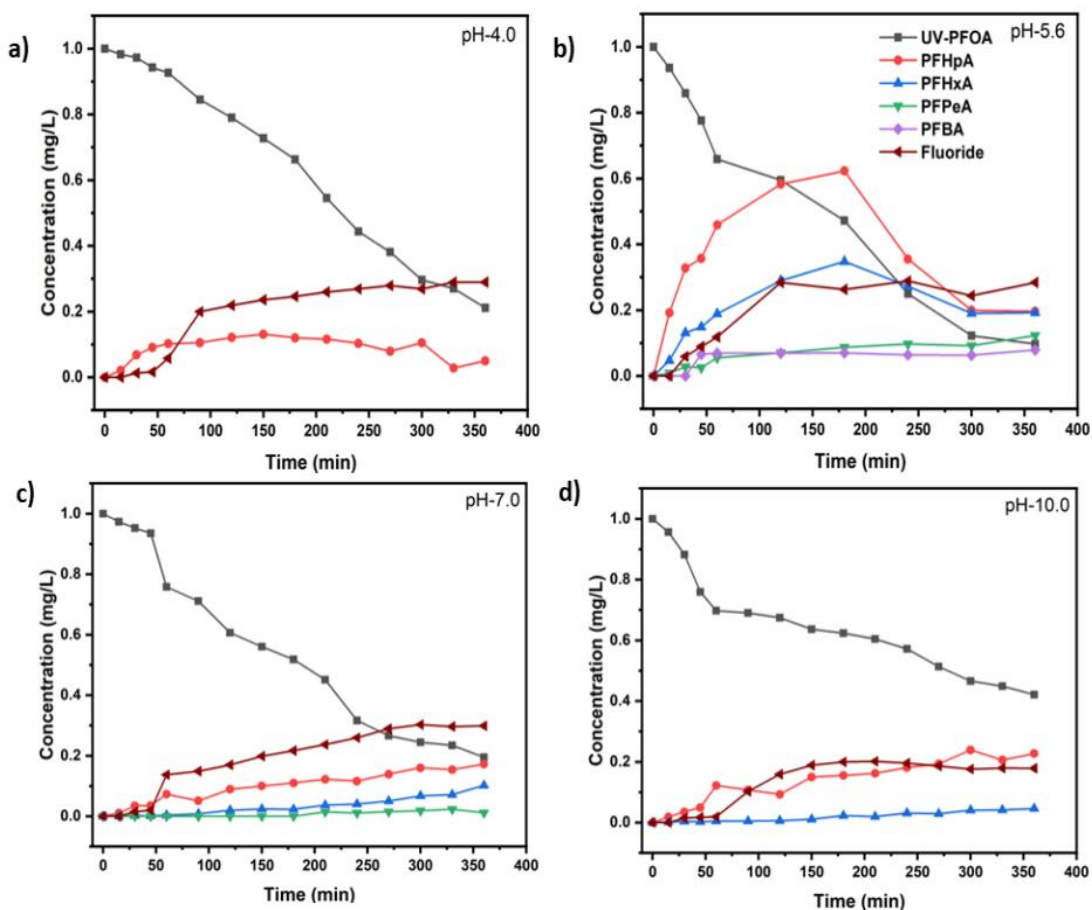


Figure 4.18. Removal of PFOA, production of transformation products, and fluoride release upon UV irradiation at pH 4.0 (a), pH 5.6 (b), pH 7.0 (c), and pH 10.0 (d).

Table 4.2. Rate constant, Half-life, %age decomposition, and- defluorination at different pH values for 1 mg L⁻¹ PFOA.

pH value	$k(s^{-1})$	$t_{1/2}$ (min)	Decomposition (%)	Fluoride release (%)
4.0	$(8.85 \pm 1.13) \times 10^{-5}$	130 ± 2	85.2 ± 1.6	29.0 ± 3.5
5.6	$(1.08 \pm 0.30) \times 10^{-4}$	107 ± 2	90.3 ± 2.5	28.8 ± 4.8
7.0	$(7.57 \pm 1.70) \times 10^{-5}$	152 ± 3	80.5 ± 4.0	30.3 ± 5.4
10.0	$(4.00 \pm 1.15) \times 10^{-5}$	288 ± 3	57.9 ± 1.8	20.2 ± 3.5

Our results indicate a remarkable effect of the initial pH on the decomposition kinetics of PFOA, as well as the formation of the main TPs and major mineralization products. Similar observations concerning the influence of pH were recently reported by Wang and Zhang, and others [210–212]. In particular, Wang and Zhang [210] investigated the influence of pH on PFOA decomposition, which was inhibited at alkaline pH. They suggested that the initial decomposition of PFOA is mediated by hydrated electrons (e_{aq}^-), generated through photolysis of OH^- and dominating, at alkaline pH, over the direct PFOA photolysis. Since OH^- ions produce e_{aq}^- , one could expect unaffected photolysis of PFOA. This assumption was also confirmed by Wang and Zhang [210], but only in the absence of oxygen. The influence of oxygen during PFOA photolysis was also recently investigated by Giri et al. [212]. Giri et al., as well as Wang and Zhang both observed negative effects of dissolved oxygen (DO) during PFOA photolysis, especially at alkaline pH. Wang and Zhang [210] postulated that, in the presence of oxygen at alkaline pH, e_{aq}^- is scavenged by O_2 to produce $O_2^{\bullet-}$.

Recently, we demonstrated that our system configuration produces more $O_2^{\bullet-}$ than $\bullet OH$ radicals [213]. Therefore, the initial decomposition of PFOA should be significantly inhibited at alkaline pH in the presence of O_2 . In our experimental set-up, we used deionized water without purging it with nitrogen gas, which caused DO to be present at the beginning of the UV treatment. Therefore, we can assume that, at alkaline pH, the presence of DO inhibits PFOA decomposition as postulated by Wang and Zhang [210] and Giri et al. [212].

Overall, our results are consistent with those of Wang and Zhang [210] and Giri et al. [212]. However, the two-stage decomposition reaction observed for PFOA in our study can also be due to differences in the system configurations, leading to different kinetics involving H_2O_2 production as well as other factors (*vide infra*).

Our UV system configuration has a tremendous impact on the decomposition kinetics and generation of radical species, as recently demonstrated [213]. Therefore, we are aware that the intensity of our UV lamp might also have an important effect on PFOA decomposition. Our UV light intensity was considerably weaker as compared to those

reported by Wang and Zhang and Giri et al. [210,212], resulting in lower photon flux and slower reaction kinetics. Therefore, the determination of lower degradation rate constants is justified. Apart from these differences, Wang and Zhang [210] observed H₂O₂ formation from recombination of hydrogen peroxide radicals (HO₂[•]) in their system within 60 minutes, reaching an optimum level of 300 μM H₂O₂ between 20 min and 30 min. We also measured H₂O₂ formation in our system but at a significantly lower concentration, close to the limit of detection (data not shown).

As demonstrated by Wang and Zhang [210], it is very reasonable that high yields of e_{aq}^- during oxygen-free photolysis decompose PFOA. The presence of high quantities of oxygen will scavenge e_{aq}^- and form O₂^{•-}, especially at alkaline pH. In our system configuration, we measured DO consumption of 2 mg L⁻¹ within 180 min of UV treatment PFOA. Thus, we assume that rapid degradation of PFOA in the initial stage of our UV treatment was possibly due to hampered HO₂[•] formation.

4.3.2 Scavengers' Experiments for PFOA Decomposition

In our system configuration, we assumed that different reactive species ([•]OH, HO₂[•], and O₂^{•-}) are synergistically participating in PFOA decomposition. To further investigate the mechanism potentially driven by different reactive species, scavenger experiments were carried out. Various scavengers including methanol (MeOH), ethanol (EtOH), 2-propanol, and t-butanol (for [•]OH), as well as L-Threoascorbic acid (for reactive oxygen species, ROS, including O₂^{•-}, carbon dioxide radical, CO₂^{•-}, and [•]OH radical) were used [214–216].

We observed almost 90% PFOA decomposition without the addition of scavengers, as mentioned above. By adding different alcohols as [•]OH scavengers, we always found inhibition of PFOA decomposition, lower efficiency, and lower defluorination, as compared with the reference treatment (Fig. 4.19). Methanol, ethanol, and 2-propanol allowed for about 81 – 85 % PFOA decomposition, while t-butanol gave only 75% decomposition (Tab. 4.3).

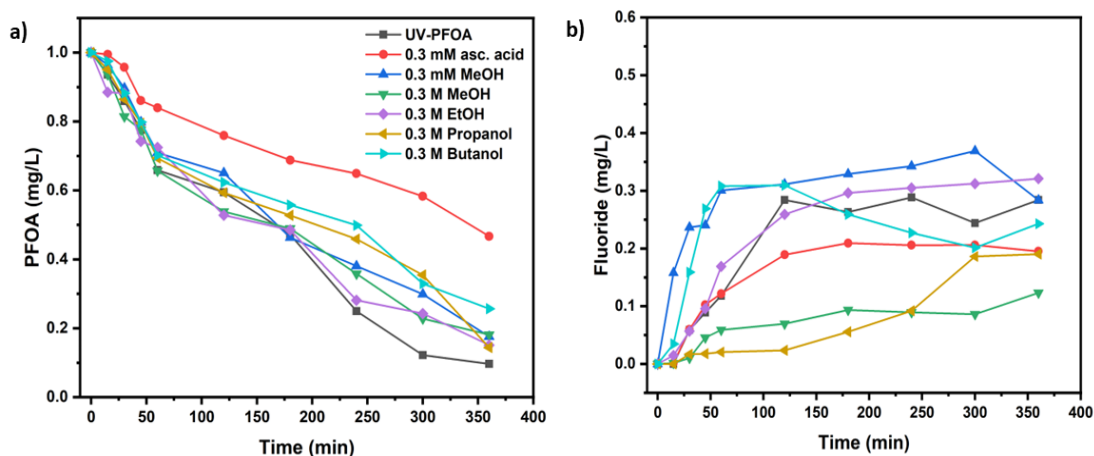


Figure 4.19. Comparative removal of PFOA in the presence of scavengers (a), fluoride release with scavengers' addition (b).

Table 4.3. Rate constant, Half-life, %age decomposition, and defluorination by different scavengers for 1 mg L^{-1} PFOA.

Scavenger & initial pH	$k \text{ (s}^{-1}\text{)}$	$t_{1/2} \text{ (min)}$	PFOA Decomposition (%)	Fluoride release (%)
0.3 mM Methanol - pH 5.1	$(8.06 \pm 1.5) \times 10^{-5}$	143 ± 3	82.6 ± 2.9	36.9 ± 1.3
0.3 M Methanol - pH-5.1	$(7.91 \pm 0.2) \times 10^{-5}$	146 ± 4	81.9 ± 2.7	12.3 ± 4.3
0.3 M Ethanol - pH-5.7	$(8.74 \pm 1.2) \times 10^{-5}$	132 ± 5	84.9 ± 1.9	32.1 ± 3.2
0.3 M Propanol - pH-5.8	$(9.00 \pm 1.9) \times 10^{-5}$	128 ± 5	85.7 ± 1.5	19.0 ± 2.8
0.3 M Butanol - pH-5.7	$(6.30 \pm 1.5) \times 10^{-5}$	183 ± 3	74.3 ± 4.2	30.8 ± 4.6
0.3 mM Ascorbic acid* - pH-4.3	$(3.52 \pm 1.3) \times 10^{-5}$	327 ± 6	53.3 ± 5.2	20.9 ± 4.2

* at $t=0$ and $t=1 \text{ h}$

The alcoholic scavengers seemed to also affect defluorination (Fig. 4.19 b). While the release of F⁻ from PFOA without scavenger started only after 20 min, we found an immediate release of F⁻ in the presence of 0.3 mM MeOH. Overall, the defluorination with 0.3 mM MeOH was the highest (around 36% after 180 min treatment time, Tab. 4.3). Individual results of PFOA decomposition with all scavengers are shown in (Fig. 4.20-4.25).

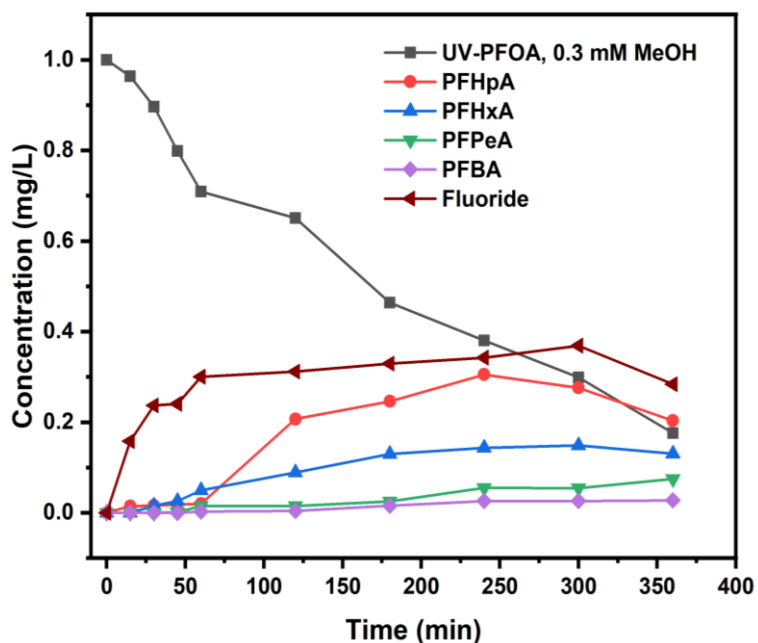


Figure:4.20 PFOA decomposition in the presence of 0.3 mM methanol as a scavenger.

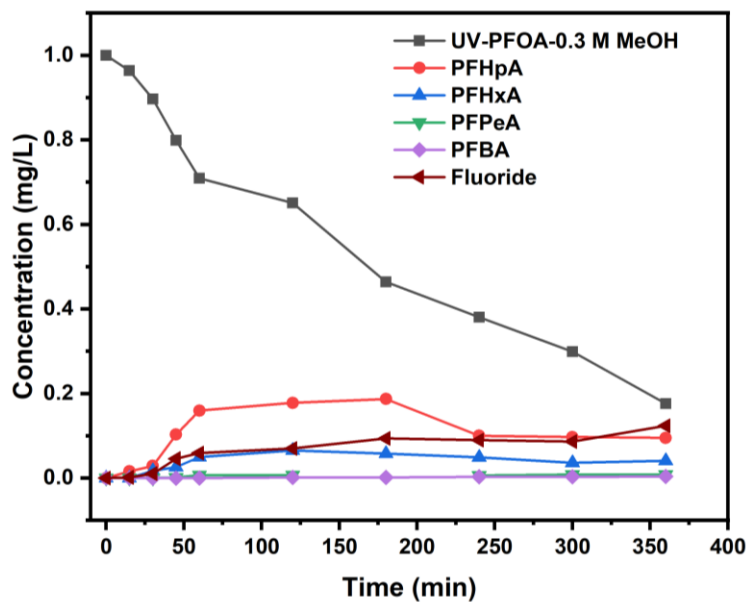


Figure:4.21 PFOA decomposition in the presence of 0.3 M methanol as a scavenger.

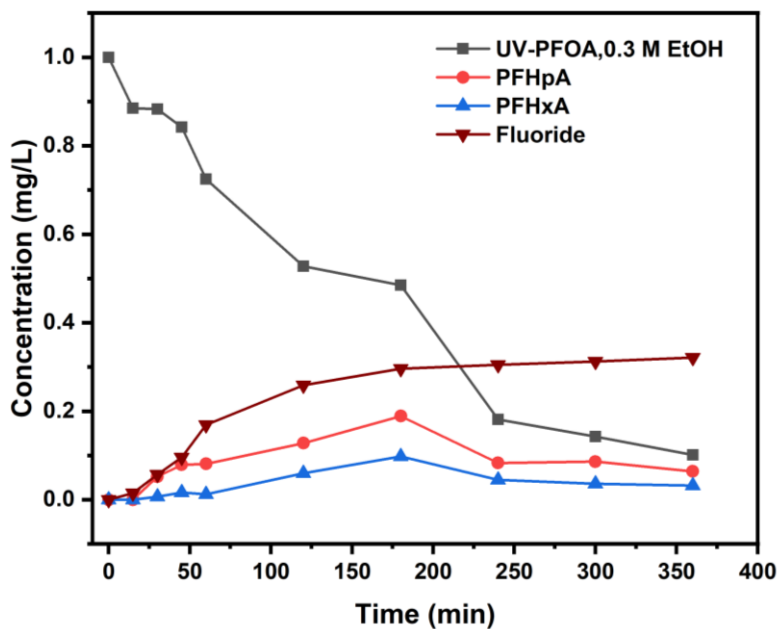


Figure:4.22 PFOA decomposition in the presence of 0.3 M ethanol as scavenger.

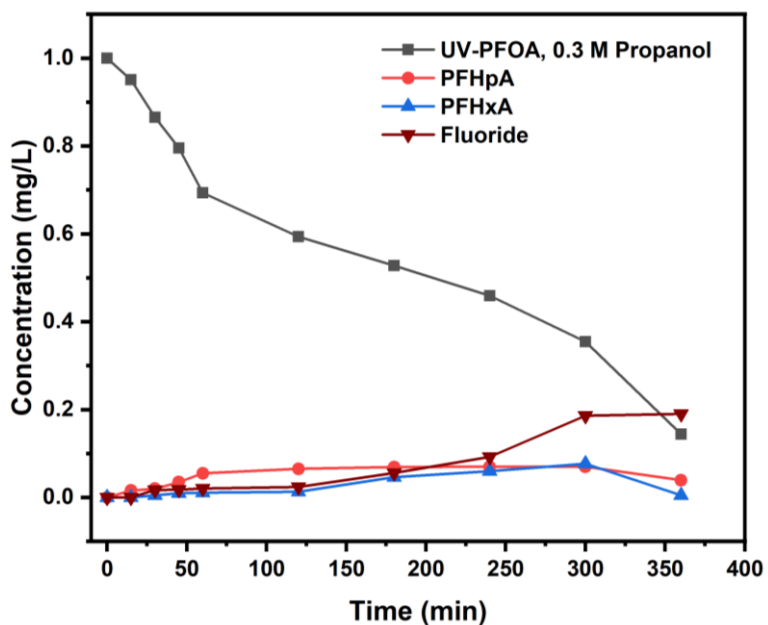


Figure:4.23 PFOA decomposition in the presence of 0.3 M propanol as scavenger.

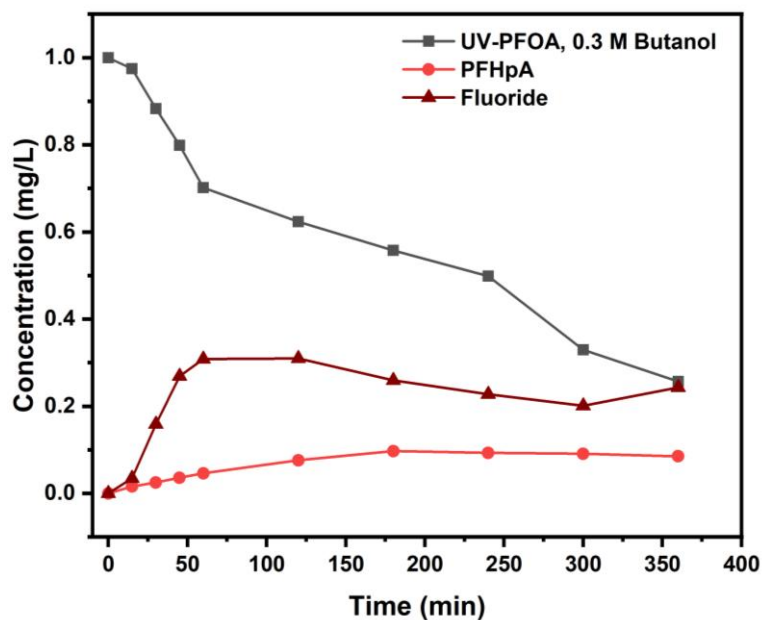


Figure:4.24 PFOA decomposition in the presence of 0.3 M t-butanol as scavenger.

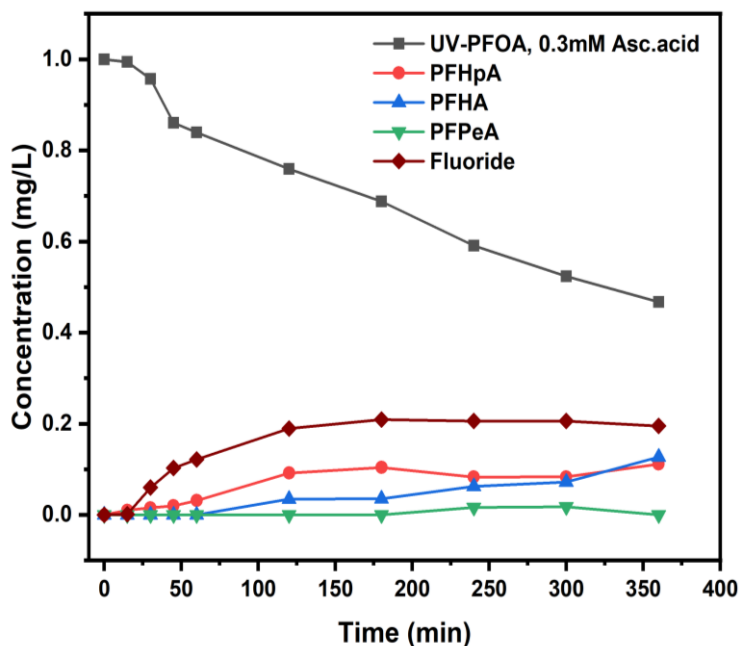


Figure:4.25 PFOA decomposition in the presence of 0.3 mM Asc. acid as a scavenger.

The addition of alcohols did not significantly affect the initial PFOA decomposition (Tab. 4.3). However, our results reveal that $\cdot\text{OH}$ radicals were being scavenged by alcohols as expected, but without inhibiting defluorination. This might be justified by the unrestricted presence of e_{aq}^- which should be mainly responsible for PFOA decomposition [209,210,212].

Recently, Chen et al. [209] studied PFOA decomposition using a UV/H₂O/alcohol system. They observed that alcohols are quenching $\cdot\text{OH}$ radicals and, thus, might produce alcohol radicals. Both species are inefficient in decomposing PFOA. They stated that during the quenching of $\cdot\text{OH}$ radicals, more hydrated electrons are produced in the presence of alcohols. Therefore, they suggested that alcohols may act as catalysts for PFOA decomposition. However, very high alcohol concentrations (65 mM) were required to achieve significant PFOA decomposition. Beyond this amount, the continuous addition of alcohol had no further effect. In addition, it has been suggested that using alcohols caused an increase in the surface tension of 10 mg L⁻¹

PFOA, with better dispersion of PFOA on the surface and, thus, enhanced decomposition.

However, we used a ten-fold lower concentration of PFOA (1 mgL^{-1}) and did not observe better decomposition. Also, as stated in section 3.1, due to the different system configurations and weaker UV intensity, our findings might not be consistent with Chen et al. [209]. Moreover, it has also been stated that alcohols protect electrons from quenching by oxygen and protons. Considering $\text{O}_2^{\bullet-}$ radical as the driving factor for PFOA decomposition, we agree with Giri et al. [212] and Wang and Zhang [210] who observed the formation of $\text{O}_2^{\bullet-}$ radicals upon quenching of electrons with DO. To further prove our assumption, we also applied ascorbic acid as an $\text{O}_2^{\bullet-}$ scavenger. Interestingly, we found the highest inhibition of PFOA decomposition (which reduced to 53% at 360 min treatment time, Fig. 19 a) with ascorbic acid, which also well corresponded with the inhibition of defluorination (Fig. 4.19 b). Ascorbic acid showed the strongest inhibition effect compared with all other scavengers applied.

Recently, Bai et al. [217] studied the effect of $\text{O}_2^{\bullet-}$ radicals on PFAS decomposition using a series of PFAA. They demonstrated the involvement of $\text{O}_2^{\bullet-}$ radicals in PFAA decomposition both theoretically, using density functional theory (DFT), and experimentally. They measured the $\text{O}_2^{\bullet-}$ decay rates in the presence of PFAA and considered the effect of solvation on $\text{O}_2^{\bullet-}$ reactivity. The possible mechanism was examined by DFT calculations, as well as the thermodynamic viability of the reaction pathway between an $\text{O}_2^{\bullet-}$ radical and $\text{C}_2\text{F}_5\text{CO}_2^-$. They concluded that the α -C atom ($\Delta G_R^\circ = -4.09 \text{ kcal mol}^{-1}$) is attacked by $\text{O}_2^{\bullet-}$, causing the C-F bond to break. Despite these findings, Metz et al. [218] critically opposed the idea based on recent results they obtained [219] and argued that they produced $\text{O}_2^{\bullet-}$ radicals by three different systems to verify the involvement of superoxide. In none of the systems were they capable of finding a correlation between $\text{O}_2^{\bullet-}$ formation and PFAS decomposition.

Interestingly, our results might support the hypothesis of $\text{O}_2^{\bullet-}$ participating in PFOA decomposition. Based on our results, we might agree with the finding of Bai et al. [217] although, as mentioned above, our findings might be caused by our system configuration that favors the generation of $\text{O}_2^{\bullet-}$ over $\bullet\text{OH}$. Nevertheless, we also

support the claim of Metz et al., as we could not completely confirm the occurrence of $O_2^{\bullet-}$ only based on the application of ascorbic acid as a scavenger. As mentioned above, ascorbic acid scavenges ROS, a rather broad variety of reactive oxygen species that includes, among others, $\bullet OH$ and $O_2^{\bullet-}$.

Therefore, we have to address this important issue in future investigations, more precisely considering the given treatment conditions and parameters, to determine the exact role of different reactive species involved in the decomposition of PFOA. Independently, we aimed to investigate whether our system can reliably decompose PFOA with reproducible results, comparable to those reported in recent literature and, ultimately, use the PFOA results to achieve decomposition of 6:2 FTAB.

4.3.3 Decomposition of 6:2 FTAB at different pH values

UV treatment of 6:2 FTAB was carried out for 360 min at four different initial pH values. The original pH of the aqueous 6:2 FTAB solution was 6.5. During the UV treatment of 1 mg L^{-1} 6:2 FTAB, complete decomposition was achieved within 360 minutes (Fig. 4.26 b). The decomposition followed more or less pseudo-first-order kinetics, with an average lifetime of 45.7 ± 1.7 min at pH 6.5 (Tab. 4.4). The time evolution of 6:2 FTAB was characterized by a first exponential decay branch, resulting in a pseudo-plateau at 60-90 min that was followed by a second exponential decay, the outcome of which was complete 6:2 FTAB degradation at around 360 min (see Figure 4.26).

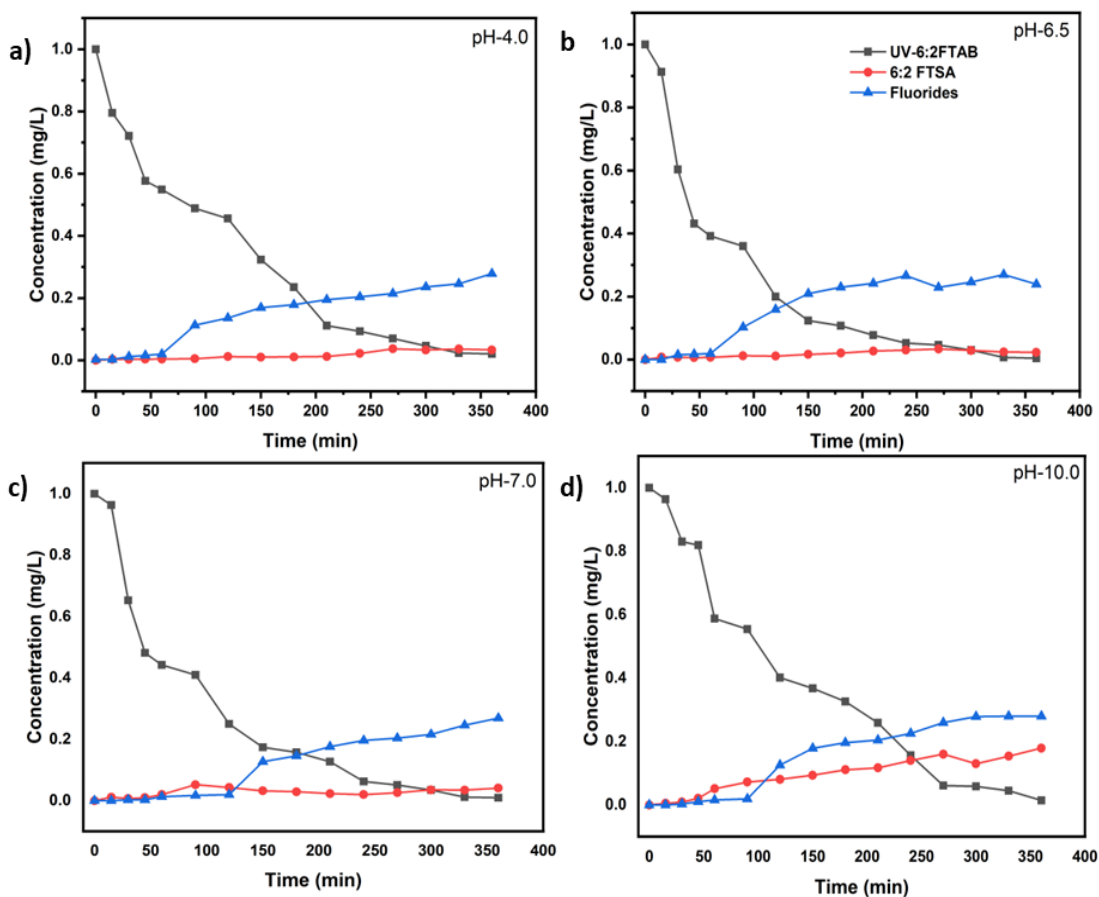


Figure 4.26. Removal of 6:2FTAB, formation of major transformation product, and fluoride release by UV irradiation at pH 4.0 (a), at pH 6.5 (b), at pH 7.0 (c), and at pH 10.0 (d).

Table 4.4. Rate constant, Half-life, %age decomposition, and fluoride release at different pH values for 1 mg L⁻¹ 6:2 FTAB.

pH value	k (s ⁻¹)	$t_{1/2}$ (min)	6:2 FTAB Decomposition (%)	Fluoride release (%)
4.0	$(1.80 \pm 0.06) \times 10^{-4}$	64.1 ± 7.2	98.0 ± 3.1	27.9 ± 5.0
6.5	$(2.52 \pm 0.16) \times 10^{-4}$	45.7 ± 1.7	99.6 ± 0.5	27.0 ± 4.7
7.0	$(2.16 \pm 0.29) \times 10^{-4}$	53.3 ± 3.9	99.1 ± 0.2	26.9 ± 3.2
10.0	$(1.97 \pm 0.14) \times 10^{-4}$	58.4 ± 6.2	98.6 ± 1.4	28.0 ± 4.2

The UV treatment of 6:2 FTAB was affected by pH as well. Lifetime followed the order $\text{pH } 4 > \text{pH } 10 > \text{pH } 7$, and the optimal pH value for the UV degradation of 6:2 FTAB was 6.5 (Tab. 4.4). Despite the different half-lives determined, we always observed complete decomposition of 6:2 FTAB within 360 min treatment time. In all cases, a two-branch bi-exponential time evolution curve could be observed in Figure 4.26.

Surprisingly, we only detected 6:2 fluorotelomer sulfonic acid (6:2 FTSA) as a major TP, with the highest concentration at alkaline pH. There is some evidence from the time evolution curves that the decomposition kinetics of 6:2 FTSA was slower at alkaline pH, where a slow accumulation of 6:2 FTSA occurred. Fluoride release started only after 60 min treatment for all four different pH values (Fig. 4.26 b), and it amounted to 26-28% (Tab. 4.4). Some shorter-chain PFAA were also identified, but only at trace level, including PFHpA, PFHxA, and PFPeA (data not shown). The rapid decomposition of 6:2 FTAB and low detection of TPs led us to assume that mineralization to carbon dioxide (CO_2) might have taken place during the UV treatment. Unfortunately, our system configuration did not allow for the measurement of CO_2 .

Many other studies reporting the decomposition of some telomer-related alcohols observed different major TPs, such as 6:2 fluorotelomer sulfonic acid (6:2 FTSA), 6:2 fluorotelomer alkyl acid, 6:2 FTAA, 6:2 FTSAm, and others (6:2 FTCA, 6:2 FTUCA, etc.) [220–225]. Surprisingly, we did not detect more TPs during 6:2 FTAB decomposition in our treatment, which might be due to kinetic effects.

As mentioned above, the decomposition of 6:2 FTAB in our treatment system followed a two-stage kinetics. In the initial stage of the UV treatment, direct photolysis of 6:2 FTAB might be reasonable. However, the participation of reactive species such as hydroxyl radicals and hydrated electrons cannot be discussed here, without further information on their presence in the UV system.

4.3.4 Scavengers experiments for 6:2 FTAB decomposition

To study the involvement of reactive species in the decomposition of 6:2 FTAB by UV photolysis, the same scavengers as for PFOA were used to better understand the role of different reactive species (Fig. 4.27 & Tab. 4.5). The application of different types of scavengers inhibited the UV decomposition of 6:2 FTAB. All scavengers had immediate inhibiting effects, except for MeOH. For either 0.3 M or 0.3 mM MeOH, the inhibition effect only occurred 30 min after the start of the UV treatment.

As mentioned above, alcohols are $\cdot\text{OH}$ scavengers. To some extent, ascorbic acid can also inhibit the reaction by scavenging both $\text{O}_2^{\cdot-}$ and $\cdot\text{OH}$ or related ROS (Fig. 4.27). The exception of 0.3 mM methanol as a scavenger could be explained based on its lower concentration as compared to other alcohols, typically used at 0.3 M concentration.

Interestingly, $\cdot\text{OH}$ was shown to play little to no role in the degradation of PFOA, but the hydroxyl radical was directly involved in the 6:2 FTAB degradation mechanism. In this framework, 0.3 mM MeOH is likely to be a poor $\cdot\text{OH}$ scavenger, and, coherently, it inhibited 6:2 FTAB decomposition to only a limited extent (Fig. 4.27 a). We also found that alcohols with a longer carbon chain caused a higher and more significant inhibition of 6:2 FTAB degradation.

Interestingly, 0.3 mM ascorbic acid inhibited 6:2 FTAB decomposition to a higher extent than either 0.3 mM or 0.3 M MeOH, but less than EtOH, 2-propanol, or t-butanol. Upon addition of 0.3 mM ascorbic acid, a higher inhibition effect was observed than for MeOH, which indicates that both hydroxyl and superoxide radicals are being scavenged by ascorbic acid, thus a greater effect of inhibition was observed in the case of ascorbic acid. All scavengers decreased fluoride release that ranged between 22 and 28%, except for t-butanol which reduced F^- release down to 17 %. The SO_4^{2-} release was observed most often at higher pH, while at lower and neutral pH values it was not observed due to low resolution.

Although the addition of ascorbic acid also inhibited the decomposition of 6:2 FTAB, the scavenging effect was not as strong as with EtOH, 2-propanol, or t-butanol. These findings lead us to assume that the decomposition mechanism of 6:2 FTAB is an

overlapping process of direct and indirect photolysis, driven by either/both hydrated electrons and/or radicals.

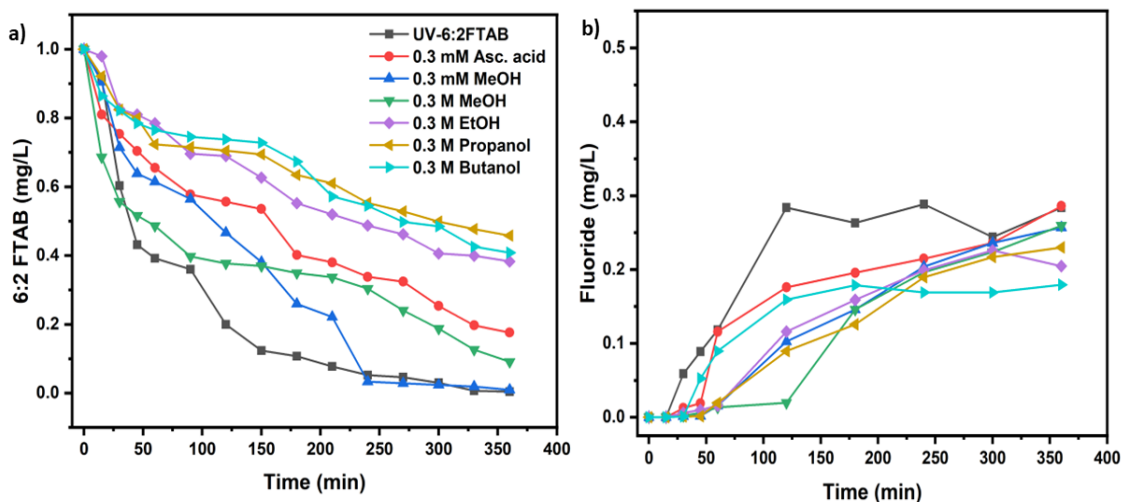


Figure 4.27. Decomposition of 6:2 FTAB in the presence of scavengers (a), fluoride release with scavengers' addition (b).

Table 4.5. Rate constant, Half-life, %age decomposition, and fluoride release with different scavengers for 1 mg L⁻¹ 6:2 FTAB.

Scavengers	$k(s^{-1})$	$t_{1/2} (min)$	6:2 FTAB Decomposition (%)	Fluoride release (%)
0.3 mM Methanol	$(2.15 \pm 0.12) \times 10^{-4}$	54 ± 4	99.0 ± 0.7	25.7 ± 4.4
0.3 M Methanol	$(1.10 \pm 0.24) \times 10^{-4}$	104 ± 8	90.9 ± 4.3	26.0 ± 2.6
0.3 M Ethanol	$(4.44 \pm 0.41) \times 10^{-5}$	260 ± 7	61.7 ± 2.9	22.6 ± 3.7
0.3 M Propanol	$(3.61 \pm 0.32) \times 10^{-5}$	319 ± 7	54.2 ± 2.6	23.0 ± 2.0
0.3 M Butanol	$(4.15 \pm 0.97) \times 10^{-5}$	279 ± 10	59.2 ± 3.5	18.0 ± 4.3
0.3 mM Ascorbic acid*	$(8.04 \pm 0.55) \times 10^{-5}$	144 ± 8	82.4 ± 4.2	25.6 ± 2.9

* at t=0 and t=1 h

The complex role of different reactive species participating in the decomposition of 6:2 FTAB was also recently described by Trouborst [223]. He studied 6:2 FTAB photolysis in a photoFate system, involving sunlight for decomposition, obtaining different TPs including mainly 6:2 FTSAm, 6:2 FTSA, and some short-chain PFAA in very low concentration. Trouborst explained the formation of 6:2 FTSAm mainly by direct photolysis but, in our UV treatment system, we did not observe the formation of 6:2 FTSAm. We assume that if 6:2 FTSAm were released, it might have volatilized due to our open-system configuration. In the study by Trouborst [223], the release of 6:2 FTSAm has been possibly ascribed to sunlight absorption by 6:2 FTAB. However, there were many degradation products, ultimately degraded to short-chain PFAA. The treatment lasted from many hours to days and the experimental setup was complicated. Moreover, the formation of 6:2 FTSA can be due to subsequent degradation of 6:2 FTSAm, but also to direct photolysis from 6:2 FTAB as we assume from our results. It has been reported [226] that biodegradation of 6:2 FTSA also produces 6:2 fluorotelomer carboxylic acid (6:2 FTCA), 6:2 fluorotelomer unsaturated carboxylic acid (6:2 FTUCA), and some short-chain PFAA [224,226]. Regarding biodegradation of 6:2 FTSA, slower and incomplete degradation was observed. We also observed the formation of some short-chain PFAA, including PFHpA, PFHxA, and PFPeA, but only at trace levels (data not shown). The individual effects of scavengers over 6:2 FTAB removal, along with 6:2 FTSA as the major TP and fluoride release, are shown in Figures 4.28-4.33.

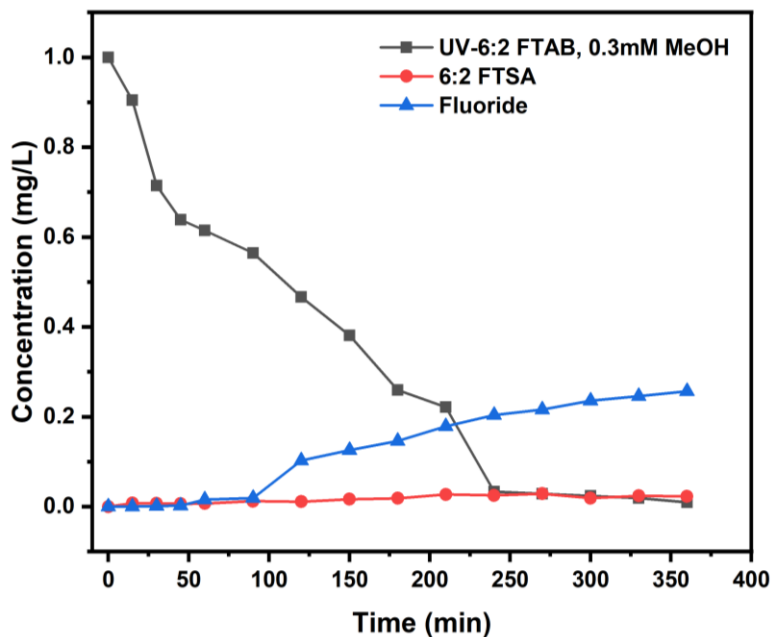


Figure:4.28 6:2 FTAB decomposition in the presence of 0.3 mM methanol as scavenger

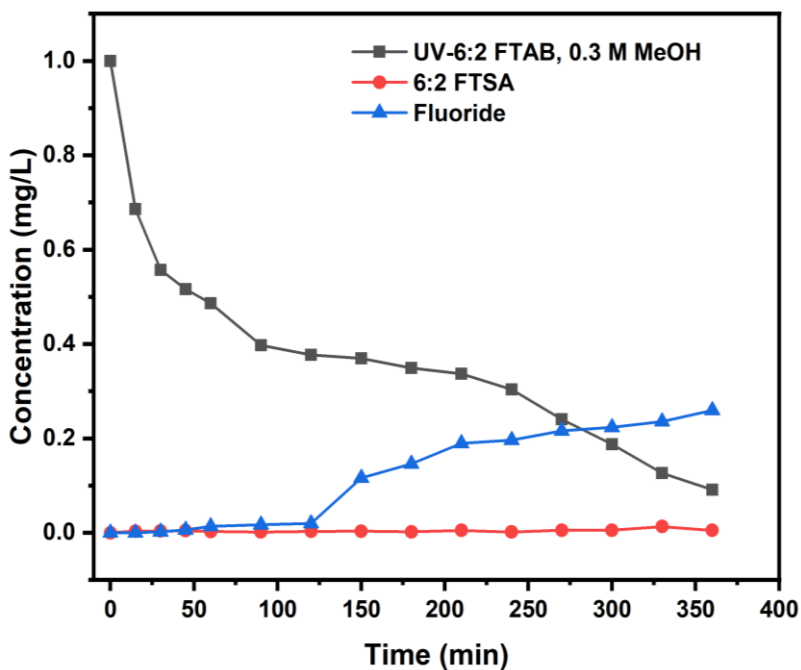


Figure:4.29 6:2 FTAB decomposition in the presence of 0.3 M methanol as scavenger

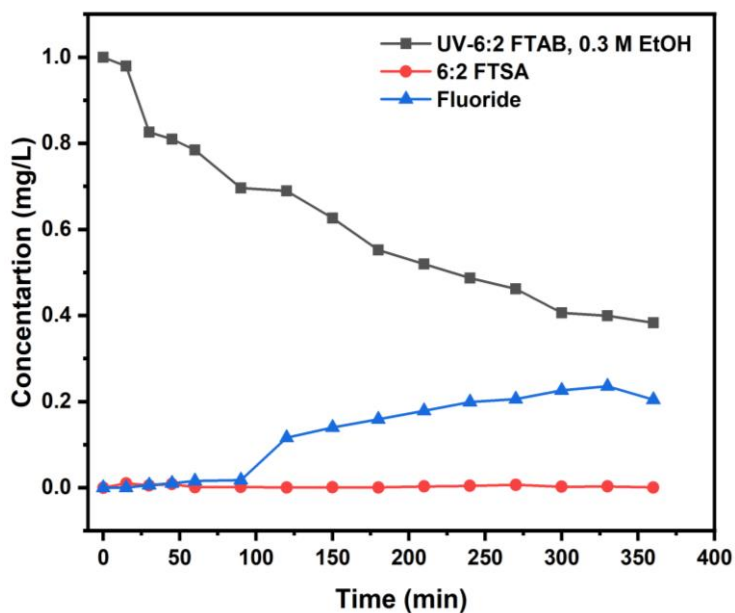


Figure:4.30 6:2 FTAB decomposition in the presence of 0.3 M ethanol as scavenger.

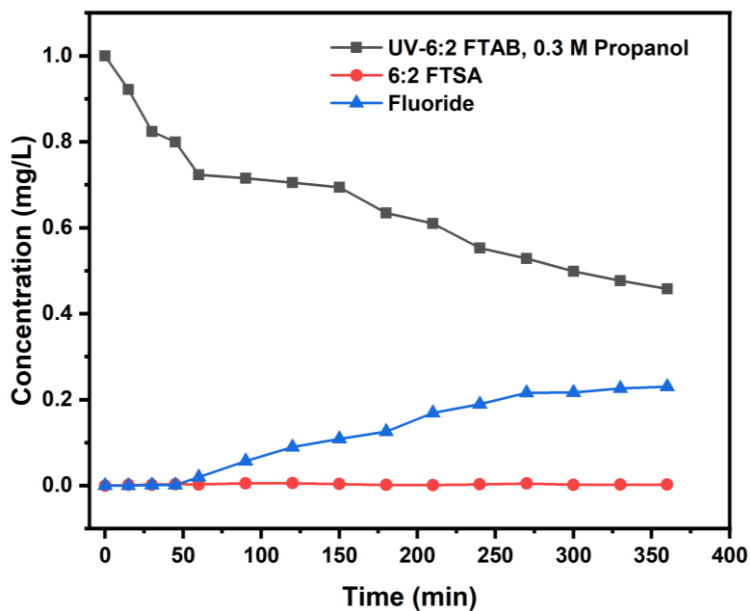


Figure:4.31 6:2 FTAB decomposition in the presence of 0.3 M propanol as scavenger.

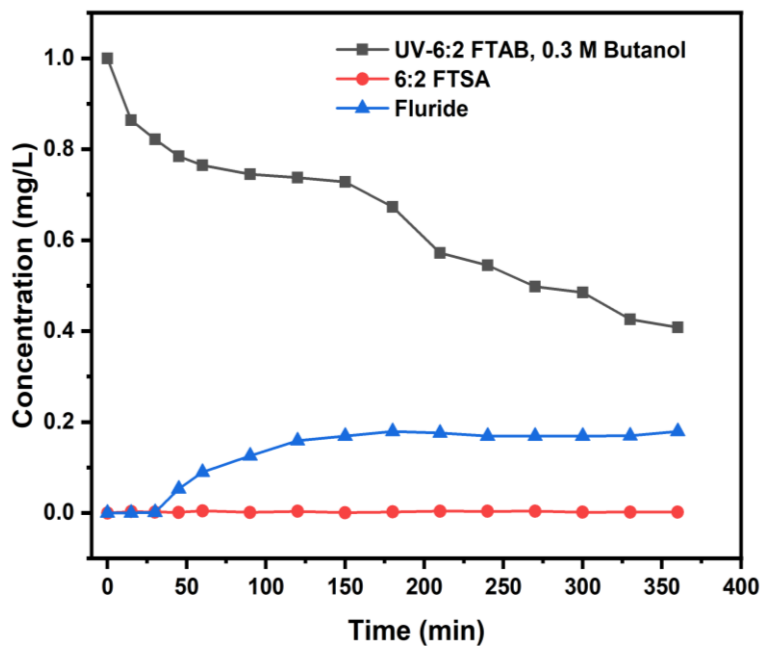


Figure:4.32 6:2 FTAB decomposition in the presence of 0.3 M t-butanol as scavenger

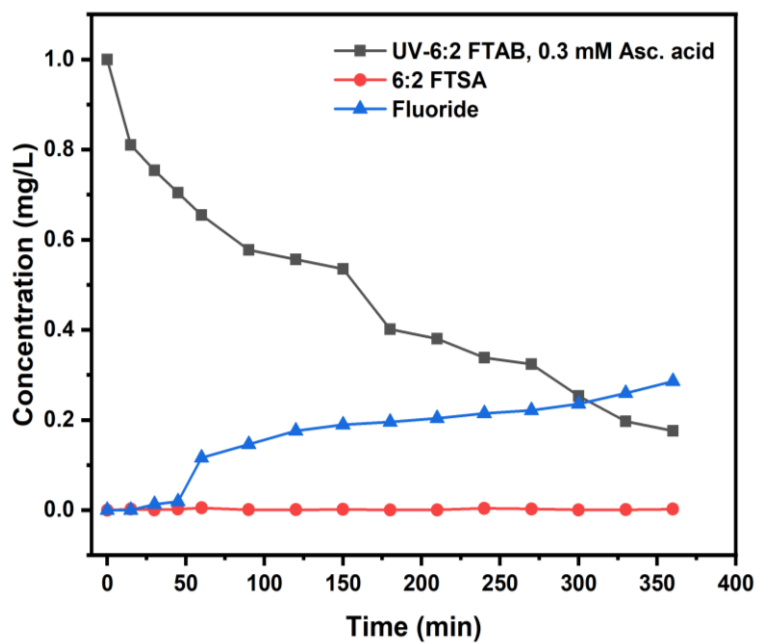


Figure:4.33 6:2 FTAB decomposition in the presence of 0.3 mM Asc. acid as scavenger

4.3.5 Proposed Mechanism of 6:2 FTAB decomposition

Based on our results, obtained from UV treatments and scavenger experiments, we propose a mechanism for the UV decomposition of 6:2 FTAB, assuming that the process is mediated by both direct and indirect photolysis. In other words, we assume that UV radiation and $\cdot\text{OH}$ play the main roles (Fig. 4.34), which is supported by experimental results including SO_4^{2-} release.

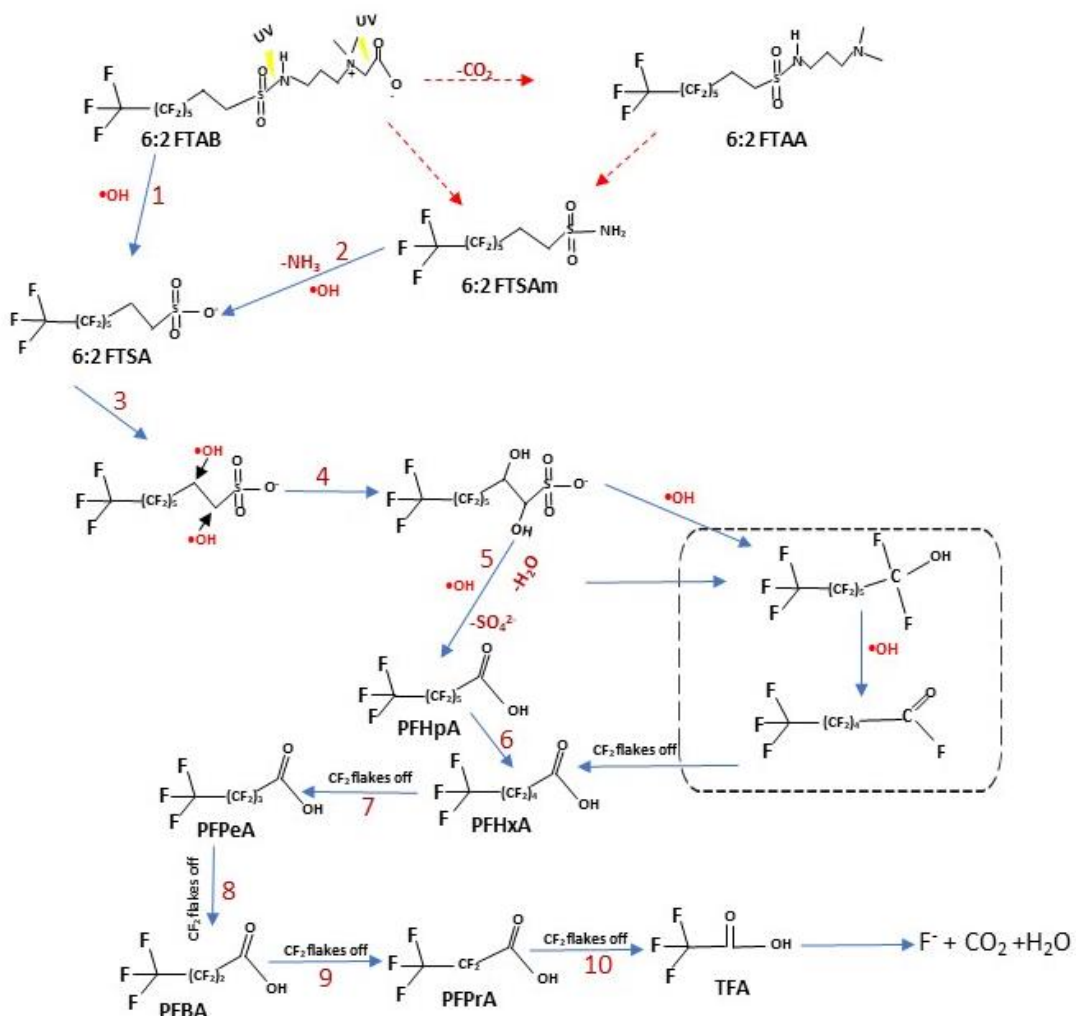


Figure 4.34. Proposed UV photolysis pathways of 6:2 FTAB. Blue arrows represent the major observed decomposition pathway, hypothesized according to the transformation products detected in this study. Red arrows indicate other reasonable decomposition routes [221,223,224,227].

The formation of 6:2 FTSA can be explained by S-N bond breaking by UV radiation (step 1), followed by $\cdot\text{OH}$ attack on the sulfur atom. We observed the formation of 6:2 FTSA in every sample but did not observe either 6:2 FTAA or 6:2 FTSA_m. The formation of 6:2 FTSA via these metabolites, as well as directly from the mother compound are both feasible [223]. The TP 6:2 FTSA would further undergo $\cdot\text{OH}$ -mediated reactions (step 4 and onwards) to form short-chain PFAA (PFHpA, PFHxA, PFPeA etc). Yang et al. [221] also studied the decomposition of 6:2 FTSA using UV/H₂O₂ and proposed a mechanism involving $\cdot\text{OH}$ attack as a prerequisite to mineralization. Furthermore, by removing CF₂ groups, shorter-chain PFAA is released. In detail, Using the mechanism of H-atom abstraction, the hydroxyl radical would first attack the 6:2 FTS-K at the positions of two unfluorinated forming an intermediate m/z 459.0. Desulfonation resulted from further reaction with hydroxyl radical, which cleaved the bond between the polyfluorinated tail and the sulfonate end group ($-\text{SO}_3^-$). The polyfluorinated tail in this process may either convert directly into the unstable alcohol C₆F₁₃OH, it could be carboxylized at the end to generate PFHpA or it could then be further degraded into PFHxA [221,223,227]. Beatriz et al. [228] studied the electrochemical decomposition of 6:2 FTAB, also observing 6:2 FTSA release and formation of short-chain PFAA, similar to our results. They also proposed the direct formation of 6:2 FTSA from the mother compound and via other metabolites.

5 Conclusions and Future Work

Initially, various dyes (Rhodamine B, Malachite Green, and Acid Blue 74) were degraded using nZVI-Fenton-like system with H₂O₂ at different pHs. Various amounts of chemicals (nZVI/H₂O₂) were optimized to investigate the performance of nZVI-Fenton-like systems. These dyes significantly degraded with various optimized loadings of nZVI as well as H₂O₂ at different pH values. Furthermore, a nZVI-Fenton-like system using metabisulfite was used to degrade Acid Blue 74 using different amounts of nZVI as well as metabisulfite. AB74 was efficiently degraded by nZVI-metabisulfite and is predicted that these nZVI-fenton-like systems could be explored to degrade different persistent organic pollutants like GLY.

Significant GLY degradation was obtained in the pH range of 3-4 using the nZVI-Fenton-like system after optimization, which encompassed a variety of conditions of nZVI loading and H₂O₂ concentration. Unfortunately, the decrease in Fenton reactivity with increasing pH prevented effective degradation from being achieved at either pH 5 or 6. GLY removal was also obtained at pH 3 with nZVI alone, without H₂O₂, but the needed loading (300 mg/L) was 15-30 times higher compared to the loading required in nZVI-Fenton. That issue would be reflected in quite high costs for water treatment with ZVI alone.

In the case of tap water, complete (100%) GLY removal was achieved at pH 4 with 20 mg/L nZVI and 150+50 μM H₂O₂ (i.e., 150 μM added at t = 0, and 50 μM added after 30 min reaction time). Overall, water treatment costs for GLY with nZVI + H₂O₂ at pH 4 would be very reasonable in terms of expenditure for chemical reagents (a total of 0.07 \$ m⁻³, of which approximately 30% for nZVI + H₂O₂, and the rest for pH-adjustment reagents). Interestingly, these same conditions would also allow for the removal of additional emerging contaminants (pharmaceuticals) from the water matrix [29,42].

Potential drawbacks of water treatment in acidic conditions are the elevated costs for pH adjustment, the increase in water conductivity following the acidification necessary for the Fenton process to work, the basification at the end of treatment to

allow for water discharge, as well as the leaching of iron from nZVI due to increased iron solubility at acidic pH. As far as pH adjustment costs are concerned, we show here that they make up ~70% of the total reagent costs in the case of treatment at pH 4, and even ~80% for treatment at pH 3. With these limitations in mind, in this work, nZVI–Fenton was also tested at pH values of 5 and 6 but, unfortunately, no GLY degradation was achieved under these conditions. Water treatment at pH 4 would be quite satisfactory, however, because overall reagent costs would still be low, and the increase in conductivity was quite small, as compared for instance to treatment at pH 3. Moreover, tap-water conductivity more than doubled upon treatment at pH 3, while a 40% increase is expected to occur at pH 4. Therefore, final water conductivity for treatment at pH 4 would still allow for water reuse in agriculture, which is a very demanding field as far as conductivity requirements are concerned. Furthermore, iron leaching from nZVI at pH 4 was low enough for treated water to meet the legal limits for safe discharge into the environment, while the same would not occur in the case of treatment at pH 3.

For PFAS decomposition, we investigated the UV photolysis of PFOA and 6:2 FTAB at different pH values (4.0, 7.0, 10.0, and the original pH values, respectively, 5.6 and 6.5). All UV treatments lasted for more than 300 min. PFOA decomposition yielded shorter-chain PFAA like PFHpA, PFHxA, and PFPeA as major TPs. The process was most effective at pH 5.6; moreover, acidic pH had only minor effects on PFOA decomposition while basic pH provided considerable inhibition. The decomposition of 6:2 FTAB was affected by pH as well, and it yielded some shorter-chain PFAA and 6:2 FTSA that were identified by LC-MS analysis.

Results of scavenger experiments indicated that alcohols did not significantly affect the decomposition of PFOA, whereas ascorbic acid carried out considerable inhibition. Considering the roles of alcohols as selective $\cdot\text{OH}$ scavengers and of ascorbic acid as a general ROS scavenger (including $\cdot\text{OH}$), these results suggest that $\cdot\text{OH}$ was not involved in the decomposition of PFOA, which likely proceeded with the contribution of e_{aq}^- and/or $\text{O}_2^{\cdot-}$.

As far as 6:2 FTAB decomposition is concerned, the major decomposition product 6:2 FTSA was likely formed via the involvement of both direct and indirect photolysis. Differently from PFOA, we found clear indications that both $\cdot\text{OH}$ (especially) and $\text{O}_2^{\cdot-}$ are involved in the decomposition of 6:2 FTAB.

No consensus exists regarding the PFAS photo-reduction mechanisms. The relative importance of specific photo-reduction pathways of PFAS is still under debate. Mechanisms regarding PFAS removal through redox reactions needs to be deeply explored considering every perspective including all kinds of reactive species. In particular, the $\text{O}_2^{\cdot-}$ role could not be elucidated clearly in this study and needs to be addressed in future work. Moreover, clarification is needed regarding the role of e_{aq}^- in the degradation of 6:2 FTAB in future work. The efficiency of the treatment might be further improved by introducing stronger UV sources (for example, vacuum UV), suitable sensitizers, and optimized pH and temperature throughout the treatment.

Even though a lot of studies have been done on how PFAS break down, there are still a few issues that need to be resolved before technological solutions are used. First and foremost, research must be done to determine how co-contaminants and organics affect the breakdown of the full range of PFAS chemicals. The majority of research works have employed a basic water matrix, and those that have looked into the effects of specific water quality parameters have mostly examined the effects of one co-contaminant, making them unrepresentative of a genuine water matrix.

Additionally, in order to shorten the time of energy-intensive UV-based operations, it is necessary to minimize treatment costs, for instance, by implementing several complementary treatments. In order to make PFAS more susceptible to removal through straightforward and affordable pre- and post-UV based treatments, such as biological processes that could encourage particular bacteria to selectively degrade remaining PFAS and/or their intermediates, the focus must be on the partial degradation of the most resistant parts of PFAS. Though additional investigation is required to determine the effectiveness of oxidative and reductive mechanisms for targeted PFAS breakdown in combined treatment techniques under more difficult circumstances, both the oxidative and the reductive strategy seem promising. The

results of these investigations would aid in determining if these processes are feasible on a large scale. Future research should concentrate on examining the toxicity of water following UV treatment in order to comprehend how toxicity varies with various treatments and to endure the safety of treated waters.

6 References

1. Abu-Zeid, M.A. Water and Sustainable Development: The Vision for World Water, Life and the Environment. *Water policy* **1998**, *1*, 9–19.
2. Ahrens, L.; Xie, Z.; Ebinghaus, R. Distribution of Perfluoroalkyl Compounds in Seawater from Northern Europe, Atlantic Ocean, and Southern Ocean. *Chemosphere* **2010**, *78*, 1011–1016.
3. Higgins, C.P.; Luthy, R.G. Sorption of Perfluorinated Surfactants on Sediments. *Environ. Sci. Technol.* **2006**, *40*, 7251–7256.
4. Björklund, J.A.; Thuresson, K.A.J.; De Wit, C.A. Perfluoroalkyl Compounds (PFACs) in Indoor Dust: Concentrations, Human Exposure Estimates, and Sources. *Environ. Sci. Technol.* **2009**, *43*, 2276–2281.
5. Sunderland, E.M.; Hu, X.C.; Dassuncao, C.; Tokranov, A.K.; Wagner, C.C.; Allen, J.G. A Review of the Pathways of Human Exposure to Poly- and Perfluoroalkyl Substances (PFASs) and Present Understanding of Health Effects. *J. Expo. Sci. Environ. Epidemiol.* **2019**, *29*, 131–147.
6. Villamar-Ayala, C.A.; Carrera-Cevallos, J.V.; Vasquez-Medrano, R.; Espinoza-Montero, P.J. Fate, Eco-Toxicological Characteristics, and Treatment Processes Applied to Water Polluted with Glyphosate: A Critical Review. *Crit. Rev. Environ. Sci. Technol.* **2019**, *49*, 1476–1514.
7. Feng, D.; Soric, A.; Boutin, O. Treatment Technologies and Degradation Pathways of Glyphosate: A Critical Review. *Sci. Total Environ.* **2020**, *742*, 140559, doi:10.1016/J.SCITOTENV.2020.140559.
8. Key, B.D.; Howell, R.D.; Criddle, C.S. Fluorinated Organics in the Biosphere. *Environ. Sci. Technol.* **1997**, *31*, 2445–2454.
9. da Silva-Rackov, C.K.O.; Lawal, W.A.; Nfodzo, P.A.; Vianna, M.M.G.R.; do Nascimento, C.A.O.; Choi, H. Degradation of PFOA by Hydrogen Peroxide and Persulfate Activated by Iron-Modified Diatomite. *Appl. Catal. B Environ.* **2016**, *192*, 253–259.
10. Yamashita, N.; Kannan, K.; Taniyasu, S.; Horii, Y.; Petrick, G.; Gamo, T. A Global

- Survey of Perfluorinated Acids in Oceans. *Mar. Pollut. Bull.* **2005**, *51*, 658–668.
11. Espinoza-Montero, P.J.; Vega-Verduga, C.; Alulema-Pullupaxi, P.; Fernández, L.; Paz, J.L. Technologies Employed in the Treatment of Water Contaminated with Glyphosate: A Review. *Molecules* **2020**, *25*, doi:10.3390/molecules25235550.
 12. Chen, S.; Liu, Y. Study on the Photocatalytic Degradation of Glyphosate by TiO₂ Photocatalyst. *Chemosphere* **2007**, *67*, 1010–1017, doi:10.1016/J.CHEMOSPHERE.2006.10.054.
 13. Assalin, M.R.; de Moraes, S.G.; Queiroz, S.C.N.; Ferracini, V.L.; Duran, N. Studies on Degradation of Glyphosate by Several Oxidative Chemical Processes: Ozonation, Photolysis and Heterogeneous Photocatalysis. <http://dx.doi.org/10.1080/03601230903404598> **2009**, *45*, 89–94, doi:10.1080/03601230903404598.
 14. Bokare, A.D.; Choi, W. Review of Iron-Free Fenton-like Systems for Activating H₂O₂ in Advanced Oxidation Processes. *J. Hazard. Mater.* **2014**, *275*, 121–135, doi:10.1016/J.JHAZMAT.2014.04.054.
 15. Tran, M.H.; Nguyen, H.C.; Le, T.S.; Dang, V.A.D.; Cao, T.H.; Le, C.K.; Dang, T.D. Degradation of Glyphosate Herbicide by an Electro-Fenton Process Using Carbon Felt Cathode. <https://doi.org/10.1080/09593330.2019.1660411> **2019**, *42*, 1155–1164, doi:10.1080/09593330.2019.1660411.
 16. Yang, Y.; Deng, Q.; Yan, W.; Jing, C.; Zhang, Y. Comparative Study of Glyphosate Removal on Goethite and Magnetite: Adsorption and Photo-Degradation. *Chem. Eng. J.* **2018**, *352*, 581–589, doi:10.1016/J.CEJ.2018.07.058.
 17. Cao, L.; Ma, D.; Zhou, Z.; Xu, C.; Cao, C.; Zhao, P.; Huang, Q. Efficient Photocatalytic Degradation of Herbicide Glyphosate in Water by Magnetically Separable and Recyclable BiOBr/Fe₃O₄ Nanocomposites under Visible Light Irradiation. *Chem. Eng. J.* **2019**, *368*, 212–222, doi:10.1016/J.CEJ.2019.02.100.
 18. Ahmed, N.; Vione, D.; Rivoira, L.; Carena, L.; Castiglioni, M.; Bruzzoniti, M.C. A Review on the Degradation of Pollutants by Fenton-Like Systems Based on Zero-Valent Iron and Persulfate: Effects of Reduction Potentials, PH, and Anions Occurring in Waste Waters. *Mol.* **2021**, *Vol. 26*, Page 4584 **2021**, *26*,

- 4584, doi:10.3390/MOLECULES26154584.
19. Vaalgamaa, S.; Vähätalo, A. V.; Perkola, N.; Huhtala, S. Photochemical Reactivity of Perfluorooctanoic Acid (PFOA) in Conditions Representing Surface Water. *Sci. Total Environ.* **2011**, *409*, 3043–3048.
 20. Taniyasu, S.; Yamashita, N.; Yamazaki, E.; Petrick, G.; Kannan, K. The Environmental Photolysis of Perfluorooctanesulfonate, Perfluorooctanoate, and Related Fluorochemicals. *Chemosphere* **2013**, *90*, 1686–1692.
 21. Evenset, A.; Carroll, J.; Christensen, G.N.; Kallenborn, R.; Gregor, D.; Gabrielsen, G.W. Seabird Guano Is an Efficient Conveyer of Persistent Organic Pollutants (POPs) to Arctic Lake Ecosystems. *Environ. Sci. Technol.* **2007**, *41*, 1173–1179.
 22. Lehnik-Habrink, P.; Hein, S.; Win, T.; Bremser, W.; Nehls, I. Multi-Residue Analysis of PAH, PCB, and OCP Optimized for Organic Matter of Forest Soil. *J. soils sediments* **2010**, *10*, 1487–1498.
 23. Liu, Z.; Ren, X.; Duan, X.; Sarmah, A.K.; Zhao, X. Remediation of Environmentally Persistent Organic Pollutants (POPs) by Persulfates Oxidation System (PS): A Review. *Sci. Total Environ.* **2023**, *863*, 160818.
 24. Jones, K.C. Persistent Organic Pollutants (POPs) and Related Chemicals in the Global Environment: Some Personal Reflections. *Environ. Sci. Technol.* **2021**, *55*, 9400–9412.
 25. Fiorilli, S.; Rivoira, L.; Cali, G.; Appendini, M.; Bruzzoniti, M.C.; Coisson, M.; Onida, B. Iron Oxide inside SBA-15 Modified with Amino Groups as Reusable Adsorbent for Highly Efficient Removal of Glyphosate from Water. *Appl. Surf. Sci.* **2017**, *411*, 457–465, doi:10.1016/J.APSUSC.2017.03.206.
 26. Sun, B.; Li, Q.; Zheng, M.; Su, G.; Lin, S.; Wu, M.; Li, C.; Wang, Q.; Tao, Y.; Dai, L. Recent Advances in the Removal of Persistent Organic Pollutants (POPs) Using Multifunctional Materials: A Review. *Environ. Pollut.* **2020**, *265*, 114908.
 27. Borggaard, O.K.; Gimsing, A.L. Fate of Glyphosate in Soil and the Possibility of Leaching to Ground and Surface Waters: A Review. *Pest Manag. Sci. Former. Pestic. Sci.* **2008**, *64*, 441–456.

28. Cerdeira, A.L.; Duke, S.O. The Current Status and Environmental Impacts of Glyphosate-resistant Crops: A Review. *J. Environ. Qual.* **2006**, *35*, 1633–1658.
29. Glass, R.L. Metal Complex Formation by Glyphosate. *J. Agric. Food Chem.* **1984**, *32*, 1249–1253.
30. András, S.; Béla, D. *Herbicides: Properties, Synthesis and Control of Weeds* 2012.
31. Giesy, J.P.; Dobson, S.; Solomon, K.R. *Ecotoxicological Risk Assessment for Roundup® Herbicide*; Springer, 2000; ISBN 146127026X.
32. Mackay, D.; Shiu, W.-Y.; Lee, S.C. *Handbook of Physical-Chemical Properties and Environmental Fate for Organic Chemicals*; CRC press, 2006; ISBN 1420044397.
33. Vereecken, H. Mobility and Leaching of Glyphosate: A Review. *Pest Manag. Sci. Former. Pestic. Sci.* **2005**, *61*, 1139–1151.
34. Benbrook, C.M. Trends in Glyphosate Herbicide Use in the United States and Globally. *Environ. Sci. Eur.* **2016**, *28*, 1–15.
35. Ahmed, N.; Vione, D.; Rivoira, L.; Castiglioni, M.; Beldean-Galea, M.S.; Bruzzoniti, M.C. Feasibility of a Heterogeneous Nanoscale Zero-Valent Iron Fenton-like Process for the Removal of Glyphosate from Water. *Molecules* **2023**, *28*, 2214.
36. Kataoka, H.; Ryu, S.; Sakiyama, N.; Makita, M. Simple and Rapid Determination of the Herbicides Glyphosate and Glufosinate in River Water, Soil and Carrot Samples by Gas Chromatography with Flame Photometric Detection. *J. Chromatogr. A* **1996**, *726*, 253–258.
37. Andreotti, G.; Koutros, S.; Hofmann, J.N.; Sandler, D.P.; Lubin, J.H.; Lynch, C.F.; Lerro, C.C.; De Roos, A.J.; Parks, C.G.; Alavanja, M.C.; et al. Glyphosate Use and Cancer Incidence in the Agricultural Health Study. *JNCI J. Natl. Cancer Inst.* **2018**, *110*, 509–516, doi:10.1093/JNCI/DJX233.
38. Blake, R.; Pallett, K. The Environmental Fate and Ecotoxicity of Glyphosate. *Outlooks pest Manag.* **2018**, *29*, 266–269.
39. Meftaul, I.M.; Venkateswarlu, K.; Dharmarajan, R.; Annamalai, P.;

- Asaduzzaman, M.; Parven, A.; Megharaj, M. Controversies over Human Health and Ecological Impacts of Glyphosate: Is It to Be Banned in Modern Agriculture? *Environ. Pollut.* **2020**, *263*, 114372.
40. Baylis, A.D. Why Glyphosate Is a Global Herbicide: Strengths, Weaknesses and Prospects. *Pest Manag. Sci. Former. Pestic. Sci.* **2000**, *56*, 299–308.
41. Xing, B.; Chen, H.; Zhang, X. Efficient Degradation of Organic Phosphorus in Glyphosate Wastewater by Catalytic Wet Oxidation Using Modified Activated Carbon as a Catalyst. *Environ. Technol.* **2018**, *39*, 749–758.
42. Thanomsit, C.; Saowakoon, S.; Wattanakornsiri, A.; Nanuam, J.; Prasatkaew, W.; Nanthanawat, P.; Mongkolvai, P.; Chalorchaoenyng, W. The Glyphosate (Roundup): Fate in Aquatic Environment, Adverse Effect and Toxicity Assessment in Aquatic Organisms. *Naresuan Univ. J. Sci. Technol.* **2020**, *28*, 65–81.
43. Bacci, F.; Campo, P. Emerging and Less Commonly Recognized Chemical Contaminants: Organic Micropollutants. **2022**.
44. Gonçalves, B.B.; Giaquinto, P.C.; dos Santos Silva, D.; de Lima, A.A.; Darosci, A.A.B.; Portinho, J.L.; Carvalho, W.F.; Rocha, T.L. Ecotoxicology of Glyphosate-Based Herbicides on Aquatic Environment. In *Biochemical toxicology-heavy metals and nanomaterials*; IntechOpen, 2019; pp. 1–24 ISBN 1789846978.
45. Tsui, M.T.K.; Chu, L.M. Aquatic Toxicity of Glyphosate-Based Formulations: Comparison between Different Organisms and the Effects of Environmental Factors. *Chemosphere* **2003**, *52*, 1189–1197.
46. Moraes, J.S.; da Silva Nornberg, B.F.; de Castro, M.R.; dos Santos Vaz, B.; Mizuschima, C.W.; Marins, L.F.F.; Martins, C. de M.G. Zebrafish (*Danio Rerio*) Ability to Activate ABC Transporters after Exposure to Glyphosate and Its Formulation Roundup Transorb®. *Chemosphere* **2020**, *248*, 125959.
47. Meftaul, I.M.; Venkateswarlu, K.; Dharmarajan, R.; Annamalai, P.; Megharaj, M. Pesticides in the Urban Environment: A Potential Threat That Knocks at the Door. *Sci. Total Environ.* **2020**, *711*, 134612.
48. von Ehrenstein, O.S.; Ling, C.; Cui, X.; Cockburn, M.; Park, A.S.; Yu, F.; Wu, J.;

- Ritz, B. Prenatal and Infant Exposure to Ambient Pesticides and Autism Spectrum Disorder in Children: Population Based Case-Control Study. *bmj* **2019**, 364.
49. Peillex, C.; Pelletier, M. The Impact and Toxicity of Glyphosate and Glyphosate-Based Herbicides on Health and Immunity. *J. Immunotoxicol.* **2020**, *17*, 163–174.
 50. Spinaci, M.; Nerozzi, C.; Mislei, B.; Blanco-Prieto, O.; Mari, G.; Galeati, G.; Bucci, D. Impact of Glyphosate and Its Formulation Roundup® on Stallion Spermatozoa. *Theriogenology* **2022**, *179*, 197–203.
 51. Eceiza, M.V.; Gil-Monreal, M.; Barco-Antoñanzas, M.; Zabalza, A.; Royuela, M. The Moderate Oxidative Stress Induced by Glyphosate Is Not Detected in *Amaranthus Palmeri* Plants Overexpressing EPSPS. *J. Plant Physiol.* **2022**, *274*, 153720.
 52. Ghimire, S.; Flury, M.; Scheenstra, E.J.; Miles, C.A. Jo Ur Na I P Re Of. *Sci. Total Environ.* **2019**, 135577.
 53. Heldt, H.W.; Piechulla, B. Nitrate Assimilation Is Essential for the Synthesis of Organic Matter. *Plant Biochem* **2005**, 275–308.
 54. Cuhra, M.; Bøhn, T.; Cuhra, P. Glyphosate: Too Much of a Good Thing? *Front. Environ. Sci.* **2016**, *4*, 28, doi:10.3389/FENVS.2016.00028/BIBTEX.
 55. Fernandez, M.R.; Zentner, R.P.; Basnyat, P.; Gehl, D.; Selles, F.; Huber, D. Glyphosate Associations with Cereal Diseases Caused by *Fusarium* Spp. in the Canadian Prairies. *Eur. J. Agron.* **2009**, *31*, 133–143.
 56. Santos, B.M.; Gilreath, J.P.; Esmel, C.E.; Siham, M.N. Effects of Sublethal Glyphosate Rates on Fresh Market Tomato. *Crop Prot.* **2007**, *26*, 89–91.
 57. Hammerschmidt, R. How Glyphosate Affects Plant Disease Development: It Is More than Enhanced Susceptibility. *Pest Manag. Sci.* **2018**, *74*, 1054–1063.
 58. Ferrante, M.; Rapisarda, P.; Grasso, A.; Favara, C.; Conti, G.O. Glyphosate and Environmental Toxicity with “One Health” Approach, a Review. *Environ. Res.* **2023**, 116678.
 59. Lesueur, C.; Pfeffer, M.; Fuerhacker, M. Photodegradation of Phosphonates in

- Water. *Chemosphere* **2005**, *59*, 685–691.
60. Grandcoin, A.; Piel, S.; Baurès, E. AminoMethylPhosphonic Acid (AMPA) in Natural Waters: Its Sources, Behavior and Environmental Fate. *Water Res.* **2017**, *117*, 187–197.
 61. Richard, S.; Moslemi, S.; Sipahutar, H.; Benachour, N.; Seralini, G.-E. Differential Effects of Glyphosate and Roundup on Human Placental Cells and Aromatase. *Environ. Health Perspect.* **2005**, *113*, 716–720.
 62. Glyphosate, R.A.R. Renewal Assessment Report 2013.
 63. Niemann, L.; Sieke, C.; Pfeil, R.; Solecki, R. A Critical Review of Glyphosate Findings in Human Urine Samples and Comparison with the Exposure of Operators and Consumers. *J. für Verbraucherschutz und Leb.* **2015**, *10*, 3–12.
 64. Kwiatkowska, M.; Huras, B.; Bukowska, B. The Effect of Metabolites and Impurities of Glyphosate on Human Erythrocytes (in Vitro). *Pestic. Biochem. Physiol.* **2014**, *109*, 34–43.
 65. Reddy, K.N.; Rimando, A.M.; Duke, S.O. Aminomethylphosphonic Acid, a Metabolite of Glyphosate, Causes Injury in Glyphosate-Treated, Glyphosate-Resistant Soybean. *J. Agric. Food Chem.* **2004**, *52*, 5139–5143.
 66. Gomes, M.P.; Smedbol, E.; Chalifour, A.; Hénault-Ethier, L.; Labrecque, M.; Lepage, L.; Lucotte, M.; Juneau, P. Alteration of Plant Physiology by Glyphosate and Its By-Product Aminomethylphosphonic Acid: An Overview. *J. Exp. Bot.* **2014**, *65*, 4691–4703.
 67. Serra, A.-A.; Nuttens, A.; Larvor, V.; Renault, D.; Couée, I.; Sulmon, C.; Gouesbet, G. Low Environmentally Relevant Levels of Bioactive Xenobiotics and Associated Degradation Products Cause Cryptic Perturbations of Metabolism and Molecular Stress Responses in Arabidopsis Thaliana. *J. Exp. Bot.* **2013**, *64*, 2753–2766.
 68. Davis, K.L.; Aucoin, M.D.; Larsen, B.S.; Kaiser, M.A.; Hartten, A.S. Transport of Ammonium Perfluorooctanoate in Environmental Media near a Fluoropolymer Manufacturing Facility. *Chemosphere* **2007**, *67*, 2011–2019.
 69. Dickman, R.A.; Aga, D.S. A Review of Recent Studies on Toxicity, Sequestration,

- and Degradation of per-and Polyfluoroalkyl Substances (PFAS). *J. Hazard. Mater.* **2022**, *436*, 129120.
70. Genualdi, S.; Jeong, N.; Dejager, L.; Begley, T. Investigation into Perfluoroalkyl Substances (PFASs) in a Cranberry Bog: Method Development and Sampling Results. *Food Addit. Contam. Part A* **2017**, *34*, 2181–2189.
 71. Park, M.; Wu, S.; Lopez, I.J.; Chang, J.Y.; Karanfil, T.; Snyder, S.A. Adsorption of Perfluoroalkyl Substances (PFAS) in Groundwater by Granular Activated Carbons: Roles of Hydrophobicity of PFAS and Carbon Characteristics. *Water Res.* **2020**, *170*, 115364.
 72. Dhore, R.; Murthy, G.S. Per/Polyfluoroalkyl Substances Production, Applications and Environmental Impacts. *Bioresour. Technol.* **2021**, *341*, 125808.
 73. Rahman, M.F.; Peldszus, S.; Anderson, W.B. Behaviour and Fate of Perfluoroalkyl and Polyfluoroalkyl Substances (PFASs) in Drinking Water Treatment: A Review. *Water Res.* **2014**, *50*, 318–340.
 74. Nguyen, T.M.H.; Bräunig, J.; Thompson, K.; Thompson, J.; Kabiri, S.; Navarro, D.A.; Kookana, R.S.; Grimison, C.; Barnes, C.M.; Higgins, C.P. Influences of Chemical Properties, Soil Properties, and Solution PH on Soil–Water Partitioning Coefficients of per-and Polyfluoroalkyl Substances (PFASs). *Environ. Sci. Technol.* **2020**, *54*, 15883–15892.
 75. Olsen, G.W.; Mair, D.C.; Church, T.R.; Ellefson, M.E.; Reagen, W.K.; Boyd, T.M.; Herron, R.M.; Medhdizadehkashi, Z.; Nobiletti, J.B.; Rios, J.A. Decline in Perfluorooctanesulfonate and Other Polyfluoroalkyl Chemicals in American Red Cross Adult Blood Donors, 2000– 2006. *Environ. Sci. Technol.* **2008**, *42*, 4989–4995.
 76. Li, F.; Duan, J.; Tian, S.; Ji, H.; Zhu, Y.; Wei, Z.; Zhao, D. Short-Chain per-and Polyfluoroalkyl Substances in Aquatic Systems: Occurrence, Impacts and Treatment. *Chem. Eng. J.* **2020**, *380*, 122506.
 77. Krafft, M.P.; Riess, J.G. Selected Physicochemical Aspects of Poly-and Perfluoroalkylated Substances Relevant to Performance, Environment and

- Sustainability—Part One. *Chemosphere* **2015**, *129*, 4–19.
78. Brusseau, M.L. Assessing the Potential Contributions of Additional Retention Processes to PFAS Retardation in the Subsurface. *Sci. Total Environ.* **2018**, *613*, 176–185.
 79. Ateia, M.; Alsaiee, A.; Karanfil, T.; Dichtel, W. Efficient PFAS Removal by Amine-Functionalized Sorbents: Critical Review of the Current Literature. *Environ. Sci. Technol. Lett.* **2019**, *6*, 688–695.
 80. Shi, Y.; Vestergren, R.; Nost, T.H.; Zhou, Z.; Cai, Y. Probing the Differential Tissue Distribution and Bioaccumulation Behavior of Per-and Polyfluoroalkyl Substances of Varying Chain-Lengths, Isomeric Structures and Functional Groups in Crucian Carp. *Environ. Sci. Technol.* **2018**, *52*, 4592–4600.
 81. Backe, W.J.; Day, T.C.; Field, J.A. Zwitterionic, Cationic, and Anionic Fluorinated Chemicals in Aqueous Film Forming Foam Formulations and Groundwater from US Military Bases by Nonaqueous Large-Volume Injection HPLC-MS/MS. *Environ. Sci. Technol.* **2013**, *47*, 5226–5234.
 82. Barzen-Hanson, K.A.; Roberts, S.C.; Choyke, S.; Oetjen, K.; McAlees, A.; Riddell, N.; McCrindle, R.; Ferguson, P.L.; Higgins, C.P.; Field, J.A. Discovery of 40 Classes of Per-and Polyfluoroalkyl Substances in Historical Aqueous Film-Forming Foams (AFFFs) and AFFF-Impacted Groundwater. *Environ. Sci. Technol.* **2017**, *51*, 2047–2057.
 83. Yadav, S.; Ibrar, I.; Al-Juboori, R.A.; Singh, L.; Ganbat, N.; Kazwini, T.; Karbassiyazdi, E.; Samal, A.K.; Subbiah, S.; Altaee, A. Updated Review on Emerging Technologies for PFAS Contaminated Water Treatment. *Chem. Eng. Res. Des.* **2022**, *182*, 667–700.
 84. Ruyle, B.J.; Pickard, H.M.; LeBlanc, D.R.; Tokranov, A.K.; Thackray, C.P.; Hu, X.C.; Vecitis, C.D.; Sunderland, E.M. Isolating the AFFF Signature in Coastal Watersheds Using Oxidizable PFAS Precursors and Unexplained Organofluorine. *Environ. Sci. Technol.* **2021**, *55*, 3686–3695, doi:10.1021/ACS.EST.0C07296/SUPPL_FILE/ES0C07296_SI_002.XLSX.
 85. Brase, R.A.; Mullin, E.J.; Spink, D.C. Legacy and Emerging Per-and

- Polyfluoroalkyl Substances: Analytical Techniques, Environmental Fate, and Health Effects. *Int. J. Mol. Sci.* **2021**, *22*, 995.
86. Wang, Y.; Munir, U.; Huang, Q. Occurrence of Per- and Polyfluoroalkyl Substances (PFAS) in Soil: Sources, Fate, and Remediation. *Soil Environ. Heal.* **2023**, *1*, 100004, doi:10.1016/J.SEH.2023.100004.
87. Barbo, N.; Stoiber, T.; Naidenko, O. V.; Andrews, D.Q. Locally Caught Freshwater Fish across the United States Are Likely a Significant Source of Exposure to PFOS and Other Perfluorinated Compounds. *Environ. Res.* **2023**, *220*, 115165, doi:10.1016/J.ENVRES.2022.115165.
88. Habib, Z.; Song, M.; Ikram, S.; Zahra, Z. Overview of Per- and Polyfluoroalkyl Substances (PFAS), Their Applications, Sources, and Potential Impacts on Human Health. *Pollut. 2024, Vol. 4, Pages 136-152* **2024**, *4*, 136–152, doi:10.3390/POLLUTANTS4010009.
89. Kurwadkar, S.; Dane, J.; Kanel, S.R.; Nadagouda, M.N.; Cawdrey, R.W.; Ambade, B.; Struckhoff, G.C.; Wilkin, R. Per- and Polyfluoroalkyl Substances in Water and Wastewater: A Critical Review of Their Global Occurrence and Distribution. *Sci. Total Environ.* **2022**, *809*, 151003, doi:10.1016/J.SCITOTENV.2021.151003.
90. Shahsavari, E.; Rouch, D.; Khudur, L.S.; Thomas, D.; Aburto-Medina, A.; Ball, A.S. Challenges and Current Status of the Biological Treatment of PFAS-Contaminated Soils. *Front. Bioeng. Biotechnol.* **2021**, *8*, 602040, doi:10.3389/FBIOE.2020.602040/BIBTEX.
91. Domingo, J.L.; Nadal, M. Human Exposure to Per- and Polyfluoroalkyl Substances (PFAS) through Drinking Water: A Review of the Recent Scientific Literature. *Environ. Res.* **2019**, *177*, 108648, doi:10.1016/J.ENVRES.2019.108648.
92. Pétré, M.A.; Genereux, D.P.; Koropecj-Cox, L.; Knappe, D.R.U.; Duboscq, S.; Gilmore, T.E.; Hopkins, Z.R. Per- And Polyfluoroalkyl Substance (PFAS) Transport from Groundwater to Streams near a PFAS Manufacturing Facility in North Carolina, USA. *Environ. Sci. Technol.* **2021**, *55*, 5848–5856,

- doi:10.1021/ACS.EST.0C07978/SUPPL_FILE/ES0C07978_SI_002.XLSX.
93. Lenka, S.P.; Kah, M.; Padhye, L.P. Occurrence and Fate of Poly- and Perfluoroalkyl Substances (PFAS) in Urban Waters of New Zealand. *J. Hazard. Mater.* **2022**, *428*, 128257, doi:10.1016/J.JHAZMAT.2022.128257.
 94. Cserbik, D.; Redondo-Hasselerharm, P.E.; Farré, M.J.; Sanchís, J.; Bartolomé, A.; Paraián, A.; Herrera, E.M.; Caixach, J.; Villanueva, C.M.; Flores, C. Human Exposure to Per- and Polyfluoroalkyl Substances and Other Emerging Contaminants in Drinking Water. *npj Clean Water* **2023**, *6*, 1–10, doi:10.1038/s41545-023-00236-y.
 95. O'Connor, J.; Bolan, N.S.; Kumar, M.; Nitai, A.S.; Ahmed, M.B.; Bolan, S.S.; Vithanage, M.; Rinklebe, J.; Mukhopadhyay, R.; Srivastava, P.; et al. Distribution, Transformation and Remediation of Poly- and per-Fluoroalkyl Substances (PFAS) in Wastewater Sources. *Process Saf. Environ. Prot.* **2022**, *164*, 91–108, doi:10.1016/J.PSEP.2022.06.002.
 96. Krippner, J.; Falk, S.; Brunn, H.; Georgii, S.; Schubert, S.; Stahl, T. Accumulation Potentials of Perfluoroalkyl Carboxylic Acids (PFCAs) and Perfluoroalkyl Sulfonic Acids (PFSAs) in Maize (*Zea Mays*). *J. Agric. Food Chem.* **2015**, *63*, 3646–3653, doi:10.1021/ACS.JAFC.5B00012/SUPPL_FILE/JF5B00012_SI_001.PDF.
 97. Zhao, L.; Cheng, Z.; Zhu, H.; Chen, H.; Yao, Y.; Baqar, M.; Yu, H.; Qiao, B.; Sun, H. Electronic-Waste-Associated Pollution of per- and Polyfluoroalkyl Substances: Environmental Occurrence and Human Exposure. *J. Hazard. Mater.* **2023**, *451*, 131204, doi:10.1016/J.JHAZMAT.2023.131204.
 98. Tansel, B. PFAS Use in Electronic Products and Exposure Risks during Handling and Processing of E-Waste: A Review. *J. Environ. Manage.* **2022**, *316*, 115291, doi:10.1016/J.JENVMAN.2022.115291.
 99. Garg, S.; Kumar, P.; Mishra, V.; Guijt, R.; Singh, P.; Dumée, L.F.; Sharma, R.S. A Review on the Sources, Occurrence and Health Risks of per-/Poly-Fluoroalkyl Substances (PFAS) Arising from the Manufacture and Disposal of Electric and Electronic Products. *J. Water Process Eng.* **2020**, *38*, 101683,

- doi:10.1016/J.JWPE.2020.101683.
100. Lucas, K.; Gaines, L.G.T.; Paris-Davila, T.; Nylander-French, L.A. Occupational Exposure and Serum Levels of Per- and Polyfluoroalkyl Substances (PFAS): A Review. *Am. J. Ind. Med.* **2023**, *66*, 379–392, doi:10.1002/AJIM.23454.
 101. Schaidler, L.A.; Balan, S.A.; Blum, A.; Andrews, D.Q.; Strynar, M.J.; Dickinson, M.E.; Lunderberg, D.M.; Lang, J.R.; Peaslee, G.F. Fluorinated Compounds in U.S. Fast Food Packaging. *Environ. Sci. Technol. Lett.* **2017**, *4*, 105–111, doi:10.1021/ACS.ESTLETT.6B00435/ASSET/IMAGES/LARGE/EZ-2016-00435Z_0001.JPEG.
 102. Abraham, K.; Monien, B.H. Transdermal Absorption of ¹³C₄-Perfluorooctanoic Acid (¹³C₄-PFOA) from a Sunscreen in a Male Volunteer – What Could Be the Contribution of Cosmetics to the Internal Exposure of Perfluoroalkyl Substances (PFAS)? *Environ. Int.* **2022**, *169*, 107549, doi:10.1016/J.ENVINT.2022.107549.
 103. Chen, Q.; Yi, S.; Ye, Q.; Zhu, Y.; Zhong, W.; Zhu, L. Insights into the Dermal Absorption, Deposition, and Elimination of Poly- and Perfluoroalkyl Substances in Rats: The Importance of Skin Exposure. *Environ. Sci. Technol.* **2022**, *56*, 16975–16984, doi:10.1021/ACS.EST.2C03181/ASSET/IMAGES/LARGE/ES2C03181_0005.JPEG.
 104. D’Ambro, E.L.; Pye, H.O.T.; Bash, J.O.; Bowyer, J.; Allen, C.; Efstathiou, C.; Gilliam, R.C.; Reynolds, L.; Talgo, K.; Murphy, B.N. Characterizing the Air Emissions, Transport, and Deposition of Per- And Polyfluoroalkyl Substances from a Fluoropolymer Manufacturing Facility. *Environ. Sci. Technol.* **2021**, *55*, 862–870, doi:10.1021/ACS.EST.0C06580/ASSET/IMAGES/LARGE/ES0C06580_0006.JPEG.
 105. DeWitt, J.C.; Shnyra, A.; Badr, M.Z.; Loveless, S.E.; Hoban, D.; Frame, S.R.; Cunard, R.; Anderson, S.E.; Meade, B.J.; Peden-Adams, M.M. Immunotoxicity of Perfluorooctanoic Acid and Perfluorooctane Sulfonate and the Role of Peroxisome Proliferator-Activated Receptor Alpha. *Crit. Rev. Toxicol.* **2009**, *39*, 76–94.

106. Gordon, S.C. Toxicological Evaluation of Ammonium 4, 8-Dioxa-3H-Perfluorononanoate, a New Emulsifier to Replace Ammonium Perfluorooctanoate in Fluoropolymer Manufacturing. *Regul. Toxicol. Pharmacol.* **2011**, *59*, 64–80.
107. Cui, L.; Zhou, Q.; Liao, C.; Fu, J.; Jiang, G. Studies on the Toxicological Effects of PFOA and PFOS on Rats Using Histological Observation and Chemical Analysis. *Arch. Environ. Contam. Toxicol.* **2009**, *56*, 338–349.
108. Trudel, D.; Horowitz, L.; Wormuth, M.; Scheringer, M.; Cousins, I.T.; Hungerbühler, K. Estimating Consumer Exposure to PFOS and PFOA. *Risk Anal. An Int. J.* **2008**, *28*, 251–269.
109. Zhao, S.; Zhou, T.; Wang, B.; Zhu, L.; Chen, M.; Li, D.; Yang, L. Different Biotransformation Behaviors of Perfluorooctane Sulfonamide in Wheat (*Triticum Aestivum* L.) from Earthworms (*Eisenia Fetida*). *J. Hazard. Mater.* **2018**, *346*, 191–198.
110. Kwak, J. Il; Lee, T.-Y.; Seo, H.; Kim, D.; Kim, D.; Cui, R.; An, Y.-J. Ecological Risk Assessment for Perfluorooctanoic Acid in Soil Using a Species Sensitivity Approach. *J. Hazard. Mater.* **2020**, *382*, 121150.
111. Li, P.; Oyang, X.; Xie, X.; Li, Z.; Yang, H.; Xi, J.; Guo, Y.; Tian, X.; Liu, B.; Li, J. Phytotoxicity Induced by Perfluorooctanoic Acid and Perfluorooctane Sulfonate via Metabolomics. *J. Hazard. Mater.* **2020**, *389*, 121852.
112. Fabrello, J.; Ciscato, M.; Masiero, L.; Finos, L.; Valsecchi, S.; Polesello, S.; Bernardini, I.; Dalla Rovere, G.; Bargelloni, L.; Massimo, M. New Compounds, Old Problems. The Case of C6O4-a Substitute of PFOA-and Its Effects to the Clam *Ruditapes Philippinarum*. *J. Hazard. Mater.* **2021**, *420*, 126689.
113. Huang, J.; Wang, Q.; Liu, S.; Lai, H.; Tu, W. Comparative Chronic Toxicities of PFOS and Its Novel Alternatives on the Immune System Associated with Intestinal Microbiota Dysbiosis in Adult Zebrafish. *J. Hazard. Mater.* **2022**, *425*, 127950.
114. Lv, G.; Sun, X. The Molecular-Level Understanding of the Uptake of PFOS and Its Alternatives (6: 2 Cl-PFESA and OBS) into Phospholipid Bilayers. *J. Hazard.*

- Mater.* **2021**, *417*, 125991.
115. Xu, C.; Yin, S.; Liu, Y.; Chen, F.; Zhong, Z.; Li, F.; Liu, K.; Liu, W. Prenatal Exposure to Chlorinated Polyfluoroalkyl Ether Sulfonic Acids and Perfluoroalkyl Acids: Potential Role of Maternal Determinants and Associations with Birth Outcomes. *J. Hazard. Mater.* **2019**, *380*, 120867.
116. Wang, S.; Huang, J.; Yang, Y.; Hui, Y.; Ge, Y.; Larssen, T.; Yu, G.; Deng, S.; Wang, B.; Harman, C. First Report of a Chinese PFOS Alternative Overlooked for 30 Years: Its Toxicity, Persistence, and Presence in the Environment. *Environ. Sci. Technol.* **2013**, *47*, 10163–10170.
117. Carrizosa, C.; Murcia, M.; Ballesteros, V.; Costa, O.; Manzano-Salgado, C.B.; Ibarluzea, J.; Iñiguez, C.; Casas, M.; Andiarena, A.; Llop, S. Prenatal Perfluoroalkyl Substance Exposure and Neuropsychological Development throughout Childhood: The INMA Project. *J. Hazard. Mater.* **2021**, *416*, 125185.
118. Ogunbiyi, O.D.; Akamo, D.O.; Oluwasanmi, E.E.; Adebajo, J.; Isafiade, B.A.; Ogunbiyi, T.J.; Alli, Y.A.; Ayodele, D.T.; Oladoye, P.O. Glyphosate-Based Herbicide: Impacts, Detection, and Removal Strategies in Environmental Samples. *Groundw. Sustain. Dev.* **2023**, 100961.
119. Tao, Y.; Fang, F.; Lv, Q.; Qin, W.; He, X.; Zhang, Y.; Zhou, Y.; Li, X.; Li, J. Highly Efficient Removal of Glyphosate from Water by Hierarchical-Pore UiO-66: Selectivity and Effects of Natural Water Particles. *J. Environ. Manage.* **2022**, *316*, 115301, doi:10.1016/J.JENVMAN.2022.115301.
120. Ajiboye, T.O.; Ogunbiyi, O.D.; Omotola, E.O.; Adeyemi, W.J.; Agboola, O.O.; Onwudiwe, D.C. Urine: Useless or Useful “Waste”? *Results Eng.* **2022**, 100522.
121. Jia, D.M.; Li, C.H.; Li, A.M. Effective Removal of Glyphosate from Water by Resin-Supported Double Valent Nano-Sized Hydroxyl Iron Oxide. *RSC Adv.* **2017**, *7*, 24430–24437.
122. Chen, M.X.; Cao, Z.Y.; Jiang, Y.; Zhu, Z.W. Direct Determination of Glyphosate and Its Major Metabolite, Aminomethylphosphonic Acid, in Fruits and Vegetables by Mixed-Mode Hydrophilic Interaction/Weak Anion-Exchange

- Liquid Chromatography Coupled with Electrospray Tandem Mass Spectrometry. *J. Chromatogr. A* **2013**, *1272*, 90–99, doi:10.1016/J.CHROMA.2012.11.069.
123. Ochoa-Herrera, V.; Sierra-Alvarez, R. Removal of Perfluorinated Surfactants by Sorption onto Granular Activated Carbon, Zeolite and Sludge. *Chemosphere* **2008**, *72*, 1588–1593.
 124. Saeidi, N.; Kopinke, F.-D.; Georgi, A. Understanding the Effect of Carbon Surface Chemistry on Adsorption of Perfluorinated Alkyl Substances. *Chem. Eng. J.* **2020**, *381*, 122689.
 125. Jing, C.; Zhang, P.; Jian, L.I.U. Photodegradation of Perfluorooctanoic Acid by 185 Nm Vacuum Ultraviolet Light. *J. Environ. Sci.* **2007**, *19*, 387–390.
 126. Jin, L.; Zhang, P. Photochemical Decomposition of Perfluorooctane Sulfonate (PFOS) in an Anoxic Alkaline Solution by 185 Nm Vacuum Ultraviolet. *Chem. Eng. J.* **2015**, *280*, 241–247, doi:10.1016/J.CEJ.2015.06.022.
 127. Hori, H.; Yamamoto, A.; Koike, K.; Kutsuna, S.; Osaka, I.; Arakawa, R. Photochemical Decomposition of Environmentally Persistent Short-Chain Perfluorocarboxylic Acids in Water Mediated by Iron (II)/(III) Redox Reactions. *Chemosphere* **2007**, *68*, 572–578.
 128. Wang, Y.; Zhang, P.; Pan, G.; Chen, H. Ferric Ion Mediated Photochemical Decomposition of Perfluorooctanoic Acid (PFOA) by 254 Nm UV Light. *J. Hazard. Mater.* **2008**, *160*, 181–186.
 129. Panchangam, S.C.; Lin, A.Y.-C.; Shaik, K.L.; Lin, C.-F. Decomposition of Perfluorocarboxylic Acids (PFCAs) by Heterogeneous Photocatalysis in Acidic Aqueous Medium. *Chemosphere* **2009**, *77*, 242–248.
 130. Li, X.; Zhang, P.; Jin, L.; Shao, T.; Li, Z.; Cao, J. Efficient Photocatalytic Decomposition of Perfluorooctanoic Acid by Indium Oxide and Its Mechanism. *Environ. Sci. Technol.* **2012**, *46*, 5528–5534.
 131. Zhao, B.; Zhang, P. Photocatalytic Decomposition of Perfluorooctanoic Acid with β -Ga₂O₃ Wide Bandgap Photocatalyst. *Catal. Commun.* **2009**, *10*, 1184–1187.

132. Verma, S.; Mezgebe, B.; Hejase, C.A.; Sahle-Demessie, E.; Nadagouda, M.N. Photodegradation and Photocatalysis of Per- and Polyfluoroalkyl Substances (PFAS): A Review of Recent Progress. *Next Mater.* **2024**, *2*, 100077, doi:10.1016/J.NXMATE.2023.100077.
133. Wang, J.L.; Xu, L.J. Advanced Oxidation Processes for Wastewater Treatment: Formation of Hydroxyl Radical and Application. *Crit. Rev. Environ. Sci. Technol.* **2012**, *42*, 251–325.
134. Manassero, A.; Passalia, C.; Negro, A.C.; Cassano, A.E.; Zalazar, C.S. Glyphosate Degradation in Water Employing the H₂O₂/UVC Process. *Water Res.* **2010**, *44*, 3875–3882, doi:10.1016/J.WATRES.2010.05.004.
135. Anipsitakis, G.P.; Dionysiou, D.D. Degradation of Organic Contaminants in Water with Sulfate Radicals Generated by the Conjunction of Peroxymonosulfate with Cobalt. *Environ. Sci. Technol.* **2003**, *37*, 4790–4797, doi:10.1021/ES0263792/ASSET/IMAGES/MEDIUM/ES0263792E00013.GIF.
136. Rezaei, F.; Vione, D. Effect of PH on Zero Valent Iron Performance in Heterogeneous Fenton and Fenton-like Processes: A Review. *Molecules* **2018**, *23*, doi:10.3390/MOLECULES23123127.
137. Deng, J.; Shao, Y.; Gao, N.; Deng, Y.; Tan, C.; Zhou, S. Zero-Valent Iron/Persulfate(Fe⁰/PS) Oxidation Acetaminophen in Water. *Int. J. Environ. Sci. Technol.* **2014**, *11*, 881–890, doi:10.1007/S13762-013-0284-2/FIGURES/8.
138. Wu, J.; Wang, B.; Cagnetta, G.; Huang, J.; Wang, Y.; Deng, S.; Yu, G. Nanoscale Zero Valent Iron-Activated Persulfate Coupled with Fenton Oxidation Process for Typical Pharmaceuticals and Personal Care Products Degradation. *Sep. Purif. Technol.* **2020**, *239*, 116534.
139. Jiang, X.; Wu, Y.; Wang, P.; Li, H.; Dong, W. Degradation of Bisphenol A in Aqueous Solution by Persulfate Activated with Ferrous Ion. *Environ. Sci. Pollut. Res.* **2013**, *20*, 4947–4953, doi:10.1007/S11356-013-1468-5/TABLES/2.
140. Hori, H.; Yamamoto, A.; Hayakawa, E.; Taniyasu, S.; Yamashita, N.; Kutsuna, S.; Kiatagawa, H.; Arakawa, R. Efficient Decomposition of Environmentally Persistent Perfluorocarboxylic Acids by Use of Persulfate as a Photochemical

- Oxidant. *Environ. Sci. Technol.* **2005**, *39*, 2383–2388.
141. Lutze, H. V; Brekenfeld, J.; Naumov, S.; von Sonntag, C.; Schmidt, T.C. Degradation of Perfluorinated Compounds by Sulfate Radicals—New Mechanistic Aspects and Economical Considerations. *Water Res.* **2018**, *129*, 509–519.
142. Kutsuna, S.; Hori, H. Rate Constants for Aqueous-phase Reactions of SO₄⁻ with C₂F₅C(O)O⁻ and C₃F₇C(O)O⁻ at 298 K. *Int. J. Chem. Kinet.* **2007**, *39*, 276–288.
143. Qian, Y.; Guo, X.; Zhang, Y.; Peng, Y.; Sun, P.; Huang, C.-H.; Niu, J.; Zhou, X.; Crittenden, J.C. Perfluorooctanoic Acid Degradation Using UV–Persulfate Process: Modeling of the Degradation and Chlorate Formation. *Environ. Sci. Technol.* **2016**, *50*, 772–781.
144. Zhang, B.-T.; Zhang, Y.; Teng, Y.; Fan, M. Sulfate Radical and Its Application in Decontamination Technologies. *Crit. Rev. Environ. Sci. Technol.* **2015**, *45*, 1756–1800.
145. Lutze, H. V; Kerlin, N.; Schmidt, T.C. Sulfate Radical-Based Water Treatment in Presence of Chloride: Formation of Chlorate, Inter-Conversion of Sulfate Radicals into Hydroxyl Radicals and Influence of Bicarbonate. *Water Res.* **2015**, *72*, 349–360.
146. Kim, C.; Thao, T.T.; Kim, J.-H.; Hwang, I. Effects of the Formation of Reactive Chlorine Species on Oxidation Process Using Persulfate and Nano Zero-Valent Iron. *Chemosphere* **2020**, *250*, 126266.
147. Rayaroth, M.P.; Lee, C.-S.; Aravind, U.K.; Aravindakumar, C.T.; Chang, Y.-S. Oxidative Degradation of Benzoic Acid Using Fe⁰-and Sulfidized Fe⁰-Activated Persulfate: A Comparative Study. *Chem. Eng. J.* **2017**, *315*, 426–436.
148. Neta, P.; Huie, R.E.; Ross, A.B. Rate Constants for Reactions of Inorganic Radicals in Aqueous Solution. *J. Phys. Chem. Ref. Data* **1988**, *17*, 1027–1284.
149. Wardman, P. Reduction Potentials of One-electron Couples Involving Free Radicals in Aqueous Solution. *J. Phys. Chem. Ref. Data* **1989**, *18*, 1637–1755.
150. Bennedsen, L.R.; Muff, J.; Sjøgaard, E.G. Influence of Chloride and Carbonates

- on the Reactivity of Activated Persulfate. *Chemosphere* **2012**, *86*, 1092–1097, doi:10.1016/J.CHEMOSPHERE.2011.12.011.
151. Hayat, W.; Zhang, Y.; Hussain, I.; Du, X.; Du, M.; Yao, C.; Huang, S.; Si, F. Efficient Degradation of Imidacloprid in Water through Iron Activated Sodium Persulfate. *Chem. Eng. J.* **2019**, *370*, 1169–1180.
152. Zhao, X.; Zhang, T.; Lu, J.; Zhou, L.; Chovelon, J.-M.; Ji, Y. Formation of Chloronitrophenols upon Sulfate Radical-Based Oxidation of 2-Chlorophenol in the Presence of Nitrite. *Environ. Pollut.* **2020**, *261*, 114242, doi:https://doi.org/10.1016/j.envpol.2020.114242.
153. Lim, S.; Shi, J.L.; von Gunten, U.; McCurry, D.L. Ozonation of Organic Compounds in Water and Wastewater: A Critical Review. *Water Res.* **2022**, *213*, 118053, doi:10.1016/J.WATRES.2022.118053.
154. Jönsson, J.; Camm, R.; Hall, T. Removal and Degradation of Glyphosate in Water Treatment: A Review. *J. Water Supply Res. Technol.* **2013**, *62*, 395–408, doi:10.2166/AQUA.2013.080.
155. Dombrowski, P.M.; Kakarla, P.; Caldicott, W.; Chin, Y.; Sadeghi, V.; Bogdan, D.; Barajas-Rodriguez, F.; Chiang, S.Y.D. Technology Review and Evaluation of Different Chemical Oxidation Conditions on Treatability of PFAS. *Remediat. J.* **2018**, *28*, 135–150, doi:10.1002/REM.21555.
156. Verma, S.; Varma, R.S.; Nadagouda, M.N. Remediation and Mineralization Processes for Per- and Polyfluoroalkyl Substances (PFAS) in Water: A Review. *Sci. Total Environ.* **2021**, *794*, 148987, doi:10.1016/J.SCITOTENV.2021.148987.
157. Lin, A.Y.C.; Panchangam, S.C.; Chang, C.Y.; Hong, P.K.A.; Hsueh, H.F. Removal of Perfluorooctanoic Acid and Perfluorooctane Sulfonate via Ozonation under Alkaline Condition. *J. Hazard. Mater.* **2012**, *243*, 272–277, doi:10.1016/J.JHAZMAT.2012.10.029.
158. Franke, V.; Schäfers, M.D.; Lindberg, J.J.; Ahrens, L. Removal of Per- and Polyfluoroalkyl Substances (PFASs) from Tap Water Using Heterogeneously Catalyzed Ozonation. *Environ. Sci. Water Res. Technol.* **2019**, *5*, 1887–1896, doi:10.1039/C9EW00339H.

159. Park, H.; Vecitis, C.D.; Cheng, J.; Dalleska, N.F.; Mader, B.T.; Hoffmann, M.R. Reductive Degradation of Perfluoroalkyl Compounds with Aquated Electrons Generated from Iodide Photolysis at 254 Nm. *Photochem. Photobiol. Sci.* **2011**, *10*, 1945–1953, doi:10.1039/C1PP05270E.
160. Bentel, M.J.; Yu, Y.; Xu, L.; Li, Z.; Wong, B.M.; Men, Y.; Liu, J. Defluorination of Per- and Polyfluoroalkyl Substances (PFASs) with Hydrated Electrons: Structural Dependence and Implications to PFAS Remediation and Management. *Environ. Sci. Technol.* **2019**, *53*, 3718–3728, doi:10.1021/ACS.EST.8B06648/ASSET/IMAGES/LARGE/ES-2018-06648G_0006.JPEG.
161. Huang, L.; Dong, W.; Hou, H. Investigation of the Reactivity of Hydrated Electron toward Perfluorinated Carboxylates by Laser Flash Photolysis. *Chem. Phys. Lett.* **2007**, *436*, 124–128, doi:10.1016/J.CPLETT.2007.01.037.
162. Szajdzinska-Pietek, E.; Gebicki, J.L. Pulse Radiolytic Investigation of Perfluorinated Surfactants in Aqueous Solutions. *Res. Chem. Intermed.* **2000**, *26*, 897–912, doi:10.1163/156856700X00381/METRICS.
163. Chen, Y.; Wu, F.; Lin, Y.; Deng, N.; Bazhin, N.; Glebov, E. Photodegradation of Glyphosate in the Ferrioxalate System. *J. Hazard. Mater.* **2007**, *148*, 360–365, doi:10.1016/J.JHAZMAT.2007.02.044.
164. Muneer, M.; Boxall, C. Photocatalyzed Degradation of a Pesticide Derivative Glyphosate in Aqueous Suspensions of Titanium Dioxide. *Int. J. Photoenergy* **2008**, *2008*, doi:10.1155/2008/197346.
165. Balci, B.; Oturan, M.A.; Oturan, N.; Sires, I. Decontamination of Aqueous Glyphosate, (Aminomethyl) Phosphonic Acid, and Glufosinate Solutions by Electro-Fenton-like Process with Mn²⁺ as the Catalyst. *J. Agric. Food Chem.* **2009**, *57*, 4888–4894, doi:10.1021/JF900876X/ASSET/IMAGES/LARGE/JF-2009-00876X_0007.JPEG.
166. Echavia, G.R.M.; Matzusawa, F.; Negishi, N. Photocatalytic Degradation of Organophosphate and Phosphonoglycine Pesticides Using TiO₂ Immobilized on Silica Gel. *Chemosphere* **2009**, *76*, 595–600,

- doi:10.1016/J.CHEMOSPHERE.2009.04.055.
167. Manassero, A.; Passalia, C.; Negro, A.C.; Cassano, A.E.; Zalazar, C.S. Glyphosate Degradation in Water Employing the H₂O₂/UVC Process. *Water Res.* **2010**, *44*, 3875–3882.
 168. Xue, W.; Zhang, G.; Xu, X.; Yang, X.; Liu, C.; Xu, Y. Preparation of Titania Nanotubes Doped with Cerium and Their Photocatalytic Activity for Glyphosate. *Chem. Eng. J.* **2011**, *167*, 397–402, doi:10.1016/J.CEJ.2011.01.007.
 169. Vidal, E.; Negro, A.; Cassano, A.; Zalazar, C. Simplified Reaction Kinetics, Models and Experiments for Glyphosate Degradation in Water by the UV/H₂O₂ Process. *Photochem. Photobiol. Sci.* **2015**, *14*, 366–377.
 170. López, A.; Coll, A.; Lescano, M.; Zalazar, C. Advanced Oxidation of Commercial Herbicides Mixture: Experimental Design and Phytotoxicity Evaluation. *Environ. Sci. Pollut. Res.* **2018**, *25*, 21393–21402.
 171. Garcia-Muñoz, P.; Dachtler, W.; Altmayer, B.; Schulz, R.; Robert, D.; Seitz, F.; Rosenfeldt, R.; Keller, N. Reaction Pathways, Kinetics and Toxicity Assessment during the Photocatalytic Degradation of Glyphosate and Myclobutanil Pesticides: Influence of the Aqueous Matrix. *Chem. Eng. J.* **2020**, *384*, 123315, doi:10.1016/J.CEJ.2019.123315.
 172. Lv, Y.R.; He, R.K.; Chen, Z.Y.; Li, X.; Xu, Y.H. Fabrication of Hierarchical Copper Sulfide/Bismuth Tungstate p-n Heterojunction with Two-Dimensional (2D) Interfacial Coupling for Enhanced Visible-Light Photocatalytic Degradation of Glyphosate. *J. Colloid Interface Sci.* **2020**, *560*, 293–302, doi:10.1016/J.JCIS.2019.10.064.
 173. Souza, D.R.D.; Trovõ, A.G.; Filho, N.R.A.; Silva, M.A.A.; Machado, A.E.H. Degradation of the Commercial Herbicide Glyphosate by Photo-Fenton Process: Evaluation of Kinetic Parameters and Toxicity. *J. Braz. Chem. Soc.* **2013**, *24*, 1451–1460, doi:10.5935/0103-5053.20130185.
 174. Lan, H.; He, W.; Wang, A.; Liu, R.; Liu, H.; Qu, J.; Huang, C.P. An Activated Carbon Fiber Cathode for the Degradation of Glyphosate in Aqueous Solutions by the Electro-Fenton Mode: Optimal Operational Conditions and the

- Deposition of Iron on Cathode on Electrode Reusability. *Water Res.* **2016**, *105*, 575–582, doi:10.1016/J.WATRES.2016.09.036.
175. Aquino Neto, S.; de Andrade, A.R. Electrooxidation of Glyphosate Herbicide at Different DSA® Compositions: PH, Concentration and Supporting Electrolyte Effect. *Electrochim. Acta* **2009**, *54*, 2039–2045, doi:10.1016/J.ELECTACTA.2008.07.019.
176. Zhang, M.; Wei, Y.; Zhao, K.; Mei, R.; Huang, M. Glyphosate Degradation with Industrial Wastewater Effluent by Combined Adsorption Treatment and Advanced Oxidation Processes. *Adv. Mater. Res.* **2011**, *233–235*, 369–372, doi:10.4028/WWW.SCIENTIFIC.NET/AMR.233-235.369.
177. Lan, H.; Jiao, Z.; Zhao, X.; He, W.; Wang, A.; Liu, H.; Liu, R.; Qu, J. Removal of Glyphosate from Water by Electrochemically Assisted MnO₂ Oxidation Process. *Sep. Purif. Technol.* **2013**, *117*, 30–34, doi:10.1016/J.SEPPUR.2013.04.012.
178. Sánchez-Montes, I.; Pérez, J.F.; Sáez, C.; Rodrigo, M.A.; Cañizares, P.; Aquino, J.M. Assessing the Performance of Electrochemical Oxidation Using DSA® and BDD Anodes in the Presence of UVC Light. *Chemosphere* **2020**, *238*, 124575, doi:10.1016/J.CHEMOSPHERE.2019.124575.
179. Rubí-Juárez, H.; Cotillas, S.; Sáez, C.; Cañizares, P.; Barrera-Díaz, C.; Rodrigo, M.A. Use of Conductive Diamond Photo-Electrochemical Oxidation for the Removal of Pesticide Glyphosate. *Sep. Purif. Technol.* **2016**, *167*, 127–135, doi:10.1016/J.SEPPUR.2016.04.048.
180. Ahmed, M.B.; Alam, M.M.; Zhou, J.L.; Xu, B.; Johir, M.A.H.; Karmakar, A.K.; Rahman, M.S.; Hossen, J.; Hasan, A.T.M.K.; Moni, M.A. Advanced Treatment Technologies Efficacies and Mechanism of Per- and Poly-Fluoroalkyl Substances Removal from Water. *Process Saf. Environ. Prot.* **2020**, *136*, 1–14, doi:10.1016/J.PSEP.2020.01.005.
181. Campbell, T.Y. Sonochemical Decomposition of Perfluorinated Surfactants: Chain Length Effects Thesis By. **2012**.
182. Moriwaki, H.; Takagi, Y.; Tanaka, M.; Tsuruho, K.; Okitsu, K.; Maeda, Y.

- Sonochemical Decomposition of Perfluorooctane Sulfonate and Perfluorooctanoic Acid. *Environ. Sci. Technol.* **2005**, *39*, 3388–3392, doi:10.1021/ES040342V/ASSET/IMAGES/LARGE/ES040342VF00005.JPEG.
183. Trautmann, A.M.; Schell, H.; Schmidt, K.R.; Mangold, K.M.; Tiehm, A. Electrochemical Degradation of Perfluoroalkyl and Polyfluoroalkyl Substances (PFASs) in Groundwater. *Water Sci. Technol.* **2015**, *71*, 1569–1575, doi:10.2166/WST.2015.143.
184. Schaefer, C.E.; Andaya, C.; Urriaga, A.; McKenzie, E.R.; Higgins, C.P. Electrochemical Treatment of Perfluorooctanoic Acid (PFOA) and Perfluorooctane Sulfonic Acid (PFOS) in Groundwater Impacted by Aqueous Film Forming Foams (AFFFs). *J. Hazard. Mater.* **2015**, *295*, 170–175, doi:10.1016/J.JHAZMAT.2015.04.024.
185. Marín-Marín, M.L.; Rubio-Clemente, A.; Peñuela, G. Procesos de Oxidación Avanzada Utilizados En El Tratamiento de Sustancias Perfluoroalquiladas En Agua. *Rev. UIS Ing.* **2023**, *22*, 135–150, doi:10.18273/REVUIN.V22N3-2023010.
186. Ochiai, T.; Iizuka, Y.; Nakata, K.; Murakami, T.; Tryk, D.A.; Koide, Y.; Morito, Y.; Fujishima, A. Efficient Decomposition of Perfluorocarboxylic Acids in Aqueous Suspensions of a TiO₂ Photocatalyst with Medium-Pressure Ultraviolet Lamp Irradiation under Atmospheric Pressure. *Ind. Eng. Chem. Res.* **2011**, *50*, 10943–10947, doi:10.1021/IE1017496/ASSET/IMAGES/LARGE/IE-2010-017496_0002.JPEG.
187. Zhao, B.; Lv, M.; Zhou, L. Photocatalytic Degradation of Perfluorooctanoic Acid with β -Ga₂O₃ in Anoxic Aqueous Solution. *J. Environ. Sci.* **2012**, *24*, 774–780, doi:10.1016/S1001-0742(11)60818-8.
188. Takeuchi, N.; Oishi, R.; Kitagawa, Y.; Yasuoka, K. Adsorption and Efficient Decomposition of Perfluoro Compounds at Plasma-Water Interface. *IEEE Trans. Plasma Sci.* **2011**, *39*, 3358–3363, doi:10.1109/TPS.2011.2171374.
189. Jin, L.; Zhang, P.; Shao, T.; Zhao, S. Ferric Ion Mediated Photodecomposition of Aqueous Perfluorooctane Sulfonate (PFOS) under UV Irradiation and Its Mechanism. *J. Hazard. Mater.* **2014**, *271*, 9–15.

190. Carter, K.E.; Farrell, J. Oxidative Destruction of Perfluorooctane Sulfonate Using Boron-Doped Diamond Film Electrodes. *Environ. Sci. Technol.* **2008**, *42*, 6111–6115, doi:10.1021/ES703273S/SUPPL_FILE/ES703273S-FILE003.PDF.
191. Ma, S.H.; Wu, M.H.; Tang, L.; Sun, R.; Zang, C.; Xiang, J.J.; Yang, X.X.; Li, X.; Xu, G. EB Degradation of Perfluorooctanoic Acid and Perfluorooctane Sulfonate in Aqueous Solution. *Nucl. Sci. Tech.* **2017**, *28*, 1–8, doi:10.1007/S41365-017-0278-8/FIGURES/5.
192. Wang, W.; Chen, Y.; Li, G.; Gu, W.; An, T. Photocatalytic Reductive Defluorination of Perfluorooctanoic Acid in Water under Visible Light Irradiation: The Role of Electron Donor. *Environ. Sci. Water Res. Technol.* **2020**, *6*, 1638–1648, doi:10.1039/D0EW00205D.
193. Song, Z.; Tang, H.; Wang, N.; Zhu, L. Reductive Defluorination of Perfluorooctanoic Acid by Hydrated Electrons in a Sulfite-Mediated UV Photochemical System. *J. Hazard. Mater.* **2013**, *262*, 332–338, doi:10.1016/J.JHAZMAT.2013.08.059.
194. Gu, Y.; Dong, W.; Luo, C.; Liu, T. Efficient Reductive Decomposition of Perfluorooctanesulfonate in a High Photon Flux UV/Sulfite System. *Environ. Sci. Technol.* **2016**, *50*, 10554–10561, doi:10.1021/ACS.EST.6B03261/ASSET/IMAGES/LARGE/ES-2016-032616_0003.JPEG.
195. Wang, Y.; Zhang, P. Photocatalytic Decomposition of Perfluorooctanoic Acid (PFOA) by TiO₂ in the Presence of Oxalic Acid. *J. Hazard. Mater.* **2011**, *192*, 1869–1875, doi:10.1016/J.JHAZMAT.2011.07.026.
196. Trojanowicz, M.; Bartosiewicz, I.; Bojanowska-Czajka, A.; Szreder, T.; Bobrowski, K.; Nałęcz-Jawecki, G.; Męczyńska-Wielgosz, S.; Nichipor, H. Application of Ionizing Radiation in Decomposition of Perfluorooctane Sulfonate (PFOS) in Aqueous Solutions. *Chem. Eng. J.* **2020**, *379*, 122303, doi:10.1016/J.CEJ.2019.122303.
197. Buxton, G. V.; Greenstock, C.L.; Helman, W.P.; Ross, A.B. Critical Review of Rate Constants for Reactions of Hydrated Electrons, Hydrogen Atoms and

- Hydroxyl Radicals ($\cdot\text{OH}/\cdot\text{O}^-$ in Aqueous Solution. *J. Phys. Chem. Ref. Data* **1988**, *17*, 513–886, doi:10.1063/1.555805.
198. Liao, C.H.; Kang, S.F.; Wu, F.A. Hydroxyl Radical Scavenging Role of Chloride and Bicarbonate Ions in the $\text{H}_2\text{O}_2/\text{UV}$ Process. *Chemosphere* **2001**, *44*, 1193–1200, doi:10.1016/S0045-6535(00)00278-2.
199. Kuhn, R.; Bryant, I.M.; Jensch, R.; Liebsch, S.; Martienssen, M. Photolysis of Hexamethylenediaminetetra (Methylenephosphonic Acid)(HDTMP) Using Manganese and Hydrogen Peroxide. *Emerg. Contam.* **2020**, *6*, 10–19.
200. Kuhn, R.; Jensch, R.; Fischer, T.; Keuler, K.; Bryant, I.M.; Martienssen, M. Sunlight Degradation of the Aminophosphonate Diethylenetriamine Penta-(Methylenephosphonic Acid). In Proceedings of the Solar; MDPI, 2022; Vol. 2, pp. 141–157.
201. Minella, M.; Bertinetti, S.; Hanna, K.; Minero, C.; Vione, D. Degradation of Ibuprofen and Phenol with a Fenton-like Process Triggered by Zero-Valent Iron (ZVI-Fenton). *Environ. Res.* **2019**, *179*, 108750, doi:10.1016/J.ENVRES.2019.108750.
202. Furia, F.; Minella, M.; Gosetti, F.; Turci, F.; Sabatino, R.; Di Cesare, A.; Corno, G.; Vione, D. Elimination from Wastewater of Antibiotics Reserved for Hospital Settings, with a Fenton Process Based on Zero-Valent Iron. *Chemosphere* **2021**, *283*.
203. Keenan, C.R.; Sedlak, D.L. Ligand-Enhanced Reactive Oxidant Generation by Nanoparticulate Zero-Valent Iron and Oxygen. *Environ. Sci. Technol.* **2008**, *42*, 6936–6941, doi:10.1021/es801438f.
204. Salgot, M.; Huertas, E.; Weber, S.; Dott, W.; Hollender, J. Wastewater Reuse and Risk: Definition of Key Objectives. *Desalination* **2006**, *187*, 29–40, doi:10.1016/j.desal.2005.04.065.
205. Hu, Y.S.; Zhao, Y.Q.; Sorohan, B. Removal of Glyphosate from Aqueous Environment by Adsorption Using Water Industrial Residual. *Desalination* **2011**, *271*, 150–156, doi:10.1016/J.DESAL.2010.12.014.
206. Dissanayake Herath, G.A.; Poh, L.S.; Ng, W.J. Statistical Optimization of

- Glyphosate Adsorption by Biochar and Activated Carbon with Response Surface Methodology. *Chemosphere* **2019**, *227*, 533–540, doi:10.1016/J.CHEMOSPHERE.2019.04.078.
207. Balabanič, D.; Hermosilla, D.; Merayo, N.; Klemenčič, A.K.; Blanco, A. Comparison of Different Wastewater Treatments for Removal of Selected Endocrine-Disruptors from Paper Mill Wastewaters. *J. Environ. Sci. Heal. Part A* **2012**, *47*, 1350–1363.
208. Cheng, M.; Zeng, G.; Huang, D.; Lai, C.; Xu, P.; Zhang, C.; Liu, Y. Hydroxyl Radicals Based Advanced Oxidation Processes (AOPs) for Remediation of Soils Contaminated with Organic Compounds: A Review. *Chem. Eng. J.* **2016**, *284*, 582–598.
209. Chen, Z.; Teng, Y.; Wang, W.; Hong, R.; Huang, L.; Wang, X.; Zhu, F.; Li, H.; Hao, S.; Wu, B.; et al. Enhanced UV Photoreductive Destruction of Perfluorooctanoic Acid in the Presence of Alcohols: Synergistic Mechanism of Hydroxyl Radical Quenching and Solvent Effect. *Appl. Catal. B Environ.* **2022**, *316*, 121652, doi:https://doi.org/10.1016/j.apcatb.2022.121652.
210. Wang, Y.; Zhang, P. Effects of PH on Photochemical Decomposition of Perfluorooctanoic Acid in Different Atmospheres by 185 Nm Vacuum Ultraviolet. *J. Environ. Sci.* **2014**, *26*, 2207–2214.
211. Qu, Y.; Zhang, C.-J.; Chen, P.; Zhou, Q.; Zhang, W.-X. Effect of Initial Solution PH on Photo-Induced Reductive Decomposition of Perfluorooctanoic Acid. *Chemosphere* **2014**, *107*, 218–223.
212. Giri, R.R.; Ozaki, H.; Okada, T.; Taniguchi, S.; Takanami, R. Factors Influencing UV Photodecomposition of Perfluorooctanoic Acid in Water. *Chem. Eng. J.* **2012**, *180*, 197–203, doi:https://doi.org/10.1016/j.cej.2011.11.049.
213. Kuhn, R.; Jensch, R.; Bryant, I.M.; Fischer, T.; Liebsch, S.; Martienssen, M. Photodegradation of Ethylenediaminetetra (Methylenephosphonic Acid)–The Effect of the System Configuration. *J. Photochem. Photobiol. A Chem.* **2020**, *388*, 112192.
214. Wang, L.; Li, B.; Dionysiou, D.D.; Chen, B.; Yang, J.; Li, J. Overlooked Formation

- of H₂O₂ during the Hydroxyl Radical-Scavenging Process When Using Alcohols as Scavengers. *Environ. Sci. Technol.* **2022**, *56*, 3386–3396.
215. Dewhirst, R.A.; Fry, S.C. The Oxidation of Dehydroascorbic Acid and 2, 3-Diketogulonate by Distinct Reactive Oxygen Species. *Biochem. J.* **2018**, *475*, 3451–3470.
216. Poljsak, B.; Ionescu, J.G. Pro-Oxidant vs. Antioxidant Effects of Vitamin C. *Handb. Vitam. C Res. Dly. Requir. Diet. sources Advers. Eff.* **2009**, *153*.
217. Bai, L.; Jiang, Y.; Xia, D.; Wei, Z.; Spinney, R.; Dionysiou, D.D.; Minakata, D.; Xiao, R.; Xie, H.-B.; Chai, L. Mechanistic Understanding of Superoxide Radical-Mediated Degradation of Perfluorocarboxylic Acids. *Environ. Sci. Technol.* **2021**, *56*, 624–633.
218. Metz, J.; Javed, H.; Mathieu, J.; Long, M.; Alvarez, P.J.J. Comment on “Mechanistic Understanding of Superoxide Radical-Mediated Degradation of Perfluorocarboxylic Acids.” *Environ. Sci. Technol.* **2022**, *56*, 5287–5288.
219. Javed, H.; Metz, J.; Eraslan, T.C.; Mathieu, J.; Wang, B.; Wu, G.; Tsai, A.-L.; Wong, M.S.; Alvarez, P.J.J. Discerning the Relevance of Superoxide in PFOA Degradation. *Environ. Sci. Technol. Lett.* **2020**, *7*, 653–658.
220. Plumlee, M.H.; McNeill, K.; Reinhard, M. Indirect Photolysis of Perfluorochemicals: Hydroxyl Radical-Initiated Oxidation of N-Ethyl Perfluorooctane Sulfonamido Acetate (N-EtFOSAA) and Other Perfluoroalkanesulfonamides. *Environ. Sci. Technol.* **2009**, *43*, 3662–3668.
221. Yang, X.; Huang, J.; Zhang, K.; Yu, G.; Deng, S.; Wang, B. Stability of 6:2 Fluorotelomer Sulfonate in Advanced Oxidation Processes: Degradation Kinetics and Pathway. *Environ. Sci. Pollut. Res.* **2014**, *21*, 4634–4642, doi:10.1007/s11356-013-2389-z.
222. D’Agostino, L.A.; Mabury, S.A. Identification of Novel Fluorinated Surfactants in Aqueous Film Forming Foams and Commercial Surfactant Concentrates. *Environ. Sci. Technol.* **2014**, *48*, 121–129.
223. Trouborst, L. Aqueous Photolysis of 6:2 Fluorotelomer Sulfonamide Alkylbetaine.; 2016.

224. Martin, J.W.; Mabury, S.A.; O'Brien, P.J. Metabolic Products and Pathways of Fluorotelomer Alcohols in Isolated Rat Hepatocytes. *Chem. Biol. Interact.* **2005**, *155*, 165–180.
225. Esfahani, E.B.; Zeidabadi, F.A.; Zhang, S.; Mohseni, M. Photo-Chemical/Catalytic Oxidative/Reductive Decomposition of per-and Poly-Fluoroalkyl Substances (PFAS), Decomposition Mechanisms and Effects of Key Factors: A Review. *Environ. Sci. Water Res. Technol.* **2022**, *8*, 698–728.
226. Marchington, E.B. *Identification of Known and Novel Fluorinated Compounds in AFFF Via $^9\text{-NMR}$, LC-MS/MS, and LC-Quad-TOFMS, and the Aerobic Biodegradation of 6: 2 FtS.*; Library and Archives Canada= Biblioth que et Archives Canada, 2009; ISBN 0494449268.
227. D'Agostino, L.A. *Environmental Chemistry of Perfluoroalkyl and Polyfluoroalkyl Substances in Aqueous Film Forming Foams*; University of Toronto (Canada), 2017; ISBN 0355776944.
228. Gomez-Ruiz, B.; G mez-Lav n, S.; Diban, N.; Boiteux, V.; Colin, A.; Dauchy, X.; Urtiaga, A. Boron Doped Diamond Electrooxidation of 6: 2 Fluorotelomers and Perfluorocarboxylic Acids. Application to Industrial Wastewaters Treatment. *J. Electroanal. Chem.* **2017**, *798*, 51–57.

Acknowledgements

My first thanks go to Professor Bruzzone and Professor Davide for their continuous help, support, and encouragement, which have allowed me to grow both scientifically and personally. I also extend my gratitude to Luca, who played a crucial role in guiding me during my work in the Lab. I deeply appreciate Professor Martienssen and Dr. Ramona for allowing me to work and collaborate in their Lab.

A special and heartfelt thanks to my family, especially my father, for raising me and supporting me throughout these years of study and in every aspect of life. I would also like to express my gratitude to my wife, whose unwavering love, patience, and understanding have been invaluable throughout this journey, and to my two wonderful children, who bring me joy and motivation every day. Their support has been a source of strength.

I also thank all the thesis students and colleagues for their friendship and for the moments spent together that brightened my days. Finally, I affectionately thank all my friends who have been by my side, offering support and a listening ear during difficult times.